


Fall 12-2008

Photopolymerization and Characterization of Thiol-enes and Thiourethanes

Qin Li

University of Southern Mississippi

Follow this and additional works at: <https://aquila.usm.edu/dissertations>

 Part of the [Materials Chemistry Commons](#), and the [Polymer Chemistry Commons](#)

Recommended Citation

Li, Qin, "Photopolymerization and Characterization of Thiol-enes and Thiourethanes" (2008).
Dissertations. 1146.
<https://aquila.usm.edu/dissertations/1146>

This Dissertation is brought to you for free and open access by The Aquila Digital Community. It has been accepted for inclusion in Dissertations by an authorized administrator of The Aquila Digital Community. For more information, please contact aquilastaff@usm.edu.

The University of Southern Mississippi

PHOTOPOLYMERIZATION AND CHARACTERIZATION OF
THIOL-ENES AND THIOURETHANES

by

Qin Li

Abstract of a Dissertation
Submitted to the Graduate Studies Office
of The University of Southern Mississippi
in Partial Fulfillment of the Requirements
for the Degree of Doctor of Philosophy

December 2008

COPYRIGHT BY

QIN LI

2008

The University of Southern Mississippi

PHOTOPOLYMERIZATION AND CHARACTERIZATION OF
THIOL-ENES AND THIOURETHANES

by

Qin Li

A Dissertation

Submitted to the Graduate Studies Office
of The University of Southern Mississippi
in Partial Fulfillment of the Requirements
for the Degree of Doctor of Philosophy

Approved:



December 2008

ABSTRACT

PHOTOPOLYMERIZATION AND CHARACTERIZATION OF THIOL-ENES AND THIOURETHANES

by Qin Li

December 2008

Compared to conventional acrylic monomer systems, thiol-ene photopolymerization, an efficient click process leading to the formation of dense and uniform molecular networks, has several distinct advantages including relative insensitivity to oxygen inhibition, high monomer conversion and low shrinkage. Although there has been a revival of interest in thiol-enes in the past 6 years, the structure-property relationship of these networks has not been explored in detail. For future applications, thiol-enes with higher shelf-life stability and glass transition temperatures need to be used. Sulfur containing urethanes, thiourethanes and dithiourethanes are a class of widely used materials due to their distinct properties such as high refractive index. However, the structure-property relationships of thiourethanes and dithiourethanes have not been explored in detail. This research provides a fundamental study of the photopolymerization and properties of thiol-enes and the structure-property relationships of sulfur containing urethanes. The effect of chemical structure of thiol-ene monomers on physical and mechanical properties, the photopolymerization of thiol-ene free-radical/ene cationic hybrid systems, the development and characterization of thiourethane thiol-ene networks, the effect of hydrogen bonding on the physical aging of

thiourethane thiol-ene networks, the investigation of hydrogen bonding behavior of thiourethanes and dithiourethanes and the structure-property relationships are all presented.

The first study deals with the photopolymerization and characterization of four different types of ene monomers with both primary and secondary multifunctional thiols. The results indicate that ene structures can significantly affect the rigidity and the physical and mechanical properties of the thiol-ene networks. Network density controlled by the functionality of ene monomers was found also to be a major factor in defining network properties. Networks formed from the secondary thiol-ene systems are basically equivalent to those made from primary thiol-enes with respect to physical mechanical and optical properties. The secondary thiol monomer samples evaluated were found to have excellent storage stability and relatively low odor.

The second study reports the photopolymerization kinetics of mixtures containing a trithiol and a trivinyl ether (in different molar ratios) with a cationic photoinitiator. Using the combination of real-time FTIR and rheology to follow both chemical conversion and rheological property development, a clear picture of physical property development during the complete polymerization process is obtained. This represents the first example of a thiol-ene radical/ene cationic two-step hybrid photopolymerization process in which thiol copolymerizes with vinyl ether functional groups in a rapid radical step growth process followed by vinyl ether cationic homopolymerization. The sequential thiol-vinyl ether copolymerization and the vinyl ether cationic polymerization result in

crosslinked networks with thermal and mechanical properties that are combinations of each system.

The third study concentrates on the development of novel thiourethane based thiol-ene (TUTE) films prepared from diisocyanates, tetrafunctional thiols and trienes. The incorporation of thiourethane linkages into the thiol-ene networks results in TUTE films with high glass transition temperatures. Increase of T_g was achieved by aging at room temperature and annealing the UV cured films at 85 °C. The aged/annealed film with thiol prepared from isophorone diisocyanate and cured with a 10,080 mJ/cm² radiant exposure had the highest DMA based glass transition temperature (108 °C) and a tan δ peak with a full width at half maximum (FWHM) of 22 °C, indicating a very uniform matrix structure. All of the initially prepared TUTE films exhibited good physical and mechanical properties based on pencil hardness, pendulum hardness, impact and bending tests.

The physical aging behavior of a class of photopolymerized thiourethane thiol-ene networks were characterized by thermal and spectroscopic analysis, the results of which are directly related to changes in macroscopic physical and mechanical properties. The hydrogen bonding associated with the thiourethane chemical structure exerts at most a slight retarding effect on the enthalpy relaxation, but there is a significant increase in the glass transition temperature of the thiourethane thiol-ene networks, an important implication for application of these materials and the stabilization of their physical, mechanical and thermal transition properties.

To define the difference between ordinary urethanes and thiourethanes, the hydrogen bonding behavior of a homologous family of model urethane, thiourethane and dithiourethane compounds prepared from primary isocyanates/isothiocyanates were investigated in solution, melt and solid states. The relative strengths of hydrogen bonds in these systems were evaluated, and the results compared to theoretical calculations of hydrogen bonding strength. The polyurethane and polythiourethane were found to have approximately equivalent physical and mechanical properties as a result of a similar extent of hydrogen bonding, whereas the polydithiourethane model compound, due to a lower degree of hydrogen bonding, has reduced thermal and mechanical transition temperatures as well as lower hardness values. The polythiourethane and polydithiourethane networks exhibit narrower glass transitions compared to polyurethane networks apparently the result of an efficient isocyanate/isothiocyanate-thiol reaction with little or no side products. Due to weakness of the C-S bond compared to the C-O bond, thiourethanes and dithiourethanes have lower thermal stability than corresponding urethanes. Finally the thiourethanes and dithiourethane have higher refractive index values than their urethane counterparts.

To complete the comparison study on urethane type materials, another homologous family of model urethane, thiourethane and dithiourethane prepared from both aliphatic and aromatic secondary isocyanates were comprehensively characterized by a series of spectroscopic, thermal, physical and mechanical analysis measurements to define the relative hydrogen bond strength and its correlation with properties. The

polyurethane and polythiourethane systems have similar physical and mechanical properties as a result of their similar structures and hydrogen bonding behavior, whereas the polydithiourethane, due to relatively weaker hydrogen bonding has reduced physical properties. The NMR, FTIR and XRD measurements of small molecule models in solution, melt and solid states indicate the relative hydrogen bonding strength as: urethane \approx thiourethane $>$ dithiourethane. The aromatic urethane is more stable under UV irradiation than the corresponding thiourethane analogues. Due to the weaker C-S bond compared to C-O bond, thiourethane and dithiourethane have reduced thermal stability compared to their urethane counterpart. Similar T_g values observed for polyurethane and polythiourethane systems are higher than those for the polydithiourethane, consistent with the lower hydrogen bonding in the latter.

DEDICATION

I would like to dedicate this document to my parents, my dear wife, my lovely baby and all my family members for loving, encouraging and supporting me all the way.

ACKNOWLEDGEMENTS

I would like to thank my advisor Dr. Charles E. Hoyle for guiding me with enthusiasm, encouragement, kindness, and patience. His great personality and dedication to scientific research have established a tradition for achieving excellence as not only a scientist but also a person. I thank him especially for providing me with so many opportunities to go to top-class professional conferences.

I would also like to thank my co-advisor Dr. Douglas A. Wicks for always being supportive, encouraging, and kind. I benefited from his professional guidance and advice.

I acknowledge my committee members, Dr. Janice P. Phillips, Dr. Sarah E. Morgan, Dr. Seigei I. Nazarenko, and Dr. William L. Jarrett, for their help and support leading to the successful completion of this graduate research.

Special thanks go to Dr. Hui Zhou and Dr. Huanyu Wei for their unconditional help and beneficial discussions. The assistance and support of past and present members of the Hoyle Research Group were very important for the completion of this research.

I would like to thank the Rawlins, Moore, Phillips, Mauritz, Lowe, Nazarenko and Urban research groups for kindly allowing me to use their equipment, which made the characterization in this research possible. I give additional thanks to all the friends within these groups and the department who have aided me. I would also like to thank Dr. David Magers and Dr. Edward Valente for their excellent contribution to this research.

I thank the National Science Foundation, specifically the Materials Research Science and Engineering Center (MRSEC), and Fusion UV Systems for funding this

research. In addition, materials were generously provided by Perstorp, Bruno Bock, Bayer Materials Science, Ciba Specialty Chemicals, Showa Denko K. K. and Sartomer Company.

TABLE OF CONTENTS

ABSTRACT.....	ii
DEDICATION.....	vii
ACKNOWLEDGEMENTS.....	viii
LIST OF CHARTS AND SCHEMES.....	xiii
LIST OF TABLES.....	xv
LIST OF ILLUSTRATIONS.....	xvii
CHAPTER	
I. INTRODUCTION.....	1
Photopolymerization of (Meth)acrylates and Thiol-Enes	
Hybrid Photopolymerization Systems	
Modification of Thiol-Ene Systems	
Urethane, Thiourethane and Dithiourethane	
Summary	
References	
II. OBJECTIVES.....	35
III. THE EFFECT OF THIOL AND ENE STRUCTURES ON THIOL-ENE NETWORKS: PHOTOPOLYMERIZATION, PHYSICAL, MECHANICAL AND OPTICAL PROPERTIES.....	38
Abstract	
Introduction	
Experimental	
Results and Discussion	
Conclusions	
Acknowledgements	
References	
IV. THIOL-ENE FREE-RADICAL AND VINYL ETHER CATIONIC HYBRID	

PHOTOPOLYMERIZATION.....	68
Abstract	
Introduction	
Experimental	
Results and Discussion	
Conclusions	
Acknowledgements	
References	
V. THIOURETHANE THIOL-ENE HIGH T_g NETWORKS: PREPARATION, THERMAL, MECHANICAL, AND PHYSICAL PROPERTIES.....	96
Abstract	
Introduction	
Experimental	
Results and Discussion	
Conclusions	
Acknowledgements	
References	
VI. PHYSICAL AGING OF THIOURETHANE THIOL-ENE NETWORKS.....	123
Abstract	
Introduction	
Experimental	
Results and Discussion	
Conclusions	
Acknowledgements	
References	
VII. COMPARISON OF SMALL MOLECULE AND POLYMERIC URETHANES, THIOURETHANES AND DITHIOURETHANES: HYDROGEN BONDING AND CORRELATION WITH THERMAL, PHYSICAL AND MECHANICAL PROPERTIES. PART 1.....	152
Abstract	
Introduction	
Experimental	
Results and Discussion	
Conclusions	
Acknowledgements	

References

VIII.	COMPARISON OF SMALL MOLECULE AND POLYMERIC URETHANES, THIOURETHANES AND DITHIOURETHANES: HYDROGEN BONDING AND CORRELATION WITH THERMAL, PHYSICAL AND MECHANICAL PROPERTIES. PART 2.....	209
	Abstract	
	Introduction	
	Experimental	
	Results and Discussion	
	Conclusions	
	Acknowledgements	
	References	
IX.	CONCLUSIONS AND RECOMMENDATIONS.....	249

LIST OF CHARTS AND SCHEMES

Chart

- 3.1. Chemical structures of thiols and enes.....54
- 4.1. Chemical structures of TriThiol and TriVinyl.....86
- 5.1. Structures of components.....110
- 5.2. Representative average structures of the three thiol end-capped oligomers: IPDI Thiol pentamer, H12MDI Thiol pentamer and TDI Thiol pentamer (the hydrogens are numbered and their ¹H NMR chemical shifts are listed in Table 1 under the same number).....111
- 7.1. Molecular structures of (a) N-methyl methylcarbamate, (b) N-methyl S-methylthiocarbamate and (c) N-methyl S-methyldithiocarbamate used in hydrogen bonding strength calculation.....183
- 8.1. Structures and bond length (Å) of PIHA and PIHT. Bond length values are measured by X-Ray diffraction.....232

Scheme

- 5.1. Synthesis of IPDI Thiol and formation of the corresponding TUTE film.....112
- 6.1. Preparation of thiourethane-thiol-ene films. IPDI, TDI and H12MDI were used as the diisocyanates to prepare thiourethane thiols with different structures.....138
- 7.1. Synthesis of carbamate (HIHA), thiocarbamates (HIHT and BMPHI) and dithiocarbamate (BMPHIT).....181
- 7.2. Preparation of polyurethane (3NCO-HexDiol), polythiourethanes

(3NCO-HexDithiol and HDI-TriThiol) and polydithiourethane (HDIT-TriThiol).....	182
8.1. Synthesis of carbamates (CIHA and PIHA), thiocarbamates (CIHT and PIHT) and dithiocarbamates (PITHT).....	229
8.2. Synthesis of polyurethanes, IPDI-HexDiol and TDI-HexDiol, polythiourethanes, IPDI-HexDithiol and TDI-HexDithiol, and polydithiourethane, TDIT-HexDithiol.....	230
8.3. Free radicals formed in the photolysis of aromatic urethane and thiourethane.....	231

LIST OF TABLES

Table

3.1. Shelf-life of thiol-ene formulations (1 wt% DMPA) stored in dark and at room temperature.....	55
3.2. Glass transition temperature and heat capacity change of thiol-ene networks measured by DSC.....	56
3.3. Glass transition temperature and heat capacity change of thiol-ene networks measured by DSC.....	57
3.4. Temperature at 5% weight loss ($T_{5\%}$) and temperature at the maximum degradation rate (T_{\max}) of thiol-ene films.....	58
3.5. Refractive indices of thiol-ene films.....	59
4.1. Mechanical properties of 0:100TriVinyl, 25:75 TriThiol-TriVinyl and 50:50 TriThiol-TriVinyl.....	87
5.1. ^1H NMR Chemical Shifts of the SH end-capped oligomers.....	113
5.2. T_g s ($^{\circ}\text{C}$) of aged TUTE films and 1:1 molar Tetra Thiol-Triallyl Triazine films. All T_g s were measured by DMA operating at 1Hz and 3 $^{\circ}\text{C}/\text{min}$	114
5.3. FWHM values of $\tan \delta$ peaks of aged IPDI Thiol-Triallyl Triazine films.....	115
5.4. Hardness of unaged TUTE films.....	116
5.5. Impact and elongation of unaged TUTE films.....	117
6.1. Glass transition temperatures of thiourethane-thiol-ene and the base thiol-ene networks measured with DSC operating at 10 $^{\circ}\text{C}/\text{min}$ and full width of half	

maximum (FWHM) of Tan δ peaks measured with DMA operating at 3 °C/min..	139
6.2. Enthalpy relaxation rate of thiol-ene and thiourethane-thiol-ene networks.....	140
7.1. Melting point (T_m) of small model compounds measured by DSC operating at 1 °C/min.....	184
7.2. Assignments of free and hydrogen bonded peaks in model compounds at 35°C...	185
7.3. Slope and chemical shift difference for model compounds calculated from Figure 7.5.....	186
7.4. Hydrogen bonding energy of carbamate, thiocarbamate and dithiocarbamate.....	187
7.5. Glass transition temperatures of polymer networks measured by DSC and DMA.....	188
7.6. Pendulum hardness and pencil hardness of model polymers.....	189
7.7. The yield stress (σ_y), yield strain (ϵ_y), stress at break (σ_b), strain at break (ϵ_b) and Young's modulus (E) of polymer networks.....	190
7.8. Densities and refractive indices of polymer networks.....	191
8.1. Table 8.1. Temperature dependence chemical shift coefficients, $\Delta\delta/\Delta T$, and variation in chemical shift, $\Delta\delta$, of model compounds.....	233
8.2. Hydrogen-bonding metrics from crystal structures.....	234
8.3. Crystallographic data for crystal structures.....	235
8.4. Melting point of model compounds measured by DSC at a heating rate of 1 °C/min	
8.5. Polymer glass transition temperatures.....	236
8.6. Temperature at 5% weight loss ($T_{5\%}$) values of polymers.....	237

LIST OF ILLUSTRATIONS

Figure

1.1. Conventional free-radical chain growth polymerization mechanism.....	25
1.2. Figure 1.2. The free-radical step growth mechanism of thiol-ene photopolymerization.....	26
1.3. The $\tan \delta$ vs. temperature plot of TriThiol-TriVinyl networks.....	27
1.4. Mechanism of cationic photopolymerization.....	28
1.5. Structures of urethane, thiourethane and dithiourethane.....	29
1.6. Methods to synthesis linear polythiourethane.....	30
1.7. Suggested mechanism of amine catalyzed thiol-isocyanate reaction.....	31
1.8. Physically crosslinked networks formed through hydrogen bonding between urethane linkages.....	32
1.9. Schematic representation of polyurethane segments.....	33
1.10. Structures of dithiocarbamates.....	34
3.1. Percent conversion of thiol group as a function of irradiation time (SH:C=C = 1:1 mol/mol). Light intensity = 0.625 mW/cm^2	60
3.2. Percent conversion of acrylate group as a function of irradiation time (SH:C=C = 1:1 mol/mol). Light intensity = 0.625 mW/cm^2	61
3.3. DSC curves of thiol-ene networks measured at a heating rate of $10 \text{ }^\circ\text{C/min}$	62
3.4. Persoz pendulum hardness of thiol-ene networks.....	63
3.5. Impact resistance of thiol-ene networks.....	64

3.6. Elongation and cracking resistance of thiol-ene networks.....	65
3.7. Pencil hardness of thiol-ene films.....	66
3.8. TGA curves of thiol-ene films.....	67
4.1. Real-time IR percent conversion versus time plots of 50:50 TriThiol-TriVinyl: (a) thiol and (b) vinyl ether. Irradiance (full arc) is 1.87 mW/cm ²	88
4.2. Real-time IR percent conversion versus time plots of pure TriVinyl. Irradiance (full arc) is 1.87 mW/cm ²	89
4.3. Real-time IR percent conversion versus time plots of 25:75 TriThiol-TriVinyl: (a) thiol and (b) vinyl ether. Irradiance (full arc) is 1.87 mW/cm ²	90
4.4. Time dependence of (A) dynamic storage modulus, G' , and (B) complex viscosity, η^* , of different concentrations of TriThiol/TriVinyl mixtures at constant shear frequency ($\omega=10\text{ rad s}^{-1}$) and 25 °C: O (pure TriVinyl); Δ (25:50 TriThiol-TriVinyl); \square (50:50 TriThiol-TriVinyl). Irradiance is $\sim 7.5\text{ mW/cm}^2$	91
4.5. Time dependence of G' and G'' at 25 °C and 10 rad s ⁻¹ for the photopolymerization process of pure TriVinyl. The arrow shows the t_{gel} obtained from intersection point of G' and G'' . Irradiance is $\sim 7.5\text{ mW/cm}^2$	92
4.6. Time dependence of G' and G'' at 25 °C and 10 rad s ⁻¹ for the UV polymerization process of 25:75 TriThiol-TriVinyl. The inset-plot shows the same figure at a smaller scale; the arrow shows the t_{gel} obtained from intersection point of G' and G'' . Irradiance is $\sim 7.5\text{ mW/cm}^2$	93
4.7. Tan δ versus temperature plots for films formed from (a) pure TriVinyl, (b) 25:75	

TriThiol-TriVinyl, and (c) 50:50 TriThiol-TriVinyl. DMA plots obtained with scan rate 3 °C/min and frequency 1 Hz.....	94
4.8. Tensile strain versus stress plots of 1-mm thick samples of (a) pure TriVinyl, (b) 25:75 TriThiol-TriVinyl, and (c) 50:50 TriThiol-TriVinyl.....	95
5.1. Figure 5.1. (a) RTIR spectra of thiol (2575 cm ⁻¹) and ene (3083 cm ⁻¹) in thiol-ene photopolymerization. Percent conversion of thiol group as a function of irradiation time of (b) IPDI Thiol-Triallyl Triazine, (c) H12MDI Thiol-Triallyl Triazine, and (d) TDI Thiol-Triallyl Triazine mixtures. Light intensity is 18.7 mW/cm ² and 1 wt% of DMPA is used as photoinitiator.....	118
5.2. 1 st and 2 nd DSC heating scans and first DSC cooling scans for unaged IPDI Thiol-Triallyl Triazine films polymerized with UV radiant exposure of 10,080 mJ/cm ² . All scans at 10 °C/min.....	119
5.3. T _g s of (a) unaged and (b) aged IPDI Thiol-Triallyl Triazine films determined from 1 st and 2 nd DSC heating scans at 10 °C/min.....	120
5.4. (a) Tan δ peaks for aged IPDI Thiol-Triallyl Triazine unannealed films. (b) Tan δ peaks for aged IPDI Thiol-Triallyl Triazine annealed (18 h, 85 °C) films. (c) T _g obtained from tan δ peak maxima in (a) and (b) vs. light radiant exposure. DMA scans obtained at 1Hz and 3 °C/min.....	121
5.5. (a) T _g of aged H12MDI Thiol-Triallyl Triazine films, and (b) T _g s of aged TDI Thiol-Triallyl Triazine films obtained by DMA at 1Hz and 3 °C/min. Annealed samples were heated at 85 °C for 18 h.....	122

6.1. Schematic illustration of DSC measurements of enthalpy relaxation.....	141
6.2. Tensile stress and strain of unannealed and annealed (T_g-10 °C for 20 h) IPDI Thiol-TTT film measured at room temperature.....	142
6.3. Pendulum hardness of IPDI Thiol-TTT film measured at room temperature.....	143
6.4. Refractive index of IPDI Thiol-TTT and Tetra Thiol-TTT films measured at room temperature.....	144
6.5. Enthalpy relaxation of IPDI Thiol-TTT film annealed for 1 h at various temperatures measured with DSC.....	145
6.6. Enthalpy relaxation of TetraThiol-TTT film annealed at various temperatures measured with DSC.....	146
6.7. Relaxed enthalpy of all thiol-ene films as a function of annealing temperature...	147
6.8. DSC curve of (a) Tetra Thiol-TTT network and (b) IPDI Thiol-TTT network annealed for different time periods.....	148
6.9. Enthalpy relaxation of thiol-ene and thiourethane thiol-ene networks as a function of annealing time (t_a) at T_g-10 °C.....	149
6.10. FTIR spectra of the NH group of the IPDI Thiol-TTT network measured at different conditions: (a) unannealed, (b) immediately after annealing at T_g-10 °C for 20h, and (c) when the annealed sample is cooled to 25 °C. The thermal history has been removed by heating at 150 °C for 30 min before FTIR measurements.....	150
6.11. Hydrogen bonding fraction of samples a, b and c in Figure 6.10.....	151
7.1. IR spectra of model compounds dissolved in chloroform. Note that the “bump” in	

the spectra for HIHA, HIHT and BMPHT between 3400 and 3500 cm ⁻¹ is an instrumental artifact.....	192
7.2. The ¹ H NMR spectra of 3.7 mM HIHA in CDCl ₃ and d-DMSO.....	193
7.3. Chemical shift difference between NH protons in d-DMSO and CDCl ₃	194
7.4. FTIR spectra of HIHA, HIHT, BMPHI and BMPHIT measured at different temperatures. The arrows indicate the direction of peak intensity as a function of temperature increase.....	195
7.5. Peak deconvolution of the IR spectra of BMPHI and BMPHIT measured at 35 °C.....	196
7.6. Hydrogen bonding fractions of model compounds.....	197
7.7. Contributions of different hydrogen bonding acceptors of BMPHI and BMPHIT model compounds.....	198
7.8. The ¹ H NMR spectra of HIHA measured at temperatures from 35 °C to 105 °C with a 10 °C interval.....	199
7.9. The chemical shift value of NH proton for model compounds as a function of temperature.....	200
7.10. Thermogravimetric analysis of polymer networks.....	201
7.11. Hydrogen bonding fraction of polymer networks as a function of temperature...	202
7.12. Contributions of different hydrogen bonding acceptors of HDI-TriThiol and HDIT-TriThiol.....	203
7.13. DSC scans of polymer networks.....	204

7.14. Storage modulus (E') and $\tan \delta$ of polymer networks measured by DMA operating at 3 °C/min.....	205
7.15. DSC curves of 3NCO-HexDiol and 3NCO-HexDithiol networks annealed for different times.....	206
7.16. The enthalpy relaxation of 3NCO-HexDiol and 3NCO-HexDithiol as a function of sub- T_g aging time.....	207
7.17. Stress-strain curve of model compounds measured at a strain rate of 10 %/min...	208
8.1. The ^1H NMR spectra of 3.7 mM CIHA in $\text{CDCl}_3/\text{d-DMSO}$ solvent mixtures. The numbers in the figure indicate the volume ratios of the two solvents.....	238
8.2. (a) Chemical shift values of NH protons of model compounds as a function of volume ratio of d-DMSO/ CDCl_3 . (b) Chemical shift difference between NH protons in d-DMSO and CDCl_3	239
8.3. The ^1H NMR spectra of CIHA measured at different temperature.....	240
8.4. Chemical shift of model compounds as a function of temperature.....	241
8.5. FTIR spectra of CIHA and CIHT measured at temperatures from 45 to 95°C with a 10 degrees interval. The arrows indicate the direction of temperature increase...	242
8.6. $F_{b,\text{NH}}$ of carbamates, thiocarbamates and dithiocarbamate as a function of temperature.....	243
8.7. UV spectra of PIHA, PIHT and PITHT before and after photolysis conducted by exposing all samples dissolved in CH_2Cl_2 (0.06 mM) to the output of a medium pressure mercury lamp for 20 min.....	244

8.8. UV spectra of model compound solutions (in CH ₂ Cl ₂) with equal absorbance at 254 nm before and after photolysis conducted by exposing all samples to the output of a Rayonet photoreactor equipped with 254 nm lamp.....	245
8.9. Hydrogen bonding fraction of polymers as a function of temperature.....	246
8.10. DSC curves of polymers.....	247
8.11. Thermogravimetric analysis of polymers.....	248

CHAPTER I

INTRODUCTION

Photopolymerization is the process in which low molecular weight species (monomers, oligomers and prepolymers) are transformed into high molecular weight molecules to yield solid materials upon exposure to either visible or ultraviolet (UV) light. The light source can be either a laser or a polychromatic lamp.^{1,2} The advantages and benefits of UV photopolymerization are well known since their early industrial applications in the mid-late 1970s:^{1,3,4}

- 1) Rapid cure rate
- 2) Energy and space saving
- 3) Zero Volatile Organic Compounds (VOCs)
- 4) Low-temperature operation
- 5) Application versatility

As a result of these advantages, UV polymerization has received increasing industrial attention for the last three decades. Due to more strict VOC regulations and increasing energy costs, the use of UV polymerizations has expanded into numerous fields including decorative and protective coatings, adhesives, printing inks, optics and electronics.¹

A typical UV polymerization formulation includes photoinitiators, monomers, oligomers, prepolymers and various additives. After absorbing light, photoinitiators

generate active species, e.g. free radicals and ions, which initiates the polymerization of reactive compounds, e.g. monomers, oligomers and prepolymers. For practical considerations, e.g. viscosity, various additives may also be included in the formulation. The initiation and photopolymerization rates can be controlled by the combination of lamp and chemical systems. The dose, light intensity and wavelength of UV light affect the polymerization rate. Other factors include the reactivity of the monomers and oligomers, absorption of photoinitiators and monomers, oxygen inhibition, temperature, and pigmentation.²

Photopolymerization of (Meth)acrylates and Thiol-Enes

(Meth)acrylates are the most widely used reactive components in photopolymerization due to their versatility and properties of the resultant polymers. The polymerization of acrylic monomers follows the conventional free-radical chain growth mechanism shown in Figure 1.1. The photoinitiator generates a radical species, which in turn forms a free radical via dissociation. The polymerization is then initiated by the addition of free radicals to the monomer double bond, leading to a free-radical chain process. The very rapid chain growth process and coupling of growing chain ends produce crosslinked molecular species in the early stages of polymerization,^{5,6} resulting in gelation and subsequent vitrification of the system at very low double bonds conversion. The undesired result of this process is stress built up within the polymer

network. A coincident phenomenon of this is an increase in viscosity, which kinetically traps free radicals within the network. These trapped active species continue to react, resulting in significant changes in polymer properties over a long time period.⁵⁻⁷ In multifunctional (meth)acrylates systems, pendent and terminal double bonds having different reactivities lead to cyclization reactions, resulting in density differences in the final networks. This inhomogeneity is typically characterized by a broad glass transition region.⁸ The nature of the free-radical polymerization of multifunctional (meth)acrylates makes it very difficult to control the structure, physical and mechanical properties of the resultant polymer network.

Thiol-ene photopolymerizations, which undergo a free-radical step growth mechanism, provide better control of the final network structures and thus superior physical and mechanical properties. As shown in Figure 1.2., once a radical is generated (with or without photoinitiators), it adds across the double bond of the ene monomer to produce a carbon centered radical which then abstracts a hydrogen from another thiol monomer, yielding a new thiyl radical that allows the process to continue. Polymerization proceeds by this two-step process until termination occurs via radical coupling.⁸

The gel point of multifunctional thiol-ene polymerizations is given by:⁹

$$\alpha = \sqrt{\frac{1}{r(f_{\text{thiol}} - 1)(f_{\text{ene}} - 1)}} \quad (1)$$

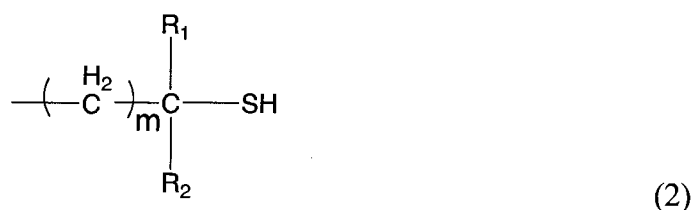
where $r (< 1)$ is the molar ration of thiol and ene functional groups, and f_{thiol} and f_{ene} are

the functionality of thiol and ene monomers, respectively. Compared with traditional acrylates, thiol-ene free radical polymerizations have a delayed onset of gelation, thereby forming network structures with less inner-stress.⁸ One of the most important aspects of thiol-ene photopolymerization is its relative insensitivity to oxygen inhibition, which generally suppresses free-radical polymerizations under ambient conditions. In this case, the peroxide radicals generated by the introduction of oxygen abstracts a thiol hydrogen, resulting in a new thiyl radical.¹⁰ This process allows propagation to proceed, leaving the polymerization rates almost unaffected.

A particularly important feature of thiol-ene systems is the uniform network density that gives polymers exceptional physical properties, such as high impact resistance without stress cracking or shattering.⁸ This feature is demonstrated by the polymerization of a trifunctional ene (tris(4-(vinylloxy)butyl) trimellitate (TriVinyl)) with a trifunctional thiol (trimethylol propane tris(3-mercaptopropionate) (TriThiol)) which yields a network with a narrow glass transition region (about 20 °C) as illustrated by the $\tan \delta$ vs. temperature curve in Figure 1.3. The dynamic mechanical properties of other thiol-ene networks reported in the literature^{11, 12} also show very narrow glass transition regions indicative of highly uniform structures. The properties of inhomogeneous polyacrylate networks can be significantly altered by the introduction of multifunctional thiols as a comonomer. The resultant networks have much more uniform structures as

evidenced by narrower glass transitions as compared with their pure polyacrylate analogues.¹³

The properties of thiol-ene networks heavily depend on the structure of each component. Almost all of the thiols used in reported thiol-ene photopolymerizations have been primary.^{8, 11-14} Although primary thiol-ene systems are very photochemically reactive, their storage stability is of concern. The short shelf-life of certain primary thiol-ene mixtures limits their applications where a long storage time before use is important. Possible reasons for the limited shelf-life of thiol-enes have been extensively studied and reviewed.^{8, 15-17} In order to extend the shelf-life of thiol-ene mixtures, numerous types of stabilizers, including sulfur, triallyl phosphates and the aluminum salt of N-nitrosophenylhydroxylamine have been used to prevent ambient thermal free-radical polymerization. Recently, there have been reports of photocurable thiol-enes based on a series of hindered multifunctional or secondary thiols, depicted by the following structure



where R_1 is an alkyl moiety, such as a methyl or a phenyl group, and R_2 is either a proton or an alkyl group.¹⁸⁻²² A commercialized secondary thiol, the pentaerythritol tetrakis(3-mercaptopbutylate) (s-4T), has recently been reported for use in numerous applications

including spacers, color filters and light sensitive coatings for LCD displays.^{19, 21, 23-28}

However, to the best of our knowledge there has not been a detailed evaluation of basic mechanical and thermal properties of thiol-ene systems as a function of ene structure.

Hybrid Photopolymerization Systems

To overcome the limitation of a single type of photopolymerization system and thereby synthesize polymers with unique properties, efforts have been undertaken to create simultaneously or sequentially polymerized hybrid systems, i.e., simultaneous free-radical and cationic photopolymerization process.²⁹⁻³⁸ It is well known that (meth)acrylate free-radical photopolymerizations suffer from oxygen inhibition and relatively high polymerization shrinkage, while cationic ring opening polymerizations (oxetanes and oxiranes) are characterized by water inhibition and low reaction rates. The combination of free-radical and cationic polymerizations is a feasible way to overcome their respective limitations. The mechanism of cationic photopolymerization initiated by the direct photolysis of sulfonium salts is shown in Figure 1.4.³⁹ Cationic photopolymerization systems are industrially important due to advantages including lower toxicity of monomers, insensitivity to oxygen, low shrinkage, and excellent adhesion.

Representative examples include the free-radical acrylate/cationic epoxide hybrid systems reported by Decker et. al.^{30, 31} and Jessop et.al.⁴⁰ The oxygen sensitivity of the

acrylate is reduced, while its ultimate conversion is enhanced in hybrid photopolymerization of acrylates and epoxides. In addition, hybrid acrylate/epoxide systems form polymer matrices with superior hardness as compared to either neat acrylate or neat epoxide based networks while being more flexible than the neat epoxide polymer. Ortiz et al.^{41, 42} investigated free-radical thiol-ene/cationic epoxide hybrid systems which were cured by photopolymerization and thermally induced polymerization at temperatures over 100 °C. During the initial photopolymerization process, the epoxide functional groups only achieve very low conversions because the growing cationic chain ends are readily terminated by the polysulfide formed in the system.^{41, 42} Hence, a subsequent thermal polymerization at temperatures over 100 °C must be used to fully cure the formulation which, to some degree, negates the general advantage of photopolymerization. A photocurable free radical thiol-ene/vinyl ether cationic hybrid system would resolve this problem.

Modification of Thiol-Ene Systems

As described earlier, thiol-ene polymers exhibit unique physical and mechanical properties, such as network uniformity and low internal stress, which is critical in many applications including optical elements^{43, 44} and dental restoratives.⁴⁵ However, the addition of thiols across double bonds yields flexible thioether linkages. Thus, the glass transition temperatures (T_g) are generally near or below room temperature, limiting the

application of these materials. The glass transition temperature can be increased by selecting more rigid thiol and ene structures, but there are few if any viable options. Limited T_g enhancement can be achieved by utilizing ene monomers with rigid structures, such as triallyl-1,3,5-triazine-2,4,6(1H,3H,5H)-trione. One alternative is to incorporate multifunctional acrylates, which act as ene monomers reacting either with thiols or themselves.^{12, 46} The resultant polymers have glass transitions as high as ~ 80 °C (as determined by DMA at 1 Hz).⁴⁷ But the uniformity of the networks, a critical criteria in several applications, is greatly reduced as indicated by the broadened $\tan \delta$ peaks compared with those of pure thiol-ene networks with full-width at half maximum (FWHM) values of 15~20 °C. Thus there is a need to develop thiol-ene based systems with high T_g s and narrow glass transition regions.

Physical aging is a widely reported phenomenon for many linear polymers.^{48, 49} Upon annealing at temperatures below the glass transition temperature, a vitrified polymer in a thermodynamic non-equilibrium state will approach the thermodynamic equilibrium with coincident changes in physical properties, including a decrease in specific volume and enthalpy relaxation.^{48, 49} The process is related to changes in various microstructural and macrostructural properties.⁴⁸ The physical aging behavior of polymers is affected by various factors such as temperature, time, and chemical structure. For example, hydrogen bonds offer physical linkages within polymer matrices that

restrict segmental and chain motions, thus affecting the relaxation process. This has been discussed previously in literature.⁵⁰⁻⁵³ McGonigle et al.⁵⁰ prepared a series of linear polystyrene copolymers capable of forming hydrogen bonds and measured their enthalpic relaxation and free volume changes using differential scanning calorimetry (DSC) and positron annihilation lifetime spectroscopy (PALS). The physical aging process of these copolymers was shown to be sensitive to the formation of hydrogen bonds, resulting in a slower relaxation rate during aging process as compared to the polystyrene homopolymer. Thus it is important to determine the effect of hydrogen bonding on the physical aging process in thiourethane-thiol-ene networks.

Urethane, Thiourethane and Dithiourethane

Polyurethanes are high performance materials widely used in such applications as coatings, elastomers, and biomedical devices due to their extraordinary combination of physical and mechanical properties.⁵⁴⁻⁵⁶ Thiourethanes and dithiourethanes are obtained when one or both of the oxygens in the urethane structure is substituted with sulfur.

Dyer et al. reported two different reactions for preparing linear polythiourethanes.⁵⁷ Polyaddition involves the reaction of diisocyanate and dithiol catalyzed by tri-n-propylamine in a co-solvent system of chlorobenzene and o-dichlorobenzene. Polycondensation (Figure 1.6) utilizes the interfacial polymerization technique which yields polymers with high polydispersity. Although the reaction rate of

the polycondensation method is high, the polyaddition method exhibits better control of the molecular weight distribution. When appropriate basic catalysts are used, the isocyanate-thiol reaction can be very efficient.⁵⁸

In addition to tri-n-propylamine, various tertiary amines, such as triethylamine, tri-n-butylamine, 1-ethylpiperidine, 1,4-diazabicyclo (2,2,2) octane (DABCO) and benzyldimethylamine, are able to catalyze the thiol-isocyanate reaction.^{58, 59} DABCO and triethylamine are particularly efficient catalysts. The catalytic ability of the amine is proportional to its base strength.⁵⁸ In addition, steric hindrance around the nitrogen atom will greatly reduce the catalytic efficiency. Using the 1-butanethiol-phenyl isocyanate system as an example, the proposed mechanism of amine catalyzed thiol-isocyanate reaction is shown in Figure 1.7.⁵⁸ Due to the lower basicity of sulfur, which makes the thiol less able to attack the isocyanate carbonyl group, the spontaneous thiol-isocyanate reaction (step 1 in Figure 1.7) is usually slower than the corresponding alcohol-isocyanate reaction. One of the unique features of the thiol-isocyanate reaction is that the thiourethane formed in step 2 has some catalytic effect on the thiol-isocyanate reaction in step 3, but it is not active enough for side reactions with an isocyanate⁵⁸⁻⁶⁰ that generates allophanates generally found in alcohol-isocyanate reactions.⁶¹

Although the reactions of thiols and isocyanates shown in Figure 1.5 have been known for a long time,^{57, 62} and the resultant thiourethanes are widely used in many

modern applications including optical lenses and advanced coatings,⁶³⁻⁶⁵ the basic properties of thiourethanes have not been characterized to the same extent as their urethane counterparts. Although limited literature can be found on synthesis, catalysis, reaction kinetics, thermal dynamic transitions and hydrogen bonding,^{57, 58, 62, 66, 67} detailed comparisons of urethane, thiourethane and dithiourethane properties have not been made. Some of the physical and chemical properties of the linear polythiourethanes prepared from methylenebis (4-phenylisocyanate) and 1,6-hexanediisocyanate with a series of difunctional thiols were briefly described by Dyer et al. in a 1960 paper.⁵⁷ In the work the dilute solution viscosity of the polythiourethane was very low (0.06-0.12), indicating a low molecular weight. Polythiourethanes have been reported to have higher melting points than their polyurethane analogues due to greater molar cohesive energy⁶⁸⁻⁷⁰ and possess an intermediate hydrolyzability in aqueous base between that of aromatic and aliphatic urethanes.⁷¹ Polythiourethane are claimed to be insoluble in most organic solvents, with only very polar solvents such as dimethylformamide and dimethyl sulfoxide being able to dissolve them.⁵⁷

Hydrogen bonding is a vital factor in determining the microscopic and macroscopic properties of polyurethanes, including phase behavior, glass transition temperature, strength and stiffness.^{72, 73} Hydrogen bonding involves a donor A-H and an acceptor B. The electronegativity of A must be high in order to alter the electron density,

and thus partially deshield the proton. The donor B should have either a lone electron pair or polarizable π electrons.^{74, 75} Strong hydrogen bonds are formed between donors that are electron deficient and acceptors with high electron density. Hydrogen bonds formed by neutral donors and acceptors are generally moderate in strength. Weak hydrogen bonds are formed when A is slightly more electroneutral than H or when B has only π electrons.

In the past 60 years, the hydrogen bonding behavior of both segmented systems and polymer blends of polyurethanes have been thoroughly investigated.^{72, 73, 76-81} Polyurethane morphology is greatly affected by the hydrogen bonding between the urethane repeat units (Figure 1.8). This hydrogen bonding can create a physically crosslinked network which imparts greatly enhanced physical properties. Polyurethanes comprised of a diisocyanate, a glycol extender (or diamine), and a long chain polyether or polyester polyol form materials comprised of both soft and hard segments (Figure 1.9). The hard segments are characterized by a high concentration of urethane groups that provide stiffness via hydrogen bonding. The soft segment is generally characterized by the long chain polyol that gives the polymer film flexibility. The microphase-separated structure formed determines the elastic properties of linear urethane block copolymers, with the hard domains behaving as physical crosslinks. By changing the chemical structure of the components, the morphology can be optimized for performance desired.

The nature of hydrogen bonding in thiourethanes and dithiourethanes has not been characterized to the same extent as their urethane analogues. Although sporadic reports occur in literature,^{82, 83} neither a direct comparison of the hydrogen bonding behavior of urethane, thiourethane and dithiourethane nor the correlation of thiourethane/dithiourethane structures with their properties has been made. Wheeler et al.⁸³ investigated a homologous family of alanine-based dithiocarbamates (Figure 1.10) by X-ray crystallography. Although the self-assembly of these molecules relies on the formation of the carboxylic acid dimers via strong hydrogen bonding, the variation in molecular alignment arises from the formation of N-H---S=C and N-H---O=C hydrogen bonds. Compared to a C=O group, the hydrogen bond acceptor, C=S group, forms weaker hydrogen bonding. The reported hydrogen bond length (for H---S=C) ranges from 2.60 to 2.70 Å,⁸³⁻⁸⁵ longer than that of H---O=C (less than 2.2 Å).^{75, 83} A comprehensive investigation of the hydrogen bonding capability of aliphatic and aromatic urethane, thiourethane and dithiourethane has not been conducted to date, and their effect on the physical and mechanical properties of the corresponding polymers has not been reported.

A number of techniques, including infrared (FTIR) and Raman spectroscopy, nuclear magnetic resonance spectroscopy (NMR), electronic absorption spectroscopy, X-ray diffraction (XRD), and neutron scattering spectroscopy have been used to measure hydrogen bonding.⁷⁵ FTIR, historically the most important spectroscopic method, is

sensitive to the presence of hydrogen bonds which cause measurable changes in vibrational modes. Most of the work in this area has focused on measuring the variation in the stretching frequency of the bonds adjacent to hydrogen bonds, e.g. N-H and C=O in the case of the N-H---O=C pair. As functional groups (e.g. NH, OH, C=O) are involved in hydrogen bonding, their characteristic bands will shift to lower frequencies. There has been a great deal of literature trying to correlate this frequency shift ($\Delta\nu$) with hydrogen bond enthalpy (ΔH).⁸⁶⁻⁸⁸ However, the use of $\Delta\nu$ to predict the strength of hydrogen bonding, as represented by ΔH , is limited due to the lack of a general relationship between them for different hydrogen bonding pairs. Nonetheless, from a comparison of the absorbance of the free and the hydrogen bonded peak, an estimate of the percent of functional groups involved in hydrogen bonding can be approximated^{78, 80}

$$F_{b,NH} = \frac{1}{1 + 3.46 \frac{A_{f,NH}}{A_{b,NH}}} \quad (3)$$

$$F_{b,C=O} = \frac{1}{1 + 1.2 \frac{A_{f,C=O}}{A_{b,C=O}}} \quad (4)$$

where $A_{f,NH}$, $A_{f,C=O}$, $A_{b,NH}$, and $A_{b,C=O}$ are the absorbance of free and hydrogen bonded NH and carbonyl groups, respectively.

X-ray diffraction has been proved useful in investigating hydrogen bonded systems.⁸⁹ Hydrogen bonding is assumed to exist, if the sum of van der Waals radii of

donor A and acceptor B is greater than the measured distance between A and B, $R(A\cdots B)$.

The distance values, $R(A\cdots B)$ and also $H\cdots B$, are reported as measures of relative hydrogen bond strength, although the latter value may not be that accurate due to difficulty in locating a hydrogen atom. The shorter the distance the stronger the hydrogen bond. Neutron diffraction⁹⁰ complements X-ray diffraction, since this method can accurately determine hydrogen bonds lengths.

The NMR chemical shift is very sensitive to environment changes of the protons involved in hydrogen bonds, making this technique very useful in characterizing these systems.⁹¹ Generally, dissolution of hydrogen bonds by diluting or heating, will move proton resonance shifts to lower ppm values and vice versa. It is believed the shifts in proton resonance signal are determined by two factors: (1) anisotropic magnetic currents in acceptor B, and (2) polarization of the AH bond by B.⁹² Usually (2) is more important than (1), because B provides a strong electric field near A-H which deforms the proton electron distribution, leading to a decrease in density and increase in asymmetry of the proton electron density. This effect decreases the shielding of the proton, thus resulting in a downfield shift upon hydrogen bond forming. However, if the acceptor is an aromatic molecule, (1) dominates (2), because the induced ring current generates a secondary magnetic field, that causes an upfield shift in proton resonance. Unlike FTIR, the observed peak is a weighted average of associated and unassociated protons due to the

much slower time scale of NMR spectroscopy as compared to the exchange rate of hydrogen-bonded systems.

Summary

The photopolymerization of thiol-ene and the properties of the resultant polymer networks, e.g. uniform network density and late gel point, have been discussed. The shelf-life stability of conventional thiol-ene systems composed of primary thiols are of concern, and this issue addressed by using secondary thiol monomers. From a practical point of view, there is a need to determine the structure-property relationships of different thiol (primary and secondary)-ene (allyl ether, vinyl ether and acrylate) polymers. Hybrid photopolymerization systems, used to circumvent the limitations of a single system, is an area that has attracted extensive attention. It would be advantageous to generate networks formed through consecutive free-radical and cationic photopolymerizations. Another way to modify thiol-ene networks is to incorporate rigid monomer structures as well as urethane/thiourethane groups able to form hydrogen bonds. The preparation and basic properties of polythiourethanes were reviewed to provide critical insight for the work described later in this document. Finally, the effect of hydrogen bonding on the morphology and properties of polyurethanes as well as the methods used to investigate hydrogen bonding were described.

References

1. Fouassier, J.-P., *Photoinitiation, Photopolymerization and Photocuring*. Hanser: New York, 1993.
2. Dufour, P.; Knight, R. E.; Pincus, A.; Skelhorne, G. G.; Tanihata, T., In *Chemistry & Technology of UV & EB Formulations for Coatings, Inks & Paints*, P. K. T. Oldring, Ed. SITA Publishers: London, 1992; Vol. 1.
3. Tripp, E. P.; Weisman, J. *Modern Paint and Coatings* **1982**, 51.
4. Pasternack, G. *Radiation Curing* **1980**, 8, 14.
5. Kloosterboer, J. G. *Advances in Polymer Science* **1988**, 84, 1.
6. Kloosterboer, J. G.; Van de Hei, G. M.; Boots, H. M. *Journal of Polymer Communication* **1984**, 25, (12), 354.
7. Roffey, C. G., *Photogeneration of Reactive Species for UV Curing*. John Wiley and Sons: New York, 1997.
8. Hoyle, C. E.; Lee, T. Y.; Roper, T. *Journal of Polymer Science Part A: Polymer Chemistry* **2004**, 42, 5301.
9. Jacobine, A. F.; Glaser, D. M.; Grabek, P. J.; Mancini, D.; Masterson, M.; Nakos, S. T.; Rakas, M. A.; Woods, J. G. *Journal of Applied Polymer Science* **1992**, 45, 471.
10. Gush, D. P.; Ketley, A. D. *Modern Paint and Coatings* **1978**, November, 58.
11. Cramer, N. B.; Bowman, C. N. *Polymer Preprint* **2003**, 36, 7964.

12. Senyurt, A. F.; Wei, H.; Phillips, B.; Cole, M.; Nazarenko, S.; E., H. C.; Piland, S. G.; Gould, T. E. *Macromolecules* **2006**, , 39, (19), 6315.
13. Cramer, N. B.; Bowman, C. N. *Polymer Preprint* **2003**, 44, (1), 17.
14. Wei, H.; Li, Q.; Ojelade, M.; Madbouly, S.; Otaigbe, J. U.; Hoyle, C. E. *Macromolecules* **2007**, 40, 8788.
15. Klemm, E.; Sensfuss, S.; Holfter, U.; Flammersheim, H. J. *Angewandte Makromolekulare Chemie* **1993**, 212, 121.
16. Kuhne, G.; Diesen, J. S.; Klemm, E. *Angewandte Makromolekulare Chemie* **1996**, 242, 139.
17. Rehnberg, N.; Annby, U.; Sjorgreen, C. A.; Davidson, R. S. PCT Patent Application, WO2001044377, 2001.
18. Ikeda, H.; Miyata, H.; Murofushi, K. PCT International Application, WO2008023603, 2008.
19. Kamata, H.; Onishi, M. Japan Kokai Tokkyo Koho, JP 2006151958, 2006.
20. Katoh, T.; Kamata, H.; Onishi, M. PCT Patent Application, WO03072614, 2003.
21. Miyata, H.; Ikeda, H.; Murofushi, K.; Hattori, Y.; Urakawa, K. PCT International Application, WO2007145241, 2007.
22. Murofushi, K.; Hattori, Y. Japan Kokai Tokkyo Koho, JP 2008013690, 2008.
23. Hisama, S.; Ichinohe, D. Japan Kokai Tokkyo Koho, JP2008077067, 2008.

24. Irie, K.; Ito, H.; Taguchi, T.; Kato, T.; Murofushi, K. Japan Kokai Tokkyo Koho, JP2003252918, 2003.
25. Okamoto, M.; Waki, S.; Mase, H. Japan Kokai Tokkyo Koho, JP2008095035, 2008.
26. Suzuki, T. Japan Kokai Tokkyo Koho, JP2008065040, 2008.
27. Takebe, K. Faming Zhuanli Shenqing Gongkai Shuomingshu, CN101121825, 2008.
28. Yamauchi, T.; Ito, H.; Morishita, S.; Tani, H. Japan Kokai Tokkyo Koho, JP2004325735, 2004.
29. Ficek, B. A.; Magwood, L.; Coretsopoulos, C.; Scranton, A. B., In *Photochemistry and UV Curing: New Trends*, Fouassier, J. P., Ed. Research Signpost: India, 2006; Vol. 25, p 294.
30. Decker, C. *Polymer International* **2002**, 52, 1141.
31. Decker, C.; Nguyen, T. V. T.; Deck, D.; Weber-Koehl, E. *polymer* **2001**, 42, 5531.
32. Decker, C. *Acta Polymer* **1994**, 45, 333.
33. Dean, K.; Cook, W. D. *Macromolecules* **2002**, 35, 7942.
34. Mecerreyes, J. A.; Pomposo, J. A.; Bengoetxea, M.; Grande, H. *Macromolecules* **2000**, 33, 5846.
35. Dean, K.; Cook, W. D.; Zipper, M. D.; Burchill, P. *Polymer* **2001**, 42, 1345.

36. Lin, Y.; Stansbury, J. *Polymer* **2003**, 44, 4781.
37. Itoh, H.; Kameyama, A.; Nihikubo, T. *Journal of Polymer Science: Part A: Polymer Chemistry* **1996**, 34, 217.
38. Chen, Z. G.; Webster, D. C. *Polymer* **2006**, 47, 3715.
39. Crivello, J. V.; Dietliker, K., In *Chemistry & Technology of UV & EB Formulation for Coatings, Inks & Paints*, Bradley, G., Ed. John Wiley & Sons: New York, 1998; Vol. III, p 326.
40. Cai, Y.; Jessop, J. L. P. *Polymer* **2006**, 47, 6560.
41. Rodriguez-Parada, J. M.; Percec, V. J. *Journal of Polymer Science: Part A: Polymer Chemistry* **1986**, 24, 1363.
42. Pappas, S. P.; Tilley, M. G.; Pappas, B. C. *Journal of Photochemistry and Photobiology, A: Chemistry* **2003**, 159, 161.
43. Jethmalani, J.; W., D. A.; Abdel-Sadek, G.; Chomyn, J.; M., L. J.; Qaddoura, M. U.S. Patent Application Publication 20060052547, 2006.
44. Smith, R. A.; Herold, R. D.; Okoroafor, M. O. PCT International Application. WO0064964, 2000.
45. Lu, H.; Carioscia, J. A.; Stansbury, J. W.; Bowman, C. N. *Dental Materials* **2005**, 21, 1129.
46. Reddy, S. K.; Cramer, N. B.; Bowman, C. N. *Macromolecules* 39, (10), 3681.

47. Wei, H., Y.; Senyurt, A. F.; Jonsson, S.; Hoyle, C. E. *Journal of Polymer Science: Part A: Polymer Chemistry* **2007**, 45, (5), 822.
48. Hutchinson, J. M. *Progress in Polymer Science* **1995**, 20, 703-760.
49. Cowie, J. M. G.; Ferguson, R. *Macromolecules* **1989**, 22, 2307.
50. McGonigle, E.-A.; Cowie, J. M. G.; Arrighi, V. *Journal of Materials Science* **2005**, 40, 1869.
51. Priestley, R. D.; Rittigstein, P.; Broadbelt, L. J.; Fukao, K.; Torkelson, J. M. *Journal of Physics: Condensed Matter* **2007**, 19, 205120.
52. Yoshida, H.; Kanbara, H.; Takemura, N.; Kobayashi, Y. *Sen'i Gakkaishi* **1983**, 39, (12), T512.
53. Yoshida, H.; Nakamura, K.; Kobayashi, Y. *Polymer Journal* **1982**, 14, (11), 855.
54. Bayer, O. *Angew Chem* **1947**, A59, 257.
55. Chattopadhyay, D. K.; Raju, K. V. S. N. *Progress in Polymer Science* **2007**, 32, 352.
56. Pztrov, Z. S.; Ferguson, J. *Progress in Polymer Science* **1991**, 16, 695.
57. Dyer, E.; Osborne, D. W. *Journal of Polymer Science* **1960**, 47, 361.
58. Dyer, E.; Glenn, J. F.; Lendrat, E. G. *Journal of Organic Chemistry* **1961**, 26, 2919.
59. Klemm, E.; Stockl, C. *Makromolekulare Chemie* **1991**, 192, 153.

60. Dyer, E.; Glenn, J. F. *Journal of American Chemical Society* **1957**, 79, 366.
61. Frisch, K. C.; Ruma, L. P. *Journal of Macromolecular Science: Review* **1970**, C5, 103.
62. Hastings, G. W.; Johnston, D. *British Polymer Journal* **1971**, 3, (2), 83.
63. Dietliker, K.; Misteli, K.; Jung, T.; Studer, K. In RadTech Europe 05: UV/EB--
Join the Winning Technology (Conference Proceedings), Barcelona, Spain, Oct. 18-20,
2005; Barcelona, Spain, 2005; p 473.
64. Shinohara, N.; et al. PCT Int. Appl. WO 2004078855, 2004.
65. Tanaka, M.; et al. U.S. Patent Application 20050131203, 2005.
66. Freed, V. H.; et al. *Journal of Agriculture and Food Chemistry* **1967**, 15, (6), 1121.
67. Nagai, A.; Ochiiai, B.; Endo, T. *Journal of Polymer Science: Part A: Polymer
Chemistry*, **2005**, 43, 1554.
68. Bunn, C. W. *Journal of Polymer Science* **1955**, 16, 323.
69. Hill, R.; Walker, E. E. *Journal of Polymer Science* **1948**, 3, 609.
70. Marvel, C. S.; Kitch, A. *Journal of American Chemical Society* **1951**, 73, 1100.
71. Dyer, E.; Bartels Jr., G. W. *Journal of American Chemical Society* **1954**, 76, 591.
72. Christenson, C. P.; Harthcock, M. A.; Meadows, M. D.; Spell, H. L.; Howard, W.
L.; Creswick, M. W.; et al. *Journal of Polymer Science: Part B: Polymer Physics* **1986**, 24,
1404.

73. Mishra, A. K.; Chattopadhyay, D. K.; B., S.; Raju, K. V. S. N. *Progress in Organic Coatings* **2006**, 55, 231.
74. Jeffrey, G. A., *An Introduction to Hydrogen Bonding*. Oxford Univeristy Press: New York-Oxford 1997.
75. Joesten, M. D.; Schaad, L. J., *Hydrogen Bonding*. Marcel Dekker, Inc: New York, 1974.
76. Coleman, M. M.; Lee, K. H.; Skrovanek, D. J.; Painter, P. C. *Macromolecules* **1986**, 19, 2149-2157.
77. Lee, H. S.; Wang, Y. K.; Hsu, S. L. *Macromolecules* **1987**, 20, 2089.
78. Seymour, R. W.; Estes, G. M.; Cooper, S. L. *Macromolecules* **1970**, 3, 579.
79. Wang, C. B.; Cooper, S. L. *Macromolecules* **1983**, 16, 775.
80. Xiu, Y.; Zhang, Z.; Wang, D.; Ying, S.; Li, J. *Polymer* **1992**, 33, 1335.
81. Yen, F.-S.; Hong, J.-L. *Macromolecules* **1997**, 30, 7927.
82. Blewett, G.; Bredenkamp, M. W.; Koch, K. R. *Acta Crystallographica Section C* **2005**, C61, o469.
83. Wheeler, K. A.; Harrington, B.; Zapp, M.; Casey, E. *CrystEngComm* **2003**, 5, (59), 337.
84. Benson, R. E.; Broker, G. A.; Daniels, L. M.; Tiekink, E. R. T.; Wardell, J. L.; Young, D. J. *Acta Crystallographica Section E* **2006**, E62, o4106.

85. Tadbuppa, P. P.; Tiekinkb, E. R. T. *Acta Crystallographica Section E* **2007**, E63, o1779.
86. Badger, R. M.; Bauer, S. H. *Journal of Chemical Physics* **1937**, 5, 839.
87. Arnett, E. M.; Joris, L.; Mitchell, E.; Murty, T. S. S. R.; Gorrie, T. M.; Schleyer, P. v. R. *Journal of American Chemical Society* **1970**, 92, 2365.
88. Drago, R. S.; Epley, T. D. *Journal of American Chemical Society* **1969**, 91, 2883.
89. Speakman, J. C. *Structure and Bonding* **1972**, 12, 141.
90. Macdonald, A. L.; Speakman, J. C.; Hadzi, D. *Journal of Chemical Society: Perkin Transaction 2* **1971**, 68, 825.
91. Arnold, J. T.; Packard, M. E. *Physics Review* **1951**, 83, 210.
92. Pople, J. A.; Schneider, W. G.; Bernstein, H. J., *High-Resolution Nuclear Magnetic Resonance*. McGraw-Hill: New York, 1959; p 400.

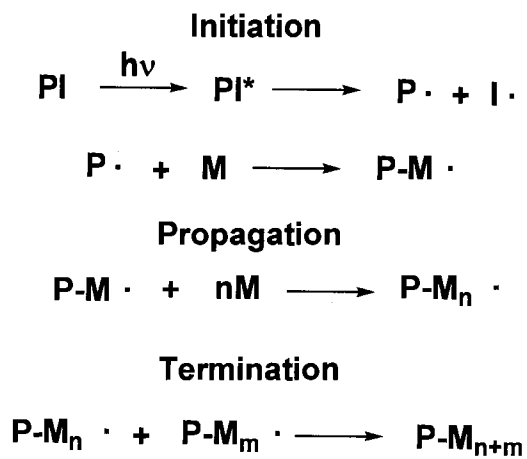


Figure 1.1. Conventional free-radical chain growth polymerization mechanism.

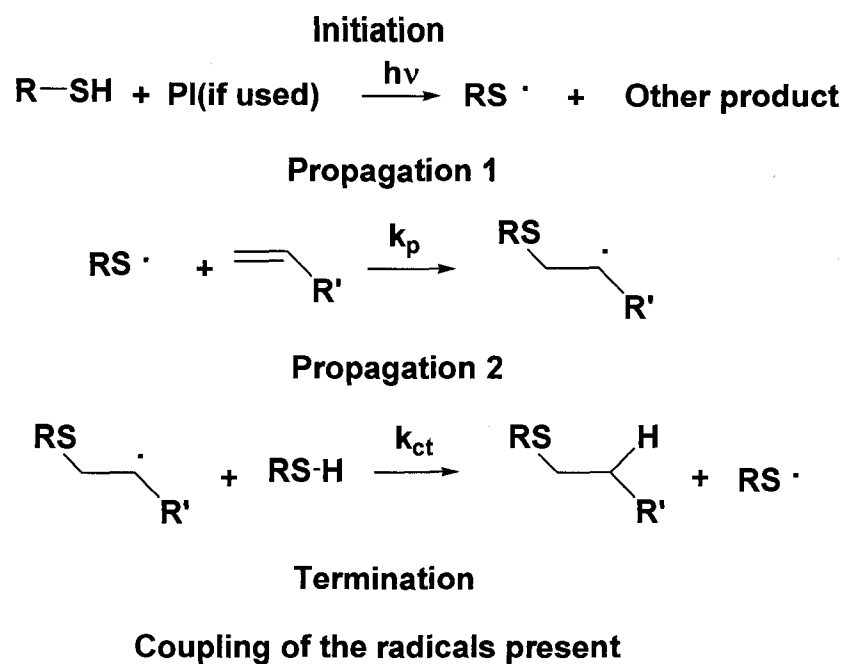


Figure 1.2. The free-radical step growth mechanism of thiol-ene photopolymerization.

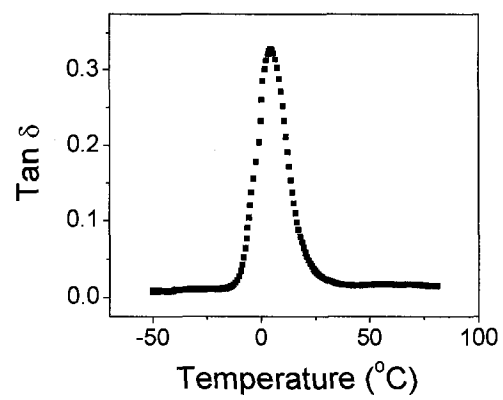


Figure 1.3. The tan δ vs. temperature plot of TriThiol-TriVinyl networks.

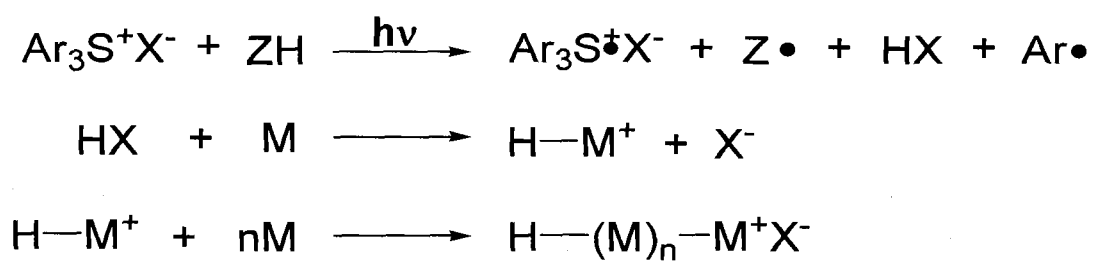


Figure 1.4. Mechanism of cationic photopolymerization.

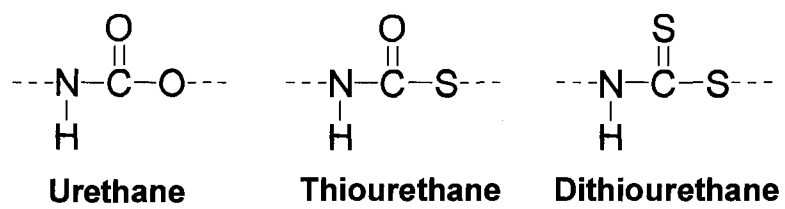


Figure 1.5. Structures of urethane, thiourethane and dithiourethane.

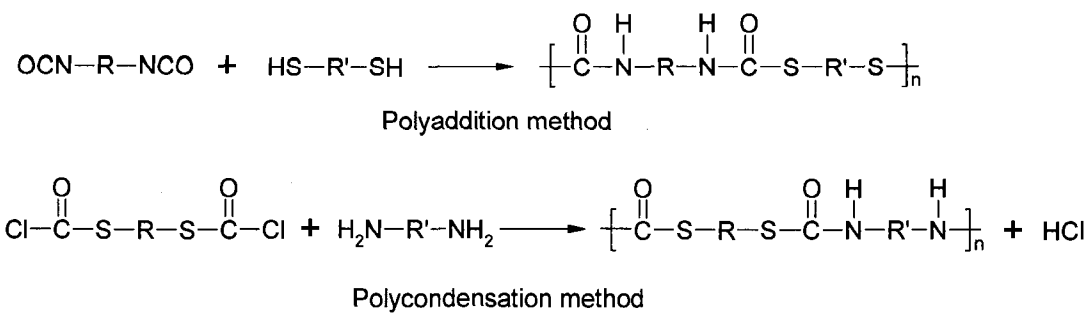


Figure 1.6. Methods to synthesis linear polythiourethane.

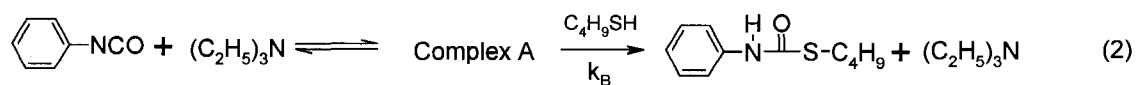
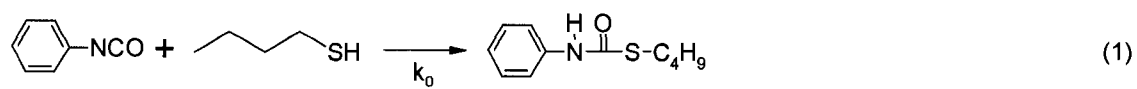


Figure 1.7. Suggested mechanism of amine catalyzed thiol-isocyanate reaction.

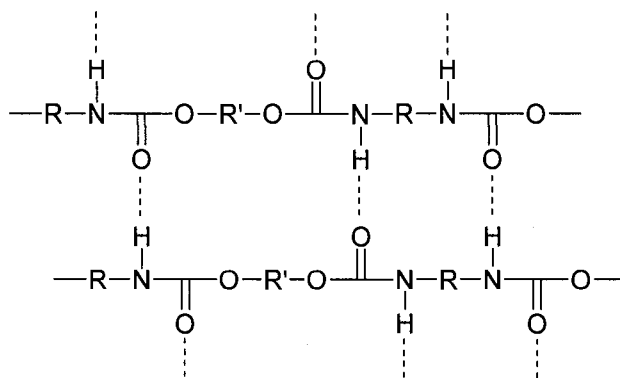


Figure 1.8. Physically crosslinked networks formed through hydrogen bonding between urethane linkages.

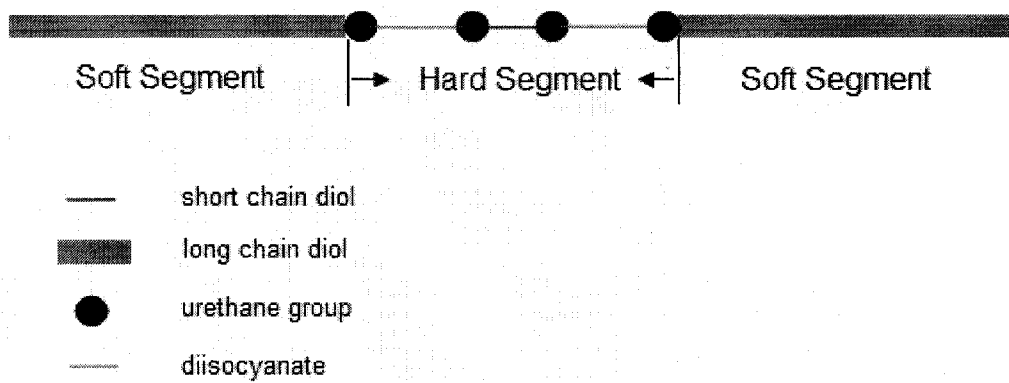


Figure 1.9. Schematic representation of polyurethane segments.

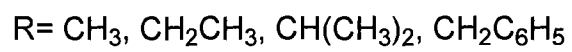
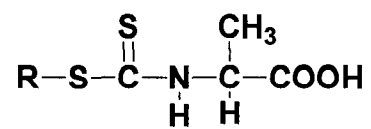


Figure 1.10. Structures of dithiocarbamates.

CHAPTER II

OBJECTIVES

As stated in the introduction it is important and necessary to improve the properties of photopolymerized thiol-ene networks through several different ways including monomer selection, mechanism selection (combining free-radical and cationic photo polymerization) and the incorporation of rigid units, e.g. thiourethanes, into the structure. Since hydrogen bonding in thiourethanes is not well characterized, it is also deemed essential to conduct a comprehensive investigation on the structure-property relationships of thiourethanes. Specifically, the goal of this work is to:

1. Establish the relationship between ene and thiol structure and the physical and mechanical properties of photocured thiol-ene networks.
2. Prepare dual cure thiol-ene free-radical/vinyl ether cationic hybrid systems and probe the effect of monomer ratio on the photopolymerization kinetics and thiol-ene network properties.
3. Enhance the glass transition temperature of thiol-ene networks by incorporating thiourethane linkages, and characterize the basic physical and mechanical properties of the resultant thiourethane thiol-ene networks.
4. Examine the effect of hydrogen bonding on physical aging of the thiourethane thiol-ene networks.
5. Investigate the hydrogen bonding behavior of thiourethanes and dithiourethanes and compare the results with urethanes; correlate the structures of thiourethane and dithiourethanes with their physical, optical, thermal and mechanical

properties.

The first objective (Chapter III) will establish the effect of ene and thiol structure on photopolymerization kinetics and network properties, providing a basic understanding of structure-property relationships of thiol-ene networks. The effect of four different enes and both conventional primary and novel secondary thiols will be examined.

The second objective (Chapter IV) will establish the method for preparing a dual cure photopolymerization system that contains a free-radically polymerizable thiol-ene and cationically polymerizable vinyl ether. The molar ratio of thiol/vinyl ether will be related to the polymerization kinetics and physical and mechanical properties of resultant hybrid polymers, such as glass transition temperature and tensile strength.

The third objective (Chapter V) will provide a novel way to prepare thiol-ene networks with enhanced glass transition temperatures and very uniform network structures for applications at elevated temperatures. DSC and DMA will be used to measure the increase in glass transition temperature by introducing thiourethane linkages. Physical and mechanical properties of the resultant thiol-ene films will be characterized to provide an understanding of the structure-property relationship of the novel thiourethane thiol-ene networks.

The fourth objective (Chapter VI) will help to probe the effect of hydrogen bonding on the physical aging of dense thiourethane thiol-ene networks, represented by entropy recovery in DSC scans and changes in macro-scale properties. The enthalpy relaxation rate of different systems will be measured and compared to draw a basic conclusion.

Finally, the fifth objective (Chapter VII and Chapter VIII) will address the need to conduct a comprehensive comparison and characterization of a homologous family of urethane, thiourethane and dithiourethane structures. The hydrogen bonding behavior of a series of small molecule and polymeric urethane, thiourethane and dithiourethane compounds will be probed and related to their physical and mechanical properties, providing a basic understanding of the sulfur containing urethane type materials. The results will benefit the future development of polythiourethanes and polydithiourethanes widely used in many modern applications.

CHAPTER III

THE EFFECT OF THIOL AND ENE STRUCTURES ON THIOL-ENE NETWORKS: PHOTOPOLYMERIZATION, PHYSICAL, MECHANICAL AND OPTICAL PROPERTIES

Abstract

The photopolymerization of four different types of ene monomers with both primary and secondary multifunctional thiols has been evaluated. To understand the effect of ene monomer structures on polymer properties, a comprehensive investigation of the basic physical, mechanical and optical properties was conducted for the secondary and primary thiol-ene networks. The results indicate that ene structures can significantly affect the rigidity and the physical and mechanical properties of the thiol-ene networks. Network density controlled by the functionality of ene monomers was found also to be a major factor in defining network properties. Networks formed from the secondary thiol-ene systems are basically equivalent to those made from primary thiol-enes with respect to physical, mechanical and optical properties. The secondary thiol monomer samples evaluated were found to have exceptional storage stability and relatively low odor.

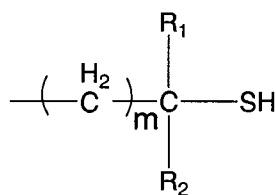
Introduction

The photopolymerization of compounds having ethylenically unsaturated bond, such as acrylates and methacrylates, often suffers from problems such as oxygen

inhibition and insufficient curing.^{1,2} The first issue is generally addressed by purging with inert gases or covering with an oxygen barrier membrane. One alternative is to expose a mixture of multifunctional thiols and multifunctional enes to light, leading to the formation of highly cross-linked networks with uniform structure in the presence of oxygen.¹⁻⁴ The photocured thiol-ene networks exhibit narrow glass transition regions and excellent mechanical and thermal properties. One of the attractive features of thiol-ene photopolymerization is that many types of enes and thiols can be incorporated into thiol-ene networks. The reactivity of three basic types of thiols, mercaptopropionate, thioglycolate and alkyl thiol, with various types of enes, such as norbornene, vinyl ether, allyl ether, allyl triazine, allyl isocyanurate, alkene, acrylate, methacrylate and styrene, have been reported in the literature.^{1,3,5,6} There have been sporadic reports dealing with the kinetics of photocured thiol-ene networks and selected physical properties. However there has not been a detailed evaluation of basic mechanical and thermal properties of thiol-ene systems as a function of ene structure.

Almost all of the thiols used in thiol-ene photopolymerization studies to date have been primary. Coincidentally, the shelf-life stability of these thiol-ene systems has been the subject of considerable concern. Possible reasons for the limited shelf-life of thiol-enes have been extensively studied and recently reviewed by Hoyle et al.^{1,7-9} In order to extend the shelf-life of thiol-ene mixture, numerous types of stabilizers, including sulfur, triallyl phosphates and the aluminum salt of N-nitrosophenylhydroxylamine have been used to prevent the ambient thermal

free-radical polymerization.¹⁰⁻¹⁴ Recently there have been reports of photocurable thiol-enes based on a series of hindered multifunctional or secondary thiols, as depicted by the following structure



where R_1 is an alkyl group, such as a methyl or a phenyl group and R_2 is either a H or an alkyl group.^{2, 15-18} A commercialized secondary thiol, pentaerythritol tetrakis(3-mercaptopbutylate) (s-4T), has been recently reported for use in numerous applications.^{15, 17, 19-24} For example, Okamoto et al. added s-4T into a (meth)acrylate photocuring formulation to prepare antistatic hard coating films with excellent transparency.¹⁹ Spacers, color filters and light sensitive coatings for liquid crystal displays were also prepared from formulations containing secondary thiols and reported to exhibit excellent storage stability and photosensitivity.²⁰⁻²³ Secondary thiols have also been produced as photocuring accelerators and for the preparation of thermally stable thiourethane containing photoinitiators.^{16, 17} Since thiol-ene resins composed of commercial secondary thiols have been reported to exhibit exceptional shelf-life stability,^{15, 17-23} it is important to evaluate the properties of networks prepared from systems incorporating a commercial secondary thiol. To the best of our knowledge, there is almost no any information about the properties of thiol-ene networks based on a commercial secondary thiol, let alone the structure-property relationships of these

materials.

Since it is important to understand physical properties of photocured thiol-ene networks in order to develop applications that combine a variety of essential properties, we decided to provide a comprehensive investigation of a series of thiol-ene networks based on four different enes and both primary and secondary thiols. The photopolymerization of these enes with both primary and secondary thiols and the physical, mechanical and optical properties of the resultant thiol-ene films have been thoroughly characterized and analyzed and basic structure-property relationships established.

Experimental

Materials

Pentaerythritol tetrakis(3-mercaptopbutylate) (s-4T) was obtained from Showa Denko K. K. and used as received. Pentaerythritol triallyl ether (APE) was obtained from Perstorp and used as received. Polyethylene Glycol (400) Diacrylate (PEGDA) was obtained from Sartomer Company and used as received. The photoinitiator, 2,2-dimethoxy-2-phenylacetophenone (DMPA) was obtained from Ciba Specialty Chemical Company and used as received. Pentaerythritol tetrakis(3-mercaptopropionate) (4T), triallyl-1,3,5-triazine-2,4,6(1H,3H,5H)-trione (TTT) and tri(ethylene glycol) divinyl ether (TEGDVE) were purchased from Aldrich Chemical Company and used as received.

Preparation

To prepare a thiol-ene coating film, 5.0 mmol of s-4T/4T, an equal molar double bond concentration of ene monomer (APE, TEGDVE, TTT) or a thiol/ene molar ratio of 20:80 (PEGDA), and 1 wt% of DMPA were charged into a clean 25 mL glass vial and mixed with the aid of sonication (the structures of all monomers are shown in Chart 3.1). The glass vial was completely wrapped with a layer of aluminum foil to prevent any prepolymerization. Once the photoinitiator was dissolved and the formulation homogeneously mixed, the mixture was evenly spread onto steel plates (for impact and mandrel bend tests) or glass (for all other tests) using a 5 mil (125 μm) draw down bar. Cured thiol-ene networks were obtained by exposing the coated glass or steel plates 10 times to the output of a Fusion high-intensity lamp system with conveyer belt (D bulb, 400 W/in. input, line speed of 10 feet/min, 3.0 W/cm²) as described elsewhere.²⁵ The thickness of cured thiol-ene films are approximately 100 \pm 20 μm . To prepare samples for shelf-life measurement, the formulations in the glass vials described above were wrapped with aluminum foil and stored in an ambient environment. It should be noted that the s-4T/4T-PEGDA samples used for shelf-life and real-time FTIR were equal molar mixtures of thiol and double bond.

Characterization

A modified Bruker IFS 99 FTIR spectrometer with a horizontal sample stage was used to monitor the photopolymerization of thiol and ene monomers and obtain real-time IR (RTIR) spectra.^{26, 27} UV light generated from an Oriel lamp system equipped with a

high pressure mercury-xenon lamp (200 W) was channel into the sample chamber through an optical fiber. The polymerization of thin layers of the above sample (~25 μm) sandwiched between two sodium chloride plates was initiated by continuous UV light irradiation within the sample chamber. The whole process was monitored by the FTIR spectrometer operating at 5 scans/s. The thermal properties of the prepared thiol-ene films were measured by a differential scanning calorimeter (DSC), TA Q1000 (TA Instruments), operating at a heating rate of 10 $^{\circ}\text{C}/\text{min}$. The second heating scan curves were used to determine the glass transition temperatures (T_g) by TA Universal Analysis software. The thermomechanical properties were measured with a TA Q800 DMA (TA Instruments) operating at 1 Hz and a heating rate of 3 $^{\circ}\text{C}/\text{min}$ (tensile mode). The peak maximum of the $\tan \delta$ plot was taken as the glass transition temperature. The thermal stability of each thiol-ene network was measured with a TA Q50 (TA Instruments, Inc.) thermal gravimetric analysis (TGA) instrument operating at a heating rate of 10 $^{\circ}\text{C}/\text{min}$. Refractive index values were measured by a Bausch&Lomb ABBE-3L refractometer at 24 $^{\circ}\text{C}$. 1-Bromonaphthalene was applied between the sample film and the prism shield. The Persoz pendulum hardness values (average of six tests) were measured following ASTM D-4366 using a BYK-Gardner pendulum hardness tester with a square frame pendulum. The direct and reverse impact resistance, the mandrel bend tests and pencil hardness tests were conducted according to ASTM D-2794, ASTM D 522-93a and ASTM D-3363, respectively.

Results and Discussion

Shelf-life and Polymerization Kinetics

As has already been reported,^{15, 17-23} resins prepared from secondary thiols exhibit excellent shelf-life stability. For reference, the shelf-life of all formulations were measured and the results are listed in Table 3.1. None of the secondary thiol-ene formulations gelled after 20 days storage at room temperature, although the viscosity of the TTT and PEGDA based samples did increase, indicating the excellent thermal stability of these formulations. The primary thiol-enes evaluated are much less stable since all formulations gelled during the 20 day storage period. Particularly interesting, the mixture of 4T and TEGDVE, the very reactive vinyl ether monomer, gelled within 12 h while the s-4T-TEGDVE mixture had a low viscosity even after 20 days.

The polymerization kinetics of each of the thiol mixed with four different types of ene monomers was next measured by real-time FTIR at room temperature. For all four types of ene monomers, as shown in Figure 3.1 the photopolymerizability of the secondary thiol, s-4T, is reduced appreciably compared to the primary thiol monomer, 4T for the light intensity used. In reactions with APE and TEGDVE, both primary and secondary thiols show very fast polymerization rates. High conversions are attained since the glass transitions of the networks formed are well below room temperature (shown in next section). In cases of the s-4T and 4T with TTT, high polymerization rates were also achieved, but with lower conversions than for the systems with APE and TEGDVE under the experimental conditions (low light intensity (0.625 mW/cm^2)). As the three

dimensional s-4T-TTT and 4T-TTT networks are formed, the glass transition temperature of the networks increases to greater than room temperature ($T_g=45\text{ }^\circ\text{C}$) hindering the further conversion of functional groups, i.e., diffusion limitation sets in under the present irradiation conditions of low light intensity at room temperature. Figure 3.1 shows that 1:1 molar functional group mixtures of 4T and s-4T with PEGDA are characterized by incomplete thiol functional group conversions. The conversion of thiol groups in PEGDA was greatly suppressed because of the high homopolymerization propensity of acrylate groups as indicated in Figure 3.2. The acrylate monomer achieved complete double bond conversions within 50 s. Herein we note that, in order to achieve high monomer conversion and eliminate the effect of unreacted monomers on polymer properties, a sample with only 20 mol% of thiol and 80 mol% of PEGDA was used to generate fully cured films for mechanical and physical testing. Also, in subsequent preparation of photocured films for physical property evaluation, complete conversions of all of the thiol-ene films was ensured by the experimental conditions used, 10 passes under the high-intensity Fusion lamp system (3.0 W/cm^2) at a belt speed of 10 fpm.

Physical, Mechanical and Optical Properties

From a practical point of view, it is important to characterize any effect of the thiol and ene structures on the physical properties of the photocured thiol-ene networks. The glass transition temperatures of the thiol-ene networks prepared from s-4T shown in Figure 3.3 and Table 3.2 were marginally higher than the networks prepared from primary thiol. These differences, which are quite small, could be due to hindered rotation

of thiol-ether linkages (-S-) afforded by the additional α -methyl group of s-4T or differences in purity of the 4T and s-4T samples. It is of interest to note that the 4T-TTT and s-4T-TTT networks have the same glass transition temperature, perhaps due to the more rigid structure of the triallyl triazine (TTT) monomer contributing to the rigidity of the networks. The rigid TTT also provides the highest T_g among the systems measured. Thiol-ene films based on the softer APE structures have much lower T_g s than the TTT based ones. The effect of lower network density and more flexible chemical structure on glass transition is exhibited by the very low T_g s of TEGDVE and PEGDA based systems. The DMA results are consistent with the DSC T_g s as shown in Table 3.3.

An interesting phenomenon is that, for networks based on TEGDVE and PEGDA which have more flexible structures and lower network densities, there is a greater change in specific heat capacity (ΔC_p) at the glass transition region (Table 3.2) consistent with increased propensity for molecular motion in the rubbery state.

The Persoz pendulum hardness of each thiol-ene network was also measured (Figure 3.4). Any small differences between the primary and secondary thiol-ene networks are inconsequential and may arise from slight structural differences. The TTT based networks exhibit the highest Persoz pendulum hardness at room temperature due to their rigid structures, which are dictated by their glassy structure at room temperature resulting in the high storage modulus at the analysis temperature (23 °C). Less energy is damped by the rigid glassy TTT based networks as attested to by the higher oscillation times (higher Persoz pendulum hardness values). PEGDA and TEGDVE networks have

medium hardness values which are higher than for the APE networks. The low damping times for the trifunctional APE based networks result from their DSC based glass transition region being located near the testing temperature (room temperature). This affords maximum energy damping in the hardness measurements.

The direct and reverse impact resistance values of the thiol-ene films are shown in Figure 3.5. Primary thiol and secondary thiol based networks do not exhibit apparent differences with respect to impact resistance values. TEGDVE based networks, benefiting from their flexible ethylene glycol units, show the highest direct impact resistance. PEGDA networks, with the same type of flexible structures as TEGDVE, do not show the high direct impact resistance values possibly due to inhomogeneities present in acrylate containing films making them too fragile to endure the impact of the tester. However, these films do perform extremely well in the reverse impact resistance tests in which the coated panels are subject to impact from the back (not directly making contact with the coating films).

The elongation and cracking resistance of each thiol-ene coating film was also measured by mandrel bending tests following an ASTM standard procedure. The coating film flexibility is indicated by the elongation values and crack resistance values. The crack lengths are simply taken as the crack resistance values, and therefore the smaller the value the better the performance. As shown in Figure 3.6, the secondary and primary thiol based thiol-ene networks performance was equivalent with respect to flexibility for a given ene. The overall better performance parameters for the TTT based films is a result

of the combination of high crosslink density and the rigid TTT structure. These TTT films exhibit fairly good mechanical properties and are tough. The higher network density also contributes to the good performance of the APE based thiol-ene films in the mandrel bending tests. The PEGDA based films formed from curing the 20/80 thiol-acrylate mixture have very poor mechanical properties and readily tear upon implementation of a light force.

Scratch resistance of network films is determined by many factors including network density and glass transition temperature. In all cases, the surface scratch resistances of the primary and secondary thiol-ene films measured are essentially identical (Figure 3.7). As a result of their high network density, and the fact that they are glasses at room temperature, the TTT based films exhibit higher pencil hardness for both the 4T and s-4T based films. The lowest pencil hardness values are obtained for the TEGDVE and PEGDA films which have low network densities and are rubbery at room temperature where the scratch resistance was measured.

The thermal stability of all of the thiol-ene networks was measured by TGA heating at 10 °C/min; the resulting weight loss curves are shown in Figure 3.8 and the resultant 5% weight loss temperatures ($T_{5\%}$) are listed in Table 3.4. Except for slight differences for the TEGDVE and APE based films at high temperatures, there are not any differentiable variations in thermal stability between primary and secondary based thiol-ene films. It is noted that the higher network densities of the TTT and APE based networks help to stabilize the network structures at elevated temperature.

Finally, the refractive indices of all of the thiol-ene films were measured at ~24 °C.

The relationship of the refractive index to other factors can be expressed by the

Lorentz-Lorenz equation²⁸

$$\frac{n^2 - 1}{n^2 + 2} = \frac{\rho N_{av} \alpha}{3M_0 \epsilon_0} \quad (1)$$

where n is the refractive index, ρ is the density of polymer, α is the average polarizability, ϵ_0 is the vacuum permittivity, N_{av} is the Avogadro constant and M_0 is the molecular weight of polymer. The dense glassy networks prepared from TTT exhibit the highest refractive index at 24 °C (Table 5). The low density and sulfur content of the PEGDA based networks lead to particularly low refractive index values.

Conclusion

The photopolymerization of four different types of enes with primary and secondary thiol was investigated and physical and mechanical properties of the thiol-ene networks measured. All ene monomers showed high reactivity with both thiols, with PEGDA homopolymerizing as well as copolymerizing with the thiol.

Higher ΔC_p values were observed for the more flexible networks based on TEGDVE and PEGDA. The flexibility, surface scratch resistance and thermal stability of films based on the primary and secondary thiols were essentially identical.

The trifunctional APE and TTT based networks with higher network densities, and in the case of TTT with a rigid ring structure, generated films with higher glass transition temperatures, pencil hardness values and refractive indices, and better mandrel

bending performance. The difunctional and flexible TEGDVE and PEGDA based networks had lower T_g s, higher ΔC_p s and better impact resistance. Finally, all of the resin mixtures prepared from the commercial secondary thiol exhibited truly exceptional shelf-life than those prepared from the primary thiols, and the secondary thiol sample evaluated had little or no objectionable odor making it particularly suitable for many applications.

Acknowledgements

This work was supported by the MRSEC Program of the National Science Foundation under Award Number DMR 0213883. We also acknowledge Fusion for UV curing systems. Materials were generously provided by Sartomer Company, Showa Denko K. K. and Ciba Specialty Chemicals.

References

1. Hoyle, C. E.; Lee, T. Y.; Roper, T. *Journal of Polymer Science Part A: Polymer Chemistry* **2004**, 42, 5301.
2. Katoh, T.; Kamata, H.; Onishi, M. PCT Patent Application, WO03072614, 2003.
3. Jacobine, A. F., In *Radiation Curing in Polymer Science and Technology III: Polymerization Mechanisms*, Fouassier, J. D.; Rabek, J. F., Eds. Elsevier: London, 1993; pp 219-268.
4. Gush, D. P.; Ketley, A. D. *Modern Paint and Coatings* **1978**, November, 58.
5. Cramer, N. B.; Bowman, C. N. *Journal of Polymer Science: Part A: Polymer Chemistry* **2001**, 39, 3311.
6. Morgan, C. R.; Magnotta, F.; Ketley, A. D. *Journal of Polymer Science: Chemistry Edition* **1977**, 15, 627.
7. Klemm, E.; Sensfuss, S.; Holfter, U.; Flammersheim, H. J. *Angewandte Makromolekulare Chemie* **1993**, 212, 121.
8. Kuhne, G.; Diesen, J. S.; Klemm, E. *Angewandte Makromolekulare Chemie* **1996**, 242, 139.
9. Rehnberg, N.; Annby, U.; Sjorgreen, C. A.; Davidson, R. S. PCT Patent Application, WO2001044377, 2001.
10. Stahly, E. E. U.S. Patent 3619393, 1971.
11. Guthrie, J. L.; Rendulic, F. J. U. S. Patent 3855093, 1974.
12. Woods, J. G.; Jacobine, A. F. *RadTech NA Technical Conference Proceedings* **1992**,

Vol. I, 173.

13. Dowling, J. P.; Richardson, S. C.; Quigley, K. U. S. Patent 5358976, 1994.
14. Rakas, M. A.; Jacobine, A. F. *Journal of Adhesives* **1992**, 36, 247.
15. Kamata, H.; Onishi, M. Japan Kokai Tokkyo Koho, JP 2006151958, 2006.
16. Ikeda, H.; Miyata, H.; Murofushi, K. PCT International Application, WO2008023603, 2008.
17. Miyata, H.; Ikeda, H.; Murofushi, K.; Hattori, Y.; Urakawa, K. PCT International Application, WO2007145241, 2007.
18. Murofushi, K.; Hattori, Y. Japan Kokai Tokkyo Koho, JP 2008013690, 2008.
19. Okamoto, M.; Waki, S.; Mase, H. Japan Kokai Tokkyo Koho, JP2008095035, 2008.
20. Hisama, S.; Ichinohe, D. Japan Kokai Tokkyo Koho, JP2008077067, 2008.
21. Suzuki, T. Japan Kokai Tokkyo Koho, JP2008065040, 2008.
22. Yamauchi, T.; Ito, H.; Morishita, S.; Tani, H. Japan Kokai Tokkyo Koho, JP2004325735, 2004.
23. Takebe, K. Faming Zhuanli Shenqing Gongkai Shuomingshu, CN101121825, 2008.
24. Irie, K.; Ito, H.; Taguchi, T.; Kato, T.; Murofushi, K. Japan Kokai Tokkyo Koho, JP2003252918, 2003.
25. Li, Q.; Zhou, H.; Douglas A. Wicks; Hoyle, C. E. *Journal of Polymer Science Part A: Polymer Chemistry* **2007**, 45, 5103.
26. Zhou, H.; Li, Q.; Lee, T. Y.; Guymon, C. A.; Johnsson, E. S.; Hoyle, C. E. *Macromolecules* **2006**, 39, 8269.

27. Wei, H.; Li, Q.; Ojelade, M.; Madbouly, S.; Otaigbe, J. U.; Hoyle, C. E.

Macromolecules **2007**, *40*, 8788.

28. Mills, N. J., In *Encyclopedia of Polymer Science and Engineering*, 2nd ed.; Mark, H.

F.; Bikales, N. M.; Overberger, C. G.; Menges, G.; Kroschwitz, J. I., Eds. John Wiley and

Sons: New York, 1987; Vol. 10, pp 493-540.

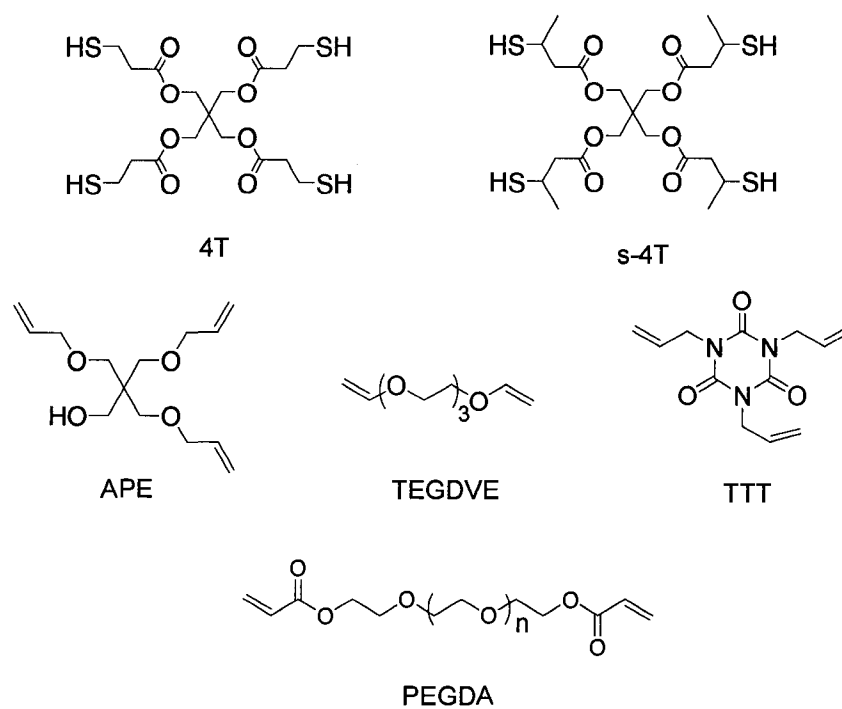


Chart 3.1. Chemical structures of thiols and enes.

Table 3.1. Shelf-life of thiol-ene formulations (1 wt% DMPA) stored in dark and at room temperature.

	APE	TEGDVE	TTT	PEGDA
4T	15 days	12 h	10 days	9 days
s-4T*	Low η	Low η	High η	High η

*Stored for 20 days

Table 3.2. Glass transition temperature and heat capacity change of thiol-ene networks measured by DSC.

	APE		TEGDVE		TTT		PEGDA	
	4T	s-4T	4T	s-4T	4T	s-4T	4T	s-4T
T _g (°C)	3	7	-30	-25	45	45	-30	-26
ΔC_p (J/g/K)	0.41	0.40	0.71	0.61	0.31	0.30	0.53	0.50

Table 3.3. Glass transition temperature of thiol-ene networks measured with DMA.

	APE		TEGDVE		TTT		PEGDA	
	4T	s-4T	4T	s-4T	4T	s-4T	4T	s-4T
Tg (°C)	8	13	-24	-20	63	64	-22	-17
E' at 23 °C (MPa)	15	20	4	7	1568	1658	15	18

Table 3.4. Temperature at 5% weight loss ($T_{5\%}$) and temperature at the maximum degradation rate (T_{max}) of thiol-ene films.

	APE		TEGDVE		TTT		PEGDA	
	4T	s-4T	4T	s-4T	4T	s-4T	4T	s-4T
$T_{5\%}$ (°C)	362	360	328	326	352	350	332	330
T_{max} (°C)	400	390	358	357	388	386	403	400

Table 3.5. Refractive indices of thiol-ene films.

APE		TEGDVE		TTT		PEGDA	
4T	s-4T	4T	s-4T	4T	s-4T	4T	s-4T
1.5350	1.5280	1.5215	1.5155	1.5622	1.5620	1.4906	1.4905

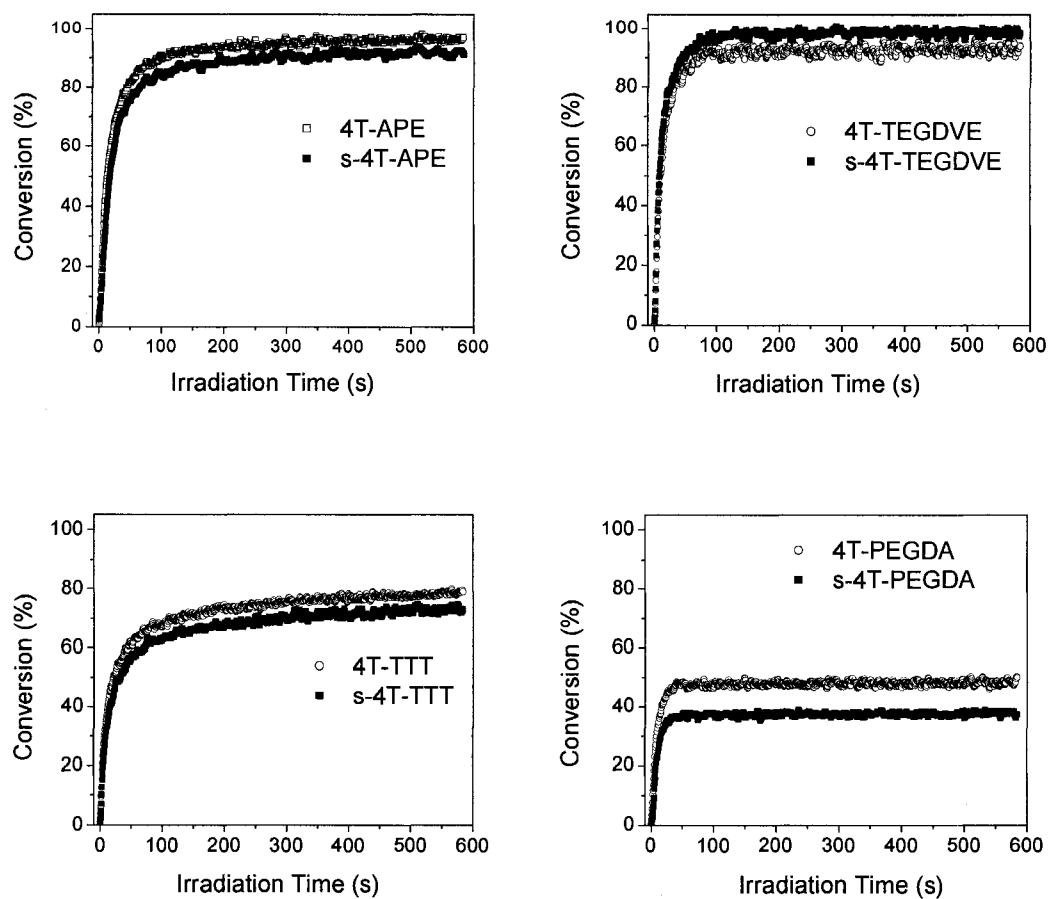


Figure 3.1. Percent conversion of thiol group as a function of irradiation time (SH:C=C = 1:1 mol/mol). Light intensity = 0.625 mW/cm².

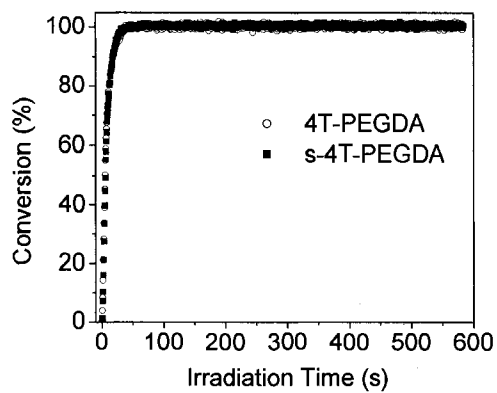


Figure 3.2. Percent conversion of acrylate group as a function of irradiation time (SH:C=C = 1:1 mol/mol). Light intensity = 0.625 mW/cm².

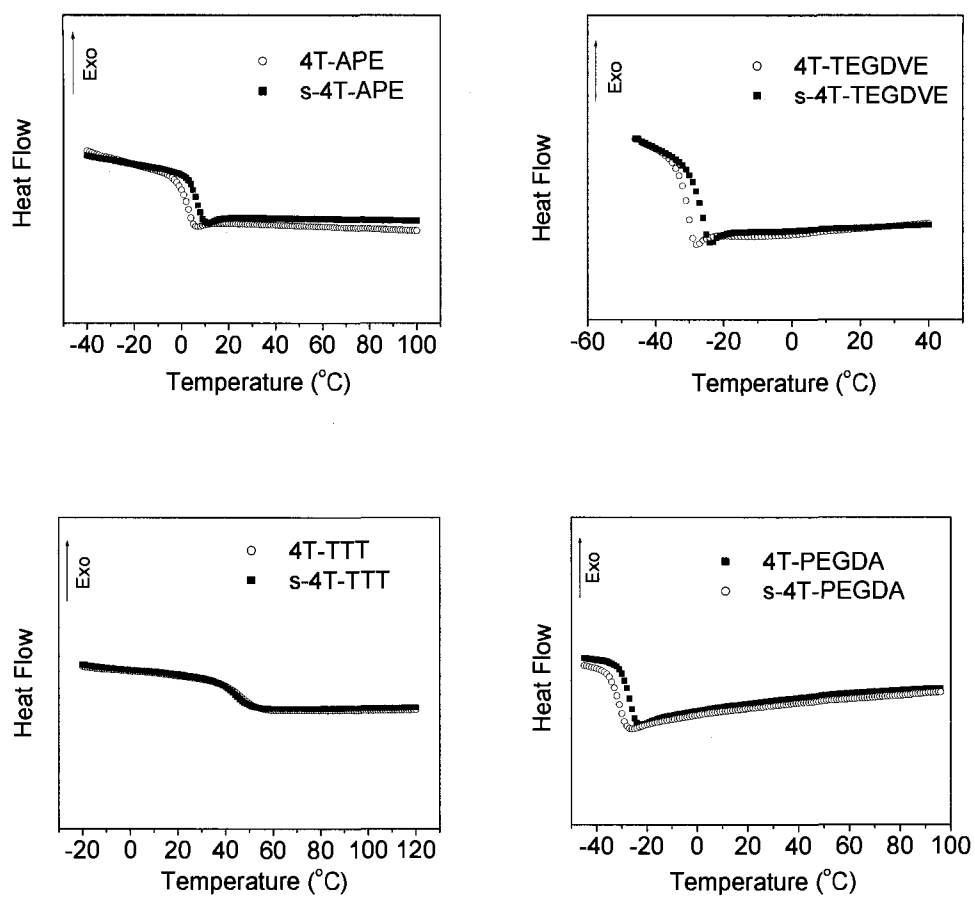


Figure 3.3. DSC curves of thiol-ene networks measured at a heating rate of 10 °C/min.

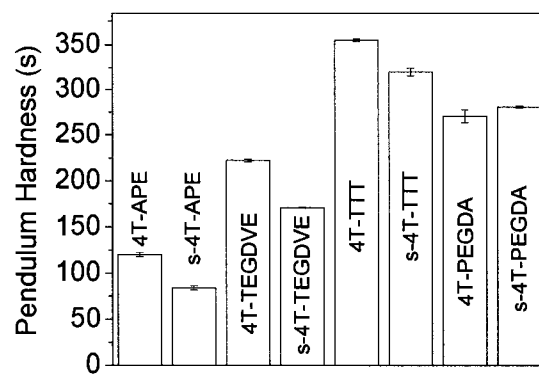


Figure 3.4. Persoz pendulum hardness of thiol-ene networks.

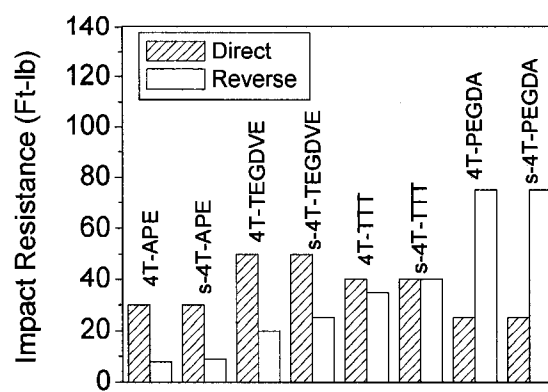


Figure 3.5. Impact resistance of thiol-ene networks.

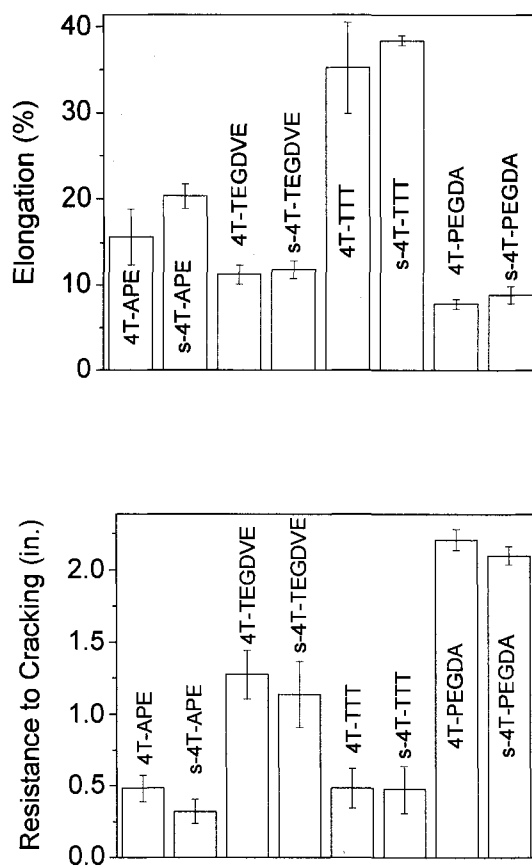


Figure 3.6. Elongation and cracking resistance of thiol-ene networks.

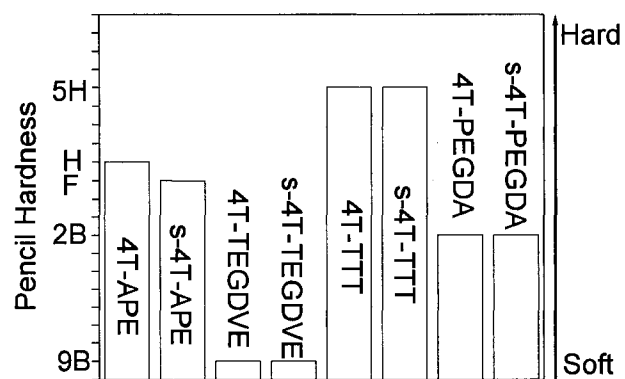


Figure 3.7. Pencil hardness of thiol-ene films.

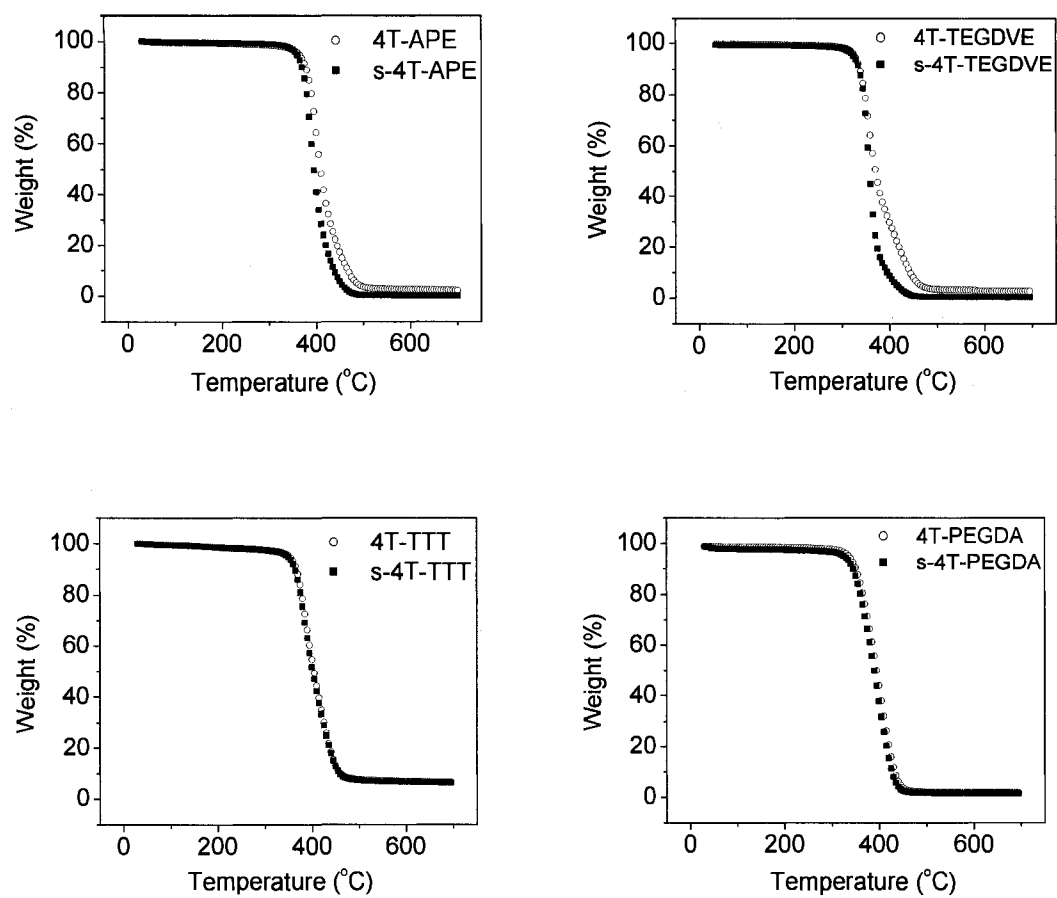


Figure 3.8. TGA curves of thiol-ene films.

CHAPTER IV
THIOL-ENE FREE-RADICAL AND VINYL ETHER CATIONIC HYBRID
PHOTOPOLYMERIZATION

Abstract

The photopolymerization kinetics of mixtures containing a trithiol and a trivinyl ether (in different molar ratios) with a cationic photoinitiator were investigated by real-time infrared and real-time rheology. Using this combination of real-time methods to follow both chemical conversion and rheological property development, a clear picture of physical property development during the complete polymerization process is obtained. This represents the first example of a thiol-ene radical/ene cationic two-step hybrid photopolymerization process in which thiol copolymerizes with vinyl ether functional groups in a rapid radical step growth process followed by vinyl ether cationic homopolymerization. The sequential thiol-vinyl ether copolymerization and the vinyl ether cationic polymerization result in crosslinked networks with thermal and mechanical properties that are combinations of each system.

Introduction

Studies of hybrid photopolymerization have primarily focused on overcoming the limitations of polymerization of a single type of system.¹ Hybrid polymerizations involving simultaneous or sequential polymerizations have led to the creation of a variety of novel polymers including interpenetrating polymer networks (IPNs)²⁻⁹ and block copolymer networks.¹⁰⁻¹² In this context, free-radical and cationic photopolymerization has received considerable attention in recent years¹⁻¹³. The primary motivation for such

multicomponent hybrid polymerizations has been to develop a system which overcomes the limitations of each of the individual systems. For example, (meth)acrylate free-radical photopolymerizations suffer from oxygen inhibition and relatively high polymerization shrinkage, while ring opening polymerizations (oxetanes and oxiranes) are characterized by water inhibition and low reaction rates. Decker et. al.^{2,3} and Jessop et.al.¹⁴ demonstrated that the oxygen sensitivity of the acrylate is reduced while its ultimate conversion is enhanced in hybrid photopolymerization of acrylates and epoxides. In addition, hybrid acrylate/epoxide systems exhibit enhancement in the resultant polymer matrix hardness compared to either neat acrylate or neat epoxide based networks. And yet the hybrid networks are more flexible than the neat epoxide polymer. Similar trends have been reported for many other hybrid monomer combinations (acrylate/vinyl ether, vinyl ether/ester).^{2,4} Stansbury et. al.⁵ reported that the moisture sensitivity of cationic photopolymerization is also reduced in methacrylate/vinyl ether hybrid systems. Oxman et.al¹⁵ investigated “sequential stage curable hybrid systems” involving an acrylate/cycloaliphatic epoxide combination in which the reaction system exhibits several discrete stages. Upon exposure to light both free-radical and cationic initiating centers were produced by a three component initiator system: the acrylate polymerized first, followed by the slower epoxide cationic polymerization. Controlling the order and timing of the sequential stages of the hybrid free-radical/cationic monomer system can be achieved either by the use of two independent initiators that are activated by distinct wavelengths of light,^{16,17} or the use of a single light source to create both the free-radical and cationic active centers simultaneously with chemical control over the sequential polymerization stages. This chemical control can be achieved in several ways including

using two separate initiators (one a free radical, the other cationic)^{3,7,9,18} or a single initiator system^{10,15,19,20} that generates both free-radical and cationic initiating species.

The unique set of properties afforded by hybrid photopolymerization systems make them attractive for a wide variety of applications, for example, medical systems, rapid prototyping resins,²¹ advanced coatings and adhesives.

There has been a revival of interest in thiol-ene photopolymerization in the past 5 years. It has been clearly shown that thiol-ene polymerization (including thiol and acrylate combinations) has distinct advantages over the polymerization of traditional acrylates related to the basic polymerization process including reduced oxygen inhibition, production of highly uniform crosslink density networks, and low shrinkage/induced stress during polymerization.²² Recently, it has been shown that polymerization of acrylate and thiol-ene mixtures exhibit interesting mechanical and impact properties.²³ In the case of binary thiol-acrylate and ternary thiol-ene-acrylate systems, free-radical step growth (thiol-ene and thiol-acrylate) and free-radical chain growth (acrylate homopolymerization) processes occur simultaneously to build up polymer networks with properties that potentially can be adapted to a wide variety of applications. In the ternary systems, since all free-radical processes occur simultaneously, chain transfer from the acrylate to the thiol-ene reaction competes with acrylate homopolymerization. In the binary thiol-acrylate systems,²⁴ acrylate homopolymerization reactions and thiol-acrylate copolymerization reactions occur simultaneously with approximately 2 to 3 acrylate-acrylate addition steps occurring per thiol-acrylate reaction. The exact kinetics depends upon the exact structure and functionality of the acrylate. We stress that in all cases involving acrylates, multiple radical processes occur simultaneously.

In an effort to evaluate processes in which multiple reaction processes occur sequentially instead of simultaneously, we have turned to thiol-vinyl ether systems. In these systems, as will be shown, depending upon the concentration of each component, sequential reactions occur involving a rapid free-radical thiol-vinyl ether process followed by a cationic vinyl ether addition process. Herein, we report initial results for a thiol-vinyl ether hybrid photopolymerization system that includes a detailed kinetic, rheological, structural and mechanical property analysis. This is the first reported example of a thiol-ene radical/cationic hybrid photopolymerization process. The results reported are indicative of the properties achievable with thiol-ene/cationic systems. The results are important since they suggest an opportunity for implementing a totally new strategy for fabricating photocurable materials for both thin film and thick crosslinked material applications. From an initially non-viscous monomer mixture, a very loose and uniform low crosslink density network with excess pendant vinyl ether groups is created by a very rapid thiol-vinyl ether free-radical polymerization followed by a subsequent cationic addition polymerization that results in a marked increase in crosslink density and formation of a unique network.

Experimental

Materials

Tris[4-(vinyloxy)butyl] trimellitate (TriVinyl) and trimethylol propane tris(3-mercaptopropionate) (TriThiol) were obtained from Aldrich Chemical Co. and Brono Bock, respectively, and used without further purification. The chemical structure of TriVinyl and the TriThiol used in this study are shown in Figure 1. The photoinitiator, CYRACURE[®] UVI 6974, triarylsulfonium hexafluoroantimonate salts mixed with

propylene carbonate, was obtained from Union Carbide Corporation. TriThiol-TriVinyl mixtures were prepared by blending the trithiol into the trivinyl ether based on molar functional group concentration. The amount of UV initiator, UVI 6974, in each case, was 2 wt%. Films on glass plates (200 μm) were photocured on a Fusion curing line (10 passes) with a D bulb (belt speed of 10 feet/min, 3.1 W/cm^2 irradiance). Thick samples (1 mm and 4 mm) were irradiated with low intensity 254-nm low-pressure mercury lamps (0.1 mW/cm^2 irradiance) Spectroline®, Model XX-15B) for 1 hours in air. Samples were then cured on the Fusion curing line (10 passes for both sides).

Characterization

Real-time infrared spectra (RTIR) were recorded on a modified Bruker 88 spectrometer designed to allow light penetration to a horizontal sample using a fiber-optic cable attached to a 200 Watt high-pressure mercury-xenon lamp source (obtained from Oriel Co.) with primary wavelengths of 313 and 366 nm and light intensity of 1.87 mW/cm^2 (ND 2.0 filter). The real-time FTIR setup has been described in detail elsewhere.²⁵ Samples were prepared by mixing vinyl ether and thiol based on the moles of each functional group. Samples of 10-15 μm thickness were placed between two sodium chloride (NaCl) salt plates. UV light intensity at the sample was measured by a calibrated radiometer (International Light IL-1400). Infrared absorption spectra of samples were obtained upon continuous UV irradiation at a scanning rate of 5-10 scans/sec. The vinyl ether double bonds were monitored at 1640 or 3116 cm^{-1} and the thiol group at 2575 cm^{-1} .

Real-time rheological measurements were performed using a Physica MCR 501 rheometer (Anton Paar, USA) with a Novacure high-pressure mercury lamp with primary

wavelengths of 313 and 366 nm and a light intensity of 7.5 mW/cm^2 (ND 2.0 filter). The lower fixture of the rheometer is a large quartz glass plate, while the top one is an 8-mm diameter metal plate. The sample thickness is 50 μm . The light was delivered to the sample via a liquid light pipe through neutral density filter (ND 2.0) for a given exposure time at a constant temperature ($25 \text{ }^\circ\text{C}$) and shear frequency (10 rad s^{-1}). Concomitant changes in viscoelastic material functions during polymerization (G' , G'' , and η^*) were measured as a function of exposure time. The measurements were carried out in the linear viscoelastic region (strain amplitude $\leq 10\%$).

Molecular relaxations of the films were recorded using a TA Q800 dynamic mechanical analyzer (DMA). DMA was conducted in the tensile mode for $19 \times 5.6 \text{ mm}$ size samples with thicknesses of 100-150 μm . Free standing film samples, obtained by removing films cured by Fusion UV curing line from glass substrates, were heated from -50 to $200 \text{ }^\circ\text{C}$ at a rate of $3 \text{ }^\circ\text{C/min}$ and at a frequency of 1 Hz in air. As described in detail in a previous publication,²³ a Tinius Olsen instrument (Model 92T) was modified with extensive help from the Tinius Olsen Testing Machine Co., Inc. to measure the energy absorbed upon moderate impact (1.13 Joules) with a steel head was used to investigate the impact resistances of the 4-mm thick samples. The typical sample dimensions were $80 \text{ mm} \times 20 \text{ mm} \times 8 \text{ mm}$ (L \times W \times H). Two photocured 4-mm plates were pressed together back to back to eliminate any contribution from the steel plate. The striking edge of the pendulum, which complied with ASTM 12.3, was made of hardened steel, tapered to have an incline angle of 45° and rounded at the edge to a radius of 3.17 mm. Tensile property measurements were obtained with a Mechanical Testing Machine (MTS-Alliance RT/10) according to ASTM D882, using a 100 N load cell with a

specimen gauge length of 40 mm at a crosshead speed of 25 mm/min. A width-thickness ratio of 8 was used for the tensile testing. Five tests were run for each sample and an average value is reported.

Results and Discussion

This paper focuses on the hybrid photopolymerization of thiol-ene and cationic systems involving the two components in Figure 1: a trithiol (designated TriThiol) and a trivinyl ether (designated TriVinyl). Each mixture contains 2 wt % of a cationic triarylsulfonium hexafluoroantimonate photoinitiator that generates both radical and cationic species upon UV light exposure leading to the initiation of both radical and cationic photopolymerization processes.²⁶ A discussion of the real-time chemical kinetics and build up of viscoelastic properties is followed by an evaluation of the final film properties of several thiol-vinyl ether combinations.

Real-Time Chemical Kinetics and Rheology

Kinetic analyses were conducted with real-time FTIR (RTIR). Resultant conversion versus irradiation time plots of the TriThiol-TriVinyl sample with 50 to 50 mol% thiol to ene functional groups (designated hereafter as 50:50 TriThiol-Trivinyl), TriVinyl, and TriThiol-TriVinyl with 25 to 75 mol% thiol to ene functional groups (designated hereafter as 25:75 TriThiol-TriVinyl) are shown in Figures 2, 3 and 4, respectively. For the 50:50 TriThiol-TriVinyl system (Figure 4.1), the vinyl ether ene conversion was a little faster than the thiol conversion and reached almost 100 % conversion (all 50 mol% of the vinyl ether ene functional groups), about 5 % greater than that of the thiol conversion (95% of the original 50 mol% thiol groups reacted). This indicates that most of the polymerization proceeds by a thiol-ene step-growth radical

process, with a minor contribution from the cationic polymerization of vinyl ether groups. For pure TriVinyl (Figure 4.2), there is about a 120 second inhibition period not seen in the 50:50 TriThiol-TriVinyl system. This is probably due in large part to the well known moisture inhibition of cationic photopolymerization. Also, the pure TriVinyl polymerizes cationically much slower than the free-radical step growth thiol-ene polymerization of 50:50 TriThiol-TriVinyl and reaches a conversion of only about 80 mol%. When TriThiol (25 mol% thiol groups of the total moles of thiol + vinyl ether functional groups) was combined with TriVinyl (75 mol % ene groups of the total moles of thiol + ene functional groups), the thiol and vinyl ether essentially copolymerized by the thiol-ene free-radical reaction in the first 70 seconds (Figure 4.3), with about 22.5 mol % of thiol functional groups (90% of the original 25 mol% thiol groups reacted) and 23 mol% of vinyl ether ene functional groups (30.7% of the original 75 mol% ene functional groups reacted) being converted. After this initial very rapid reaction involving almost exclusively thiol-vinyl ether copolymerization, the vinyl ether continued to polymerize via a cationic polymerization process reaching an ultimate conversion of about 67.5 mol% (90% of the original 75 mol% ene functional groups reacted). From the kinetics in Figures 4, it is apparent that a two-step hybrid photopolymerization involving an initial rapid free-radical thiol-ene polymerization and a subsequent slower cationic polymerization occurs for the 25:75 TriThiol-TriVinyl mixture with an excess of vinyl ether functional groups.

In the initial thiol-ene polymerization process, it is speculated that a very loose gel network is formed. According to the traditional gel-point Equation (1), which in the past has been applied to thiol-ene polymerization by Jacobine et al.,²⁷ with thiol and ene

functionalities, f_{thiol} and f_{ene} , of 3 and a thiol to ene molar ratio based on functional groups, r , of thiol to ene of 1/3, it is predicted that the gel point for the should occur at $\sim 86.6\%$ of thiol functional group conversion. The RTIR results in Figure 4.3 indicate that a near quantitative thiol conversion is attained in the initial polymerization period. This suggests that gelation occurs just at the end of the thiol-ene conversion, and thus the network formed at this point has a very low crosslink density. Then, the cationic vinyl ether homopolymerization proceeds within the framework of the initial loose gel established by the thiol-vinyl ether polymerization. To provide evidence that the thiol-vinyl ether free-radical process leads to gelation, and to provide a dynamic characterization of viscoelastic property build up during the polymerization process, we turn to real-time photo-rheological measurements.

$$\alpha \text{ (fractional conversion at gel point)} = [1/r(f_{\text{thiol}} - 1) (f_{\text{ene}} - 1)]^{1/2} \quad (1)$$

Dynamic rheology is an effective method for characterizing the curing process of thermosetting polymers and for the examination of the viscoelastic properties and transition temperatures of the cured products.²⁸⁻³⁵ It has been applied in the past to characterization of thiol-ene photopolymerization.^{36,37} The formation of polymer gels can be monitored from the time evolution of viscoelastic material functions such as G' , G'' , η^* , where the entire network forming process can be divided into two parts separated by the gel point. The light exposure time dependence of the complex dynamic viscosity and storage (elastic) modulus, η^* and G' , for 50:50 TriThiol-TriVinyl, pure TriVinyl, and 25:75 TriThiol-TriVinyl at $T = 25 \text{ }^\circ\text{C}$ and $\omega = 10 \text{ rad s}^{-1}$ is shown in Figure 4.4. Clearly, the results in Figure 4.4A and 5B show that the time evolution of the

viscoelastic properties is strongly influenced by the concentration of TriThiol in the mixtures. Considering pure TriVinyl first, after an initial induction period consistent with the results in Figure 4.2, a steady rise in both η^* and G' occurs, indicating a single curing process. Although the cationic polymerization of pure TriVinyl is relatively slow, as indicated in Figure 4.2, a conversion of greater than 80 % is achieved. Accordingly, at longer light exposure times ($t > 130$ sec) the value of G' levels off and becomes time independent. The G' plateau value at long time is indicative of the formation of an equilibrium modulus, G_{eq} : establishment of a plateau for G' is generally accepted as the primary criterion for the formation of a stable three dimensional polymer network.³¹⁻³³ In addition to the results for G' for TriVinyl, a plateau was also obtained (Figure 4.4B) for the complex dynamic viscosity, η^* .

As already indicated, photorheology results can be used to identify a gelation process associated with formation of 3D network structures. We thus compare critical viscoelastic parameters for the gelation of both pure TriVinyl and 25:75 TriThiol-TriVinyl in order to provide a clear real-time rationale for rheological property and structure development. The main goal is to provide rheological evidence for gelation at the end of an initial thiol-vinyl ether free-radical reaction for 25:75 TriThiol-TriVinyl. Figures 6 and 7 show the time dependence of G' and G'' at 25 °C and $\omega = 10 \text{ rad s}^{-1}$ for the TriVinyl and the 25:75 TriThiol-TriVinyl systems. First we consider the results in Figure 4.5. Prior to gelation, the value of G'' for the pure TriVinyl monomer is about one order of magnitude greater than G' . As expected, both G' and G'' steadily increase (no intermediate plateaus) with UV light exposure, reaching approximate equilibrium values fairly rapidly after polymerization begins. The value of G' , initially lower in

magnitude than G'' , increased more rapidly than G' , becoming greater than G'' at a very short time after the polymerization begins, following the extended induction period as previously described. The early gelation process is certainly consistent expected for multifunctional vinyl ethers. The results in Figure 4.6 for the 25:75 TriThiol-TriVinyl, indicate that, unlike that for the pure cationic polymerization process of pure TriVinyl in Figure 4.5, two distinct and apparently independent processes occur. The initial process, consistent with the kinetic results for thiol-ene polymerization in Figure 4.3, occurs during the first 20-40 seconds of light exposure and leads to a plateau in both G' and G'' . More importantly, during this initial period, which as we have indicated corresponds to the free-radical thiol-vinyl ether copolymerization process, there is an intersection of the G' and G'' curves at a point that is very near to the intermediate plateau value for each. The value for the elastic modulus G' exceeding the value for the loss modulus G'' indicates that the sample has become an infinite gel near the end of the initial thiol-ene free-radical polymerization process as previously proposed in our discussion of equation 1. The additional increase and final plateau of G' and G'' subsequent to the initial plateau is assigned to the cationic polymerization of the vinyl ether groups that are attached to the loose thiol-vinyl ether network formed initially. In summary, the real-time photo-rheological measurements of 25:75 TriThiol-TriVinyl mixture with an excess of vinyl ether functionality confirms that gelation occurs near the end of the rapid thiol-ene free-radical step-growth polymerization. The subsequent slower cationic homopolymerization of the remaining vinyl ether groups leads to additional increase in crosslink density of the network.

We note that in this paper, the exact gel time has not been presented. The relatively fast polymerization kinetics of the system studied makes it impossible to evaluate the gel point from classical frequency dependencies of the viscoelastic material functions. This is supported by the time dependencies of G' & G'' (Figure 4.5) showing a polymerization reaction time of 15 ± 5 sec. However, we made measurements of G' & G'' versus time under different shear frequencies to find out whether the crossover point is influenced by the value of shear frequency or not. These results (not shown herein) clearly indicated that the crossover point is approximately independent of the different values of shear frequency used. The behavior of the other samples was found to be similar to that of the pure TriVinyl. We thus project that the crossover point can be considered as the gel point for the specific samples of the current study. A follow up rheological paper will include complete and extensive results for gel times for a range of TriThiol and TriVinyl (as well as other multifunctional vinyl ethers) mixtures over a wide concentration regime where $\tan \delta$ versus time plots as a function of oscillation frequency will be given.

Physical, Mechanical and Thermal Properties of Polymerized Networks

Thermal and mechanical properties of the photopolymerized films of pure TriVinyl, 50:50 TriThiol-TriVinyl and 25:75 TriThiol-TriVinyl mixtures were first characterized by 1 Hz DMA scans (shown in Figure 4.7) in the tensile mode. We first note that the DMA scan results clearly show that the 50:50 TriThiol-TriVinyl film has a very narrow $\tan \delta$ peak representing a uniform network matrix resulting primarily from a free-radical thiol-ene step-growth process, while the corresponding scan for the 25:75 TriThiol-TriVinyl film is broadened and characterized by a higher temperature (just

above room temperature) at the $\tan \delta$ peak maximum. The results for the 50:50 TriThiol-TriVinyl network in Figure 4.7 are consistent with the known high uniformity of thiol-ene networks.^{21, 22} The film formed by polymerizing 25:75 TriThiol-TriVinyl, where both the thiol-ene free-radical and subsequent vinyl ether cationic polymerization occur, gives a sample that has a broader $\tan \delta$ versus temperature plot with a peak maximum at a higher temperature than the plot obtained from the sample formed by photopolymerization of 50:50 TriThiol-TriVinyl. The broadened DMA scan for the 25:75 TriThiol-TriVinyl film is indicative of a more heterogeneous network due to the cationic chain growth process which occurs subsequent to the formation of the thiol-ene network. Results for additional TriThiol-TriVinyl ether mixtures (not shown) indicate a steady increase in the $\tan \delta$ peak maximum temperature and progressive broadening with increasing vinyl ether concentration. The film produced from pure TriVinyl has a broad $\tan \delta$ plot indicative of a very heterogeneous network matrix with a main peak maximum around 84 °C and a much smaller shoulder around 57 °C. It can be concluded that, from a mechanical/thermal basis, the matrix uniformity increases with TriThiol content. In order to characterize thermal transitions, DSC scans (not shown) were also recorded for the same samples. The DSC results essentially parallel the DMA results, i. e., the film from 50:50 TriThiol-TriVinyl has a very narrow glass transition region, the film from 25:75 TriThiol-TriVinyl has a broader but still distinctive transition, while the film from the strictly cationic photopolymerization of pure TriVinyl is very broad.

In view of the observation in Figures 8 that thiol-ene/cationic mixtures can be photopolymerized to give crosslinked films with relatively narrow transitions whose peak maxima can be adjusted to a given temperature by the concentration of TriThiol, an

investigation of the impact resistances of 4-mm thick samples was conducted with a Tinius Olsen instrument modified to measure the energy absorbed upon moderate impact (1.13 Joules) with a steel head. As shown in Table 4.1, the photocured 25:75 TriThiol-TriVinyl sample absorbs about 65% of the impact energy of the striking head at room temperature, and is more effective in dissipating impact energy than the samples of 50:50 TriThiol-TriVinyl and pure TriVinyl. The energy absorption depends on the $\tan \delta$ value (at the frequency of the energy impact) at a given temperature. It is thus not surprising that the 25:75 TriThiol-TriVinyl sample has better energy absorbing ability at room temperature where it has substantial $\tan \delta$ values according to the 1 Hz DMA analysis in Figure 4.7. In other work²³, it has been shown that 1 Hz DMA values provide reasonable approximation to the impact measurements as described in the experimental section. Finally, it is noted that the amount of energy absorbed is greater than for traditional “energy absorbing” materials near room temperature, i.e., commercial ethylene vinyl acetate (EVA) often used in sports applications under the same experimental conditions were found to absorb 40-50 % of the 1.13 J impact energy.

The tensile mechanical properties were next evaluated for photocured 1-mm thick samples of 50:50 TriThiol-TriVinyl, pure TriVinyl, and 25:75 TriThiol-TriVinyl (Figure 4.8 and Table 4.1). Interesting enough, the 25:75 TriThiol-TriVinyl sample, which according to the kinetic results in Figures 4, 5 and 7 involves both an initial thiol-ene free-radical and a subsequent cationic polymerization (Figure 4.3), has both flexibility in terms of strain at break, and rigidity in terms of stress at break. This illustrates the ability of the hybrid polymerization to combine the properties of two types of systems. The energy to break is related to the area underneath a stress-strain curve. Although energy to

break is dimensionally dependent, it is one indication of material toughness. From the energy to break data in Table 4.1, it is clear that 25:75 TriThiol-TriVinyl has higher toughness than both 50:50 TriThiol-TriVinyl and pure TriVinyl. This is coincident with the high energy absorption at room temperature found for the 4-mm plates made from the 25:75 TriThiol-TriVinyl.

Conclusions

In summary, real-time infrared analysis shows that the photopolymerization of a trithiol and trivinyl ether mixture with excess vinyl ether proceeds by a rapid thiol-ene radical polymerization and a subsequent cationic vinyl ether polymerization. Dynamic rheology measurements indicate that the 25:75 TriThiol-TriVinyl sample gels at the end of the thiol-ene free-radical reaction followed by a cationic polymerization of residual vinyl ether groups. Mechanical property and impact measurements indicate an energy absorbing, tough material. The results suggest an important strategy for building networks via hybrid free-radical thiol-ene/cationic-ene polymerization processes.

Acknowledgements

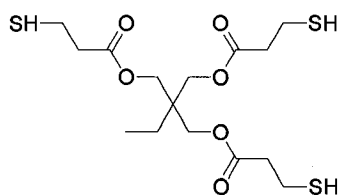
Financial support of this work by the MRSEC Program of the National Science Foundation under Award Number DMR 0213883, the Chemical and Transport System (CTS 0317646) of the National Science Foundation, and Fusion UV Systems is gratefully acknowledged. We also thank Bruno Bock for providing the thiol sample.

References

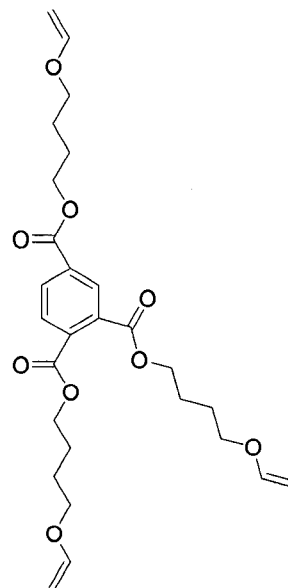
1. Ficek, B. A.; Magwood, L.; Coretsopoulos, C.; Scranton, A. B. *Photochemistry and UV Curing: New Trends*, Editor: Fouassier, J. P. Research Signpost, India, **2006**, 25, 294-300.
2. Decker, C. *Polym. Int.* **2002**, 52, 1141-1150.
3. Decker, C.; Nguyen, T. V. T.; Deck, D.; Weber-Koehl, E. *Polymer* **2001**, 42, 5531-5541.
4. Decker, C. *Acta Polymer* **1994**, 45, 333-347.
5. Lin, Y.; Stansbury, J. *Polym. Adv. Technol.* **2005**, 16, 195-199.
6. Dean, K.; Cook, W. D. *Macromolecules* **2002**, 35, 7942-7954.
7. Dean, K.; Cook, W. D.; Rey, L.; Galy, J.; Sautereau, H. *Macromolecules* **2001**, 34, 6623-6630.
8. Dean, K.; Cook, W. D.; Zipper, M. D.; Burchill, P. *Polymer* **2001**, 42, 1345-1359.
9. Lin, Y.; Stansbury, J. *Polymer* **2003**, 44, 4781-4789.
10. Degirmenci, M.; Hepuzer, Y.; Yagci, Y. *J. App. Polym. Sci.* **2002**, 85, 2389-2395.
11. Mecerreyes, J. A.; Pomposo, J. A.; Bengoetxea, M.; Grande, H. *Macromolecules* **2000**, 33, 5846-5849.
12. Itoh, H.; Kameyama, A.; Nihikubo, T. *J. Polym. Sci. Part A: Polym. Chem.* **1996**, 34, 217-225.
13. Chen, Z. G.; Webster, D. C. *Polymer* **2006**, 47, 3715-3726.
14. Cai, Y.; Jessop, J. L. P. *Polymer* **2006**, 47, 6560-6566.
15. Oxman, J. D.; Jacobs, D. W.; Trom, M. C.; Sipani, V.; Ficek, B.; Scranton, A. B. *J. Polym. Sci. Part A: Polym. Chem.* **2005**, 43, 1747-1756.

16. Decker, C. *Prog. Polym. Sci.* **1996**, 21, 593-650.
17. Kawabata, M.; Sato, A.; Sumiyoshi, I.; Kubota, T. *Appl. Optics.* **1994**, 33, 2152-2156.
18. Cho, J. D.; Hong, J. W. *J. App. Polym. Sci.* **2004**, 93, 1473-1483.
19. Crivello, J. V. *J. Polym. Sci. Part A: Polym. Chem.* **1999**, 37, 4241-4254.
20. Crivello, J. V.; Rajaraman, S.; Mowers, W. A.; Liu, S. *Macromol. Symp.* **2000**, 157, 109-119.
21. Lawton, J. *US Patent* **2004**, 6,811,937.
22. Hoyle, C. E.; Lee, T. Y.; Roper, T. *J. Polym. Sci. Part A: Polym. Chem.* **2004**, 42, 5301-5338.
23. Senyurt, A. F.; Wei, H.; Phillips, B.; Cole, M.; Nazarenko, S.; Hoyle C. E.; Piland, S. G.; Gould, T. E. *Macromolecules*, **2006**, 39(19), 6315-6317.
24. Cramer, N. B.; Bowman, C. N. *J. Polym. Sci. Part A: Polym. Chem. Part A: Polym. Chem.* **2001**, 39, 3311-3319.
25. Lee, T. Y.; Roper, T. M.; Jonsson, E. S.; Kudyakove, I.; Viswanathan, K.; Nason, C.; Guymon, C. A.; Hoyle, C. E. *Polymer* **2003**, 44, 2859.
26. Crivello, J.V.; Dietliker, K. *Chemistry & Technology of UV & EB Formulation for Coatings, Inks & Paints*, Bradley, G. Editor. John Willey & Sons Ltd., **1998**, Vol. III, 326-477.
27. Jacobine, A. F. In *Radiation Curing in Polymer Science and Technology III, Polymerization Mechanisms*; Fouassier, J.D.; Rabek, J.F., Eds.; Elsevier Applied Science: London, 1993; Chapter 7.
28. Izuka, A.; Winter, H. H.; Hashimoto, T. *Macromolecules* **1992**, 25, 2422 – 2428.
29. Adolf, D.; Martin, J. E.; Wilcoxon, J. P. *Macromolecules* **1990**, 23, 527 – 531.

30. Hodgson, D. F.; Amis, E. J. *Macromolecules* **1990**, *23*, 2512 – 2519.
31. Muller, R.; Gerard, E.; Dugand, P.; Rempp, P.; Gnanou, Y. *Macromolecules* **1991**, *24*, 1321 – 1326.
32. Takahashi, M.; Yokoyama, K.; Masuda, T.; Takigawa, T. *J. Chem. Phys.* **1994**, *101*, 798 – 804.
33. Madbouly, S. A.; Otaigbe, J. U. *Macromolecules*, **38**, **2005**, 10178-10184.
34. Madbouly, S. A.; Otaigbe, J. U.; *Macromolecules*, **39**, **2006**, 4144-4151.
35. Madbouly, S. A.; Ougizawa, T. *J. Macro. Sci. part B-Phys.* **2004**, *B43*, 819 – 832.
36. Chiou, B. S.; English, R. J.; Khan, S. A. *Macromolecules*, **29**, **1996**, 5368-5374.
37. Chiou, B. S.; Khan, S. A. *Macromolecules*, **30**, **1997**, 7322-7328.



TriThiol



TriVinyl

Chart 4.1. Chemical structures of TriThiol and TriVinyl.

Table 4.1. Mechanical properties of 0:100TriVinyl, 25:75 TriThiol-TriVinyl and 50:50 TriThiol-TriVinyl.

	50:50	25:75	0:100
Energy Absorbance (Joule)	0.15 (13%)	0.73(65%)	0 (cracked)
Stress at break (MPa)	1.0	3.0	3.3
Strain at break (%)	13.7	13.0	1.3
Energy to break (N*mm/mm ³)	49.8	128.4	14.0

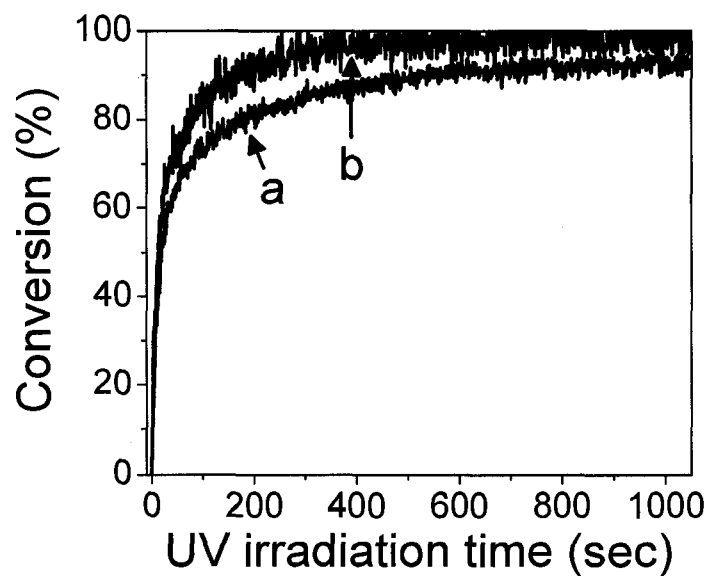


Figure 4.1. Real-time IR percent conversion versus time plots of 50:50 TriThiol-TriVinyl: (a) thiol and (b) vinyl ether. Irradiance (full arc) is 1.87 mW/cm^2 .

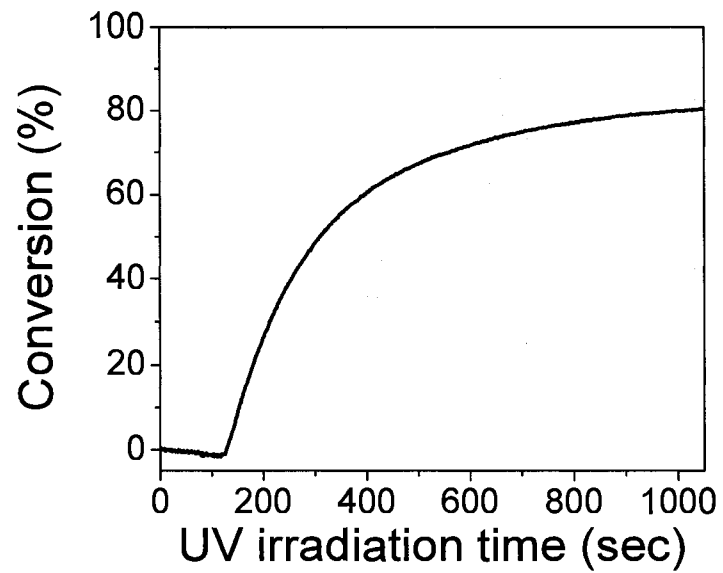


Figure 4.2. Real-time IR percent conversion versus time plots of pure TriVinyl. Irradiance (full arc) is 1.87 mW/cm^2 .

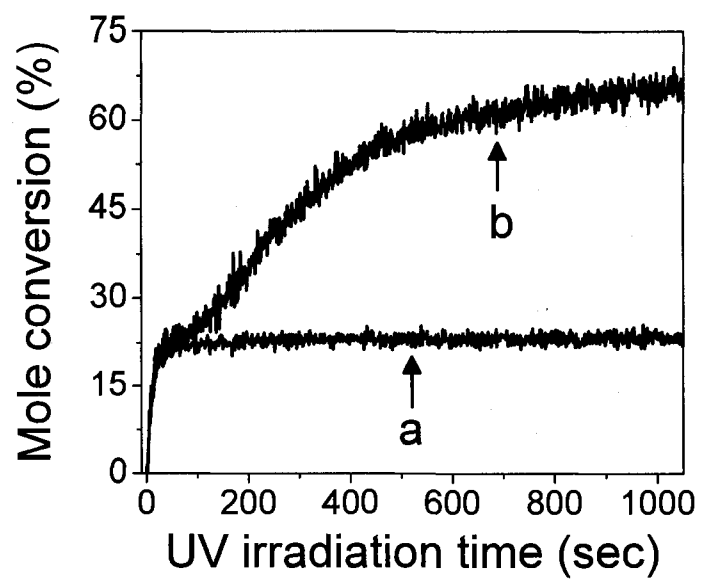


Figure 4.3. Real-time IR percent conversion versus time plots of 25:75 TriThiol-TriVinyl: (a) thiol and (b) vinyl ether. Irradiance (full arc) is 1.87 mW/cm^2 .

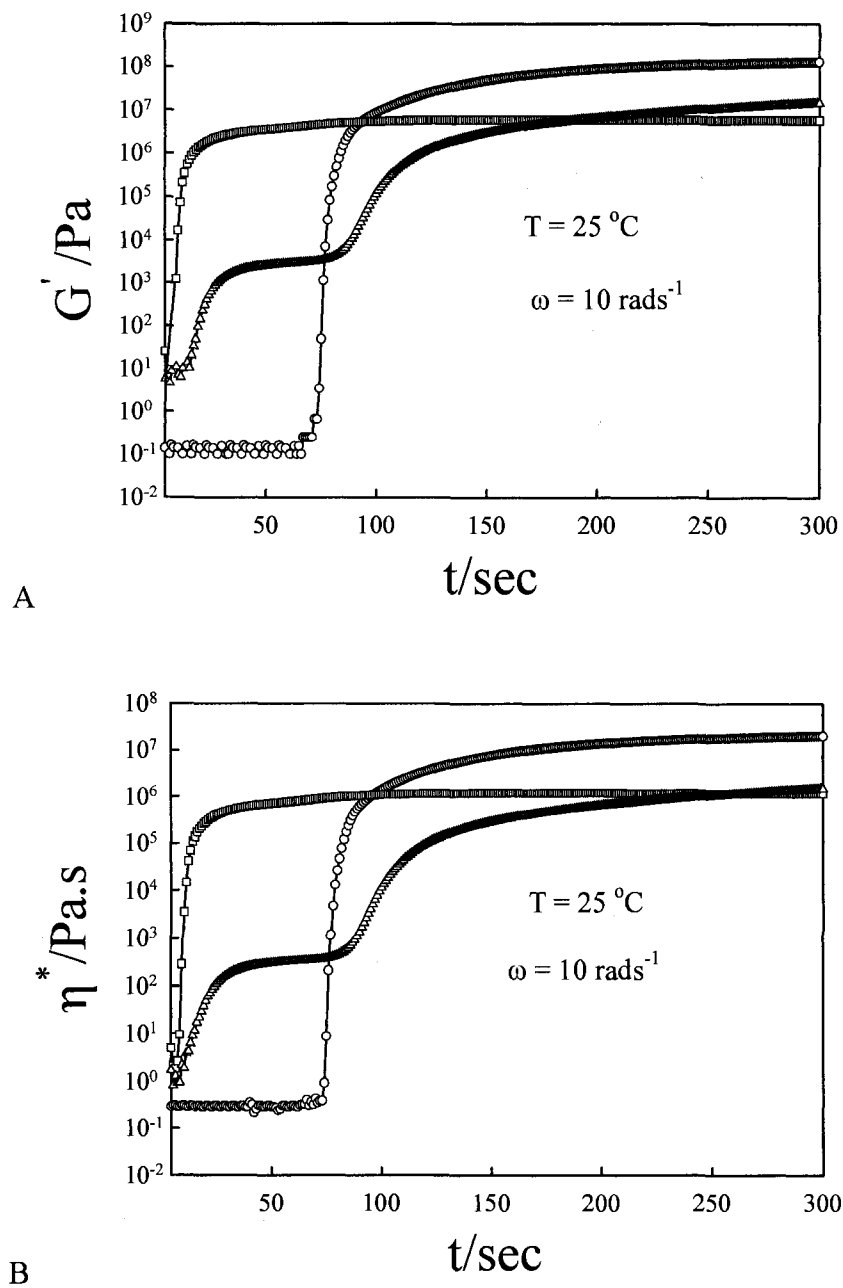


Figure 4.4. Time dependence of (A) dynamic storage modulus, G' , and (B) complex viscosity, η^* , of different concentrations of TriThiol/TriVinyl mixtures at constant shear frequency ($\omega=10\text{ rad s}^{-1}$) and $25\text{ }^\circ\text{C}$: O (pure TriVinyl); Δ (25:50 TriThiol-TriVinyl); \square (50:50 TriThiol-TriVinyl). Irradiance is $\sim 7.5\text{ mW/cm}^2$.

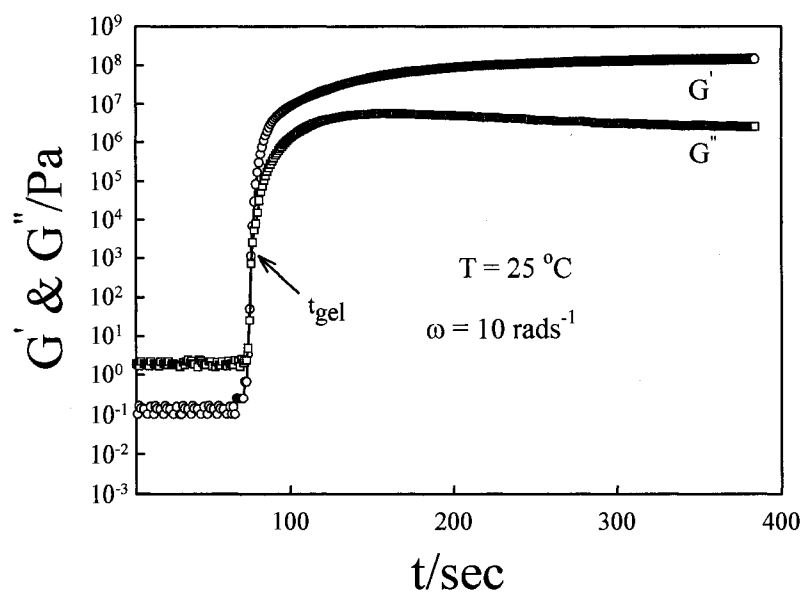


Figure 4.5. Time dependence of G' and G'' at $25 \text{ }^\circ\text{C}$ and 10 rad s^{-1} for the photopolymerization process of pure TriVinyl. The arrow shows the t_{gel} obtained from intersection point of G' and G'' . Irradiance is $\sim 7.5 \text{ mW/cm}^2$.

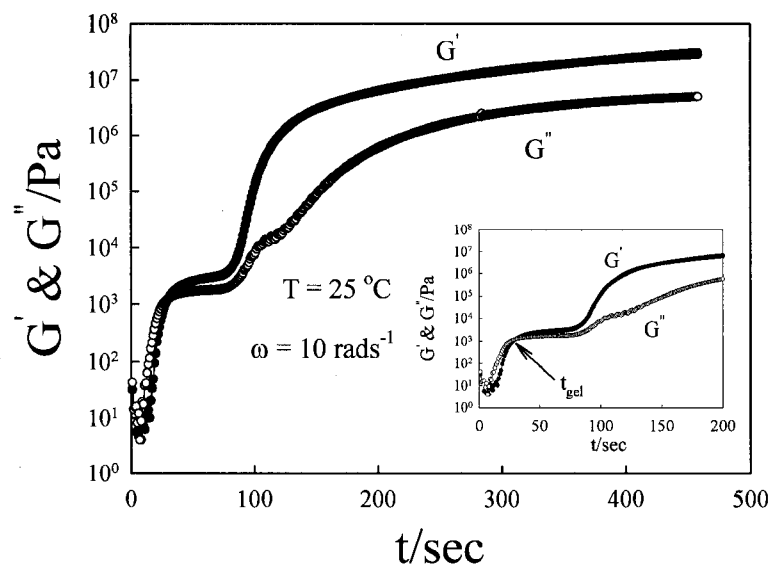


Figure 4.6. Time dependence of G' and G'' at $25\text{ }^\circ\text{C}$ and 10 rad s^{-1} for the UV polymerization process of 25:75 TriThiol-TriVinyl. The inset-plot shows the same figure at a smaller scale; the arrow shows the t_{gel} obtained from intersection point of G' and G'' . Irradiance is $\sim 7.5\text{ mW/cm}^2$.

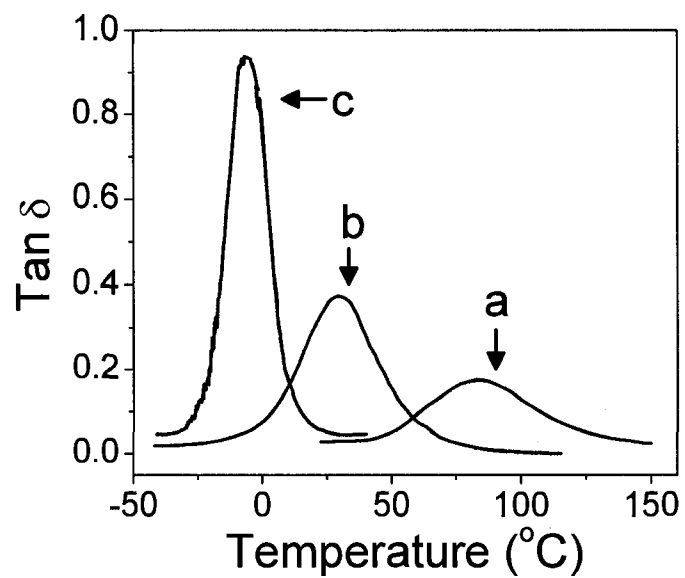


Figure 4.7. Tan δ versus temperature plots for films formed from (a) pure TriVinyl, (b) 25:75 TriThiol-TriVinyl, and (c) 50:50 TriThiol-TriVinyl. DMA plots obtained with scan rate 3 $^{\circ}\text{C}/\text{min}$ and frequency 1 Hz.

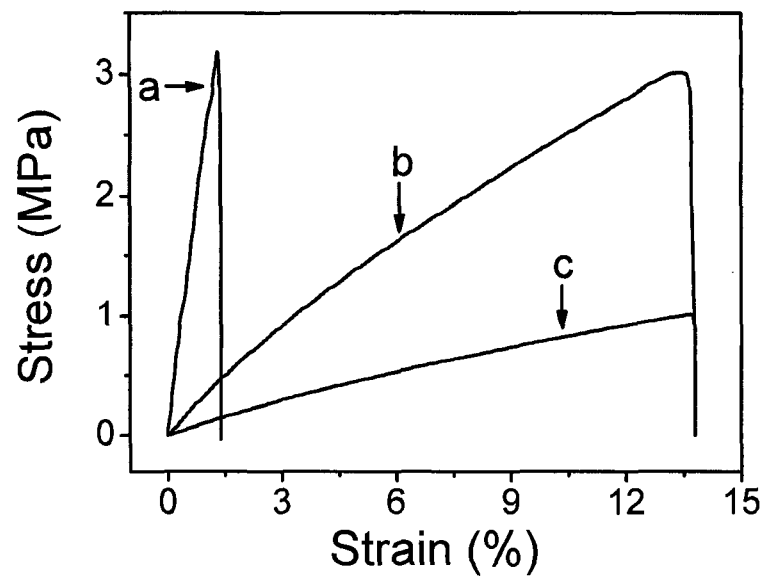


Figure 4.8. Tensile strain versus stress plots of 1-mm thick samples of (a) pure TriVinyl, (b) 25:75 TriThiol-TriVinyl, and (c) 50:50 TriThiol-TriVinyl.

CHAPTER V

THIOURETHANE THIOL-ENE HIGH T_g NETWORKS: PREPARATION, THERMAL,
MECHANICAL, AND PHYSICAL PROPERTIES

Abstract

Thiourethane based thiol-ene (TUTE) films were prepared from diisocyanates, tetrafunctional thiols and trienes. The incorporation of thiourethane linkages into the thiol-ene networks results in TUTE films with high glass transition temperatures. Increases of T_g were achieved by aging at room temperature and annealing the UV cured films at 85 °C. The aged/annealed film with thiol prepared from isophorone diisocyanate and cured with a 10,080 mJ/cm² radiant exposure had the highest DMA based glass transition temperature (108 °C) and a $\tan \delta$ peak with a full width at half maximum (FWHM) of 22 °C, indicating a very uniform matrix structure. All of the initially prepared TUTE films exhibited good physical and mechanical properties based on pencil hardness, pendulum hardness, impact and bending tests.

Introduction

An efficient process leading to the formation of highly cross-linked and uniform molecular networks results from exposure of a mixture of a multifunctional thiol and a multifunctional ene to light.¹⁻³ The uniform structure of the thiol-ene matrices is attested to by very narrow $\tan \delta$ versus temperature plots derived from dynamic mechanical analysis (DMA).^{2,3} The network uniformity is critical in applications requiring polymers

with high homogeneities, e.g. optical elements.^{4,5} Another attractive advantage of thiol-ene polymerization is the low shrinkage and consequential low stress built up in the polymeric network, which is quite desirable in applications such as dental restorative materials.⁶ Unlike acrylates, thiol-ene photopolymerizations are not very sensitive to oxygen inhibition, resulting in efficient polymerization in air.^{2,7} There is no question that thiol-ene polymers exhibit unique physical and mechanical properties which make them useful in many applications. However, the addition of thiols across double bonds results in the formation of flexible thioether linkages, and thus the glass transition temperatures (T_g) are generally limited to near or below room temperature. For applications requiring a material with a high T_g ,⁸ there are few if any viable options for thiol and ene monomer structure selection. Limited T_g enhancement can be achieved by utilizing ene monomers with rigid structures, such as triallyl-1,3,5-triazine-2,4,6(1H,3H,5H)-trione (see Chart 5.1).^{6,8}

One method for producing crosslinked thiol-ene networks with high T_g s is to add a multiacrylate comonomer which can both copolymerize with the thiol as well as homopolymerize.^{9,10} Compared with the thiol-ene copolymerization process, these two additional reaction processes result in a material with a glass transition that can be as high as ~ 80 °C (determined by DMA).¹¹ However, the corresponding high temperature glass transition regions of these ternary systems are broad compared to the traditional thiol-ene networks which can have $\tan \delta$ versus temperature plots with full width at half maximum (FWHM) typically as narrow as 15-20 °C. There is absolutely no question that generation

of thiol-ene based networks with narrow glass transition regions at high temperatures (greater than 90 °C) remains an illusive and very important goal in the thiol-ene field. Such high temperature thiol-ene networks would certainly open up new application opportunities. Herein, we describe the synthesis of multifunctional thiols connected by thiourethane groups which, when combined with a triazine triene, give networks with glass transition temperatures above 90 °C with relatively narrow FWHM values.

Experimental

Isophorone diisocyanate (IPDI), toluene diisocyanate (TDI) and dicyclohexyl methane diisocyanate (H12MDI) were obtained from Bayer and used as received. Triallyl-1,3,5-triazine-2,4,6(1H,3H,5H)-trione (Triallyl Triazine) and pentaerythritol tetrakis(3-mercapto-propionate) (Tetra Thiol) were purchased from Aldrich Chemical Co. and used as received (see Chart 5.1). The photoinitiator 2,2-dimethoxy-2-phenylacetophenone (DMPA) was obtained from Ciba Specialty Chemical Company. Other chemicals, such as anhydrous acetone, were also obtained from Aldrich Chemical Co. and used as received.

Nuclear magnetic resonance (NMR) spectra were obtained on a Mercury 300 (Varian Inc.) using 5 wt% oligomer dissolved in deuterated-chloroform. A modified Bruker IFS 88 FTIR spectrometer with a horizontal sample accessory was used to obtain real-time IR (RTIR) spectra. UV light from an Oriel lamp system equipped with a 200 Watt, high-pressure mercury-xenon bulb was channeled to the sample chamber through a

fiber-optic cable. Photoinitiated polymerization was performed by exposing a thin sample (about 25 μm) between two sodium chloride salt plates to continuous UV light. The process was monitored by the FTIR operating at a scanning rate of 5 scans/sec. Gel permeation chromatography (GPC) with a Waters 515 pump (Waters Corp.) and Waters 2414 refractive index detector were used to measure the polystyrene standard based molecular weight of thiourethane thiol oligomers.

In preparing the thiourethane thiol oligomers which are viscous liquids, 2.0 mmol of diisocyanate, 3.0 mmol Tetra Thiol and 10 mL acetone, were first charged into a one neck flask, and then 1 drop (0.2~0.3 wt%) of dibutyl tin dilaurate (DBTDL) was added. The mixture was allowed to react for 4-8 hours (until the isocyanate IR band around 2260 cm^{-1} completely disappeared) at 60 $^{\circ}\text{C}$ in an oil bath before acetone was evaporated under N_2 flow at room temperature. The different diisocyanates were chosen in order to illustrate the effect of molecular structure on the final polymer properties. The rigid triallyl triene (Triallyl Triazine) was used to ensure that the glass transition temperatures of the final films would be high. The preparation procedure of the thiourethane thiol oligomer, IPDI Thiol, formed from IPDI is shown in Scheme 5.1, as well as the procedure for forming the TUTE crosslinked films. The synthesis of H12MDI Thiol, formed from H12MDI and Tetra Thiol, and TDI Thiol, formed from TDI and Tetra Thiol, follows the same procedure.

It is necessary to point out that the product of the thiol-diisocyanate reaction are predicted to be an oligomer with number average degree of polymerization (\bar{X}_n) of 5

(pentamer) by equations (1) and (2),¹²

$$\bar{X}_n = \frac{2}{2 - f_{avg}} \quad (1)$$

$$f_{avg} = \frac{2N_A f_A}{N_A + N_B} \quad (2)$$

where f_{avg} is the average functionality of the nonstoichiometric mixture of Tetra Thiol and diisocyanates, N_A and N_B are the moles of isocyanate and thiol groups, respectively, used in the synthesis, and f_A is the functionality of isocyanate. The number average molecular weight (\bar{M}_n) of IPDI Thiol is calculated as ~1911 g/mol which is, taking into account the assumptions made in using polystyrene calibration standards, in close agreement with the \bar{M}_n of ~1573 g/mol measured by GPC. The number average structures (pentamers) prepared from the three diisocyanates (IPDI, H12MDI and TDI) and Tetra Thiol, are shown in Chart 5.2 as representatives of the oligomers and verified by ¹H NMR results in Table 5.1. The urethane protons (8) and thiol protons (1) are represented by a wide peak at 5.5-6.5 and a triplet at 1.2, respectively.

To prepare films, the thiourethane thiol oligomers (made from 2 mmol isocyanate and 3 mmol Tetra Thiol) or Tetra Thiol (2 mmol) were homogeneously mixed with 2.67 mmol Triallyl Triazine and 1 wt% DMPA and evenly spread onto glass (for pencil and Persoz pendulum hardness), aluminum (for DSC and DMA) or steel plates (for impact and bending). Cured thiol-ene films (75-150 microns) were obtained by exposing the coated plates to the output of a Fusion high intensity UV lamp system with conveyer belt. The lamp system was equipped with a D bulb (400 W/inch input,

line speed of 12.2 m/min, 3.0 W/cm²). The UV radiant exposure delivered to the coated plates was 504 mJ/cm² for every pass at a line speed of 12.2 m/min. Films were either evaluated (pencil hardness, Persoz hardness, and initial DSC) immediately after curing (both unannealed and annealed), or aged for 1 year at room temperature and then evaluated by DSC analysis (again) and DMA either directly or upon additional annealing. Annealing was conducted by heating in an oven at 85 °C, which is at least 20 °C above the 1st scan DSC T_g of all the films, for either 2 hours (for pencil and Persoz pendulum hardness measurements) or 18 hours (for DSC and DMA measurements). This annealing (both aged and unaged samples) resulted in further conversion of unreacted functionalities. A differential scanning calorimeter (DSC), TA Q1000 (TA Instruments Inc.), operating at a heating rate of 10 °C/min was used to measure thermal properties. In the case of the DSC for both aged and unaged samples, the first heating scan was from 0 °C to 180 °C (isothermal at 180 °C for 5 min) at 10 °C/min, followed by cooling to 0 °C at the same rate. The samples were then heated again from 0 °C to 180 °C to obtain the 2nd heating scan. T_g values were determined using TA Universal Analysis software. The thermomechanical spectra were obtained on a TA Q800 DMA (TA Instruments Inc.) operating at 1 Hz and a heating rate of 3 °C/min (tensile mode). The peak maximum of the tan δ plot was taken as the T_g.

For both unannealed and annealed films, the pencil (ASTM D-3363) and Persoz pendulum hardness (ASTM D-4366 using a BYK-Gardner pendulum hardness tester with a square frame pendulum) values were the average of six tests. The direct and

reverse impact resistance tests (ASTM D-2794) and the bending (mandrel) tests (ASTM D 522-93a) were conducted for unannealed samples only due to delamination considerations.

Results and Discussion

Polymerization Kinetics

The polymerization kinetics of each of the thiourethane thiols mixed with the trifunctional ene was measured via real-time FTIR. Since the C=C ene double bonds and thiols had identical conversion-time curves, to simplify, only the thiol conversion versus time plots are shown in Figure 5.1. All three systems, IPDI Thiol-Triallyl Triazine, H12MDI Thiol-Triallyl Triazine and TDI Thiol-Triallyl Triazine, had final conversions over 80% under ambient conditions with conversion rates commensurate with previous results for the Tetra Thiol-Triallyl Triazine system.⁶

DSC and DMA of Photopolymerized Networks

DSC was used to investigate the glass transition temperature of the TUTE films immediately after curing. As an example, results are shown for films prepared from an IPDI Thiol and Triallyl Triazine mixture (Figure 5.2) subjected to a radiant exposure of 10,080 mJ/cm². We point out that the glass transition increase for the second cycle is no doubt a result of increased conversion upon heating. As summarized in Figure 5.3a for samples made with Triallyl Triazine and all three thiourethane thiol oligomers (only results for IPDI Thiol-Triallyl Triazine are shown), it is obvious that for both the 1st and

2nd heating scans an increase in T_g occurs with an increase in the UV radiant exposure for each sample, and a concomitant increase in conversion of the TUTE films. Focusing on differences in the 1st and 2nd heating scans, we note that for all three samples cured using different radiant exposures, the 1st heating scan T_g is lower than the T_g of the sample after the 2nd heating cycle. The 1st heating scan since this involved heating to 180 °C (1st scan), holding the temperature for 5 min and subsequent cooling to a low temperature (see Experimental) before initiating the 2nd scan. The increase in the glass transition temperature for the 2nd scan can be explained as additional thiol-ene polymerization attained during the 1st scan. We also found by a separate FTIR analysis of annealed films that during the photocuring process a small amount of isocyanate was generated, which upon thermal annealing reacted, presumably with residual thiol. Specifically, the conversions of thiol and ene groups in IPDI Thiol-Triallyl Triazine film (UV radiant exposure=1,008 mJ/cm²) annealed at 85 °C for 18 h increased by about 7 % and 4 %, respectively. The higher conversion of thiol than ene may result from the reaction of isocyanate present in the photocured films.

Based upon the DSC results in Figure 5.3a for the unaged films (analyzed just after curing) which imply that annealing at high temperatures for short periods results in additional conversion and concomitant increase in T_g , samples were thermally aged for 1 year at room temperature to see if a long storage period (at a temperature well below the initial DSC scan T_g s) would result in an additional increase in the 1st scan DSC based T_g . Accordingly, the IPDI Thiol-Triallyl Triazine aged films were chosen as examples to

demonstrate the effect of aging on the T_g . For each IPDI Thiol-Triallyl Triazine film, the 1st DSC scan of the aged samples (Figure 5.3b) resulted in T_g s about 15 °C higher than the unaged samples (Figure 5.3a). The 2nd scans of the three aged samples were essentially identical to the 2nd scans of the unaged samples, indicating that the aging process did not affect the results of the annealing process afforded by the 1st DSC scan process. The DMAs of the aged IPDI Thiol-Triallyl Triazine films were next measured both before and after annealing at 85 °C for 18 h. The results in Figure 5.4 a-b, summarized in Figure 5.4 c, for the $\tan \delta$ vs temperature plots indicate modest increases in the peak maxima as a result of the additional annealing process, consistent with the 2nd scan DSC results. For example, the film cured with a 10,080 mJ/cm² radiant exposure had T_g s of 101 °C (unannealed) and 108 °C (annealed). A pure 1:1 molar Tetra Thiol-Triallyl Triazine polymeric film cured and aged under identical conditions has T_g s of 62 °C (unannealed) and 66 °C (annealed). For comparison, T_g s of all aged TUTE films and the Tetra Thiol-Triallyl Triazine films are listed in Table 5.2. The TUTE based networks have much higher T_g s than the Tetra Thiol-Triallyl Triazine films. As addressed above, the T_g enhancement upon annealing the aged samples results from additional reaction at 85 °C. It seems reasonable that the combination of the triallyl triazine ring rigidity and the formation of strong hydrogen bonds via the thiourethane groups results in a network with high T_g .

Another important observation of the results in Figure 5.4 is the very narrow $\tan \delta$ peaks. For a pure thiol-ene system, the FWHM value can be as narrow as 15-20 °C.² As

mentioned in the Introduction section, these narrow glass transitions imply uniform thiol-ene molecular networks resulted from the step growth free-radical mechanism^{1,2} of thiol-ene reactions. Epoxy resins upon curing by a step growth mechanism also have narrow glass transition regions indicating network uniformity. The FWHM of epoxy networks can vary from ~ 20 °C to 60 °C.¹³⁻¹⁷ The $\tan \delta$ vs. temperature plot of the aged but unannealed IPDI Thiol-Triallyl Triazine film (cured with 10,080 mJ/cm² radiant exposure) has a FWHM value of 28 °C (Table 5.3). The $\tan \delta$ peak of the aged/annealed IPDI Thiol-Triallyl Triazine film cured with the same radiant exposure has a FWHM of 22 °C. The narrowed FWHMs after annealing indicate additional reactions, e.g. thiol-ene and thiol-isocyanate.

For photopolymerized H12MDI Thiol-Triallyl Triazine and TDI Thiol-Triallyl Triazine aged films, the T_g s are also much higher than those of the Tetra Thiol-Triallyl Triazine films and, in general, further increase by the annealing process (Figure 5.5). T_g s greater than 90 °C are achieved in the aged/annealed H12MDI and TDI films cured with the 5,040 mJ/cm² and 10,080 mJ/cm² UV radiant exposure. One particularly interesting observation of the results for the TDI Thiol-Triallyl Triazine films is the decrease in the T_g for the aged/unannealed samples for the higher radiant exposures (5,040 mJ/cm² and 10,080 mJ/cm²). This may be due both to the photodegradation that is well known for aromatic polyurethanes¹⁸ and/or absorption by the aromatic urethane groups that competes with absorption by the photoinitiator.

Physical Characterization of Films

We also subjected TUTE films to some general ASTM type tests traditionally used to assess their performance immediately after curing (no aging). The results for pendulum hardness values of these TUTE films are given Table 5.4. The initially unannealed IPDI Thiol and TDI Thiol based films have pendulum hardness values of up to twice that of the H12MDI film. A 2 h annealing process at 85 °C increases the pendulum hardness values of all three films to values near 200 s. The results of pencil hardness tests in Table 5.4 are in accordance with the pendulum hardness results. The unannealed IPDI Thiol-Triallyl Triazine and TDI Thiol-Triallyl Triazine films have medium hardness, while the unannealed H12MDI Thiol-Triallyl Triazine films are much softer. As with the pendulum hardness values, after annealing at 85 °C for 2 h, presumably additional thiol-ene curing and conversion of residual isocyanate groups obtained during the photocuring process takes place and the pencil hardness of all three films increased significantly to over 5H, indicating the formation of films with surface hardness comparable to traditional hard films reported in the literature.¹⁹⁻²¹ Obviously, the increase in conversion after the annealing process results in substantial enhancement of both the pencil and pendulum hardness of the TUTE films. Direct and reverse impact resistance values of the unannealed TUTE films were also obtained (Table 5.5). H12MDI Thiol based films perform better upon impact presumably because the cyclohexyl groups in the H12MDI structure provide a mechanism for better energy dissipation.²² Annealed samples were not evaluated due to difficulties in sample preparation and delamination

from the metal substrates during the annealing process. Additional results in Table 5.5 indicate that all three unannealed films have reasonable elongations and resistance to cracking upon bending. The TDI based film has greater elongation than the other two films, consistent with the lower T_g .

Conclusions

Thiourethane-thiol-ene (TUTE) films with high glass transition temperatures were prepared from the thiol-ene polymerization of a triene with multifunctional thiol oligomers based upon three diisocyanates: IPDI, H12MDI and TDI. Further increases in T_g were achieved after the initial photocuring process by aging and/or annealing at 85 °C due to additional reaction of the thiol and ene functional groups, as well as the reaction of isocyanates formed during the photocuring process. All the aged and annealed TUTE thiol-ene films had T_g s greater than 90 °C. The hardness of the initially (unaged) cured TUTE films increased markedly after annealing. Also, the unaged TUTE films exhibit fairly good impact and bending properties. Further work will involve more extensive evaluation of both aging (at room temperature) and/or annealing at elevated temperatures and correlation with changes in physical and mechanical properties.

Acknowledgements

This work was supported by the MRSEC Program of the National Science Foundation under Award Number DMR 0213883. We also acknowledge Bayer Materials Science for providing isocyanates.

References

1. Jacobine, A. F. In Radiation Curing in Polymer Science and Technology III: Polymerization Mechanisms; Fouassier, J. D.; Rabek, J. F., Eds.; London: Elsevier, 1993; Chapter 7, pp 219-268.
2. Hoyle, C. E.; Lee, T. Y.; Roper, T. J Polym Sci Part A: Polym Chem 2004, 42, 5301.
3. Cramer, N. B.; Bowman, C.N. Polym Prep 2003, 44, 17.
4. Jethmalani, J.; Dreher A. W.; Abdel-Sadek, G.; Chomyn, J.; Li J. M.; Qaddoura, M. U.S. Pat Appl Publ 20060052547, March 9, 2006.
5. Smith, R. A.; Herold, R. D.; Okoroafor, M. O. PCT Int Appl WO0064964, November 2, 2000.
6. Lu, H.; Carioscia, J. A.; Stansbury, J. W.; Bowman, C. N. Dental Materials 2005, 21, 1129-36.
7. Gush, D. P.; Ketley, A. D. Mod Paint Coat 1978, 68, 58.
8. Bowman, C. N.; Carioscia, J. A.; Lu, H.; Stansbury, J. W. PCT Int Appl WO2005086911, September 22, 2005.
9. Senyurt, A. F.; Wei, H. Y.; Phillips, B.; Cole, M.; Nazarenko, S.; Hoyle, C. E.; Piland, S. G.; Gould, T. E. Macromolecules 2006, 39(19), 6315-17.
10. Reddy, S. K.; Cramer, N. B.; Bowman, C. N. Macromolecules 2006, 39(10), 3681.
11. Wei, H, Y.; Senyurt, A. F.; Jonsson, S.; Hoyle, C. E. J Polym Sci Part A: Polym Chem 2007, 45, 822-29.
12. Odian, G., Ed. Principles of Polymerization; John Wiley & Sons, Inc.: Hoboken, New

Jersey, 2004; Chapter 2, pp 106-107.

13. Kenyon, A. S.; Nielsen, L. E. *J Macromole Sci Chem* 1969, A3(2), 275-95.

14. Mijovic, J.; Tsay, L. *Polym* 1981, 22, 902-06.

15. Crawford, E.; Lesser, A. J. *J Polym Sci Part B: Polym Phys* 1998, 36, 1371-82.

16. Miyagawa, H.; Mohanty, A. K.; Misra, M.; Drzal, L.T. *Macromol Mater Eng* 2004, 289, 636-41.

17. Huang, J. C.; Xiao, Y.; Mya, K. Y.; Liu, X. M.; He, C. B.; Dai, J.; Siow, Y. P. *J Mater Chem* 2004, 14, 2858-63.

18. Hoyle, C. E.; Kim, K. J.; No, Y. G.; Nelson, G. L. *J Appl Polym Sci* 1987, 34(2), 763-74.

19. Diakoumakos, C. D.; Jones, F. N. *J Appl Polym Sci* 2002, 84, 576-90.

20. Xu, J. W.; Pang, W. M.; Shi, W. F. *Thin Solid Films* 2006, 514, 69-75.

21. Almeida, E.; Alves, I.; Brites, C.; Fedrizzi, L. *Prog Org Coat* 2003, 46, 8-20.

22. Seeger, N. V.; Kaman, A. J. (PPG Industries, Inc.). U.S. Patent 4,041,208, August 9, 1977.

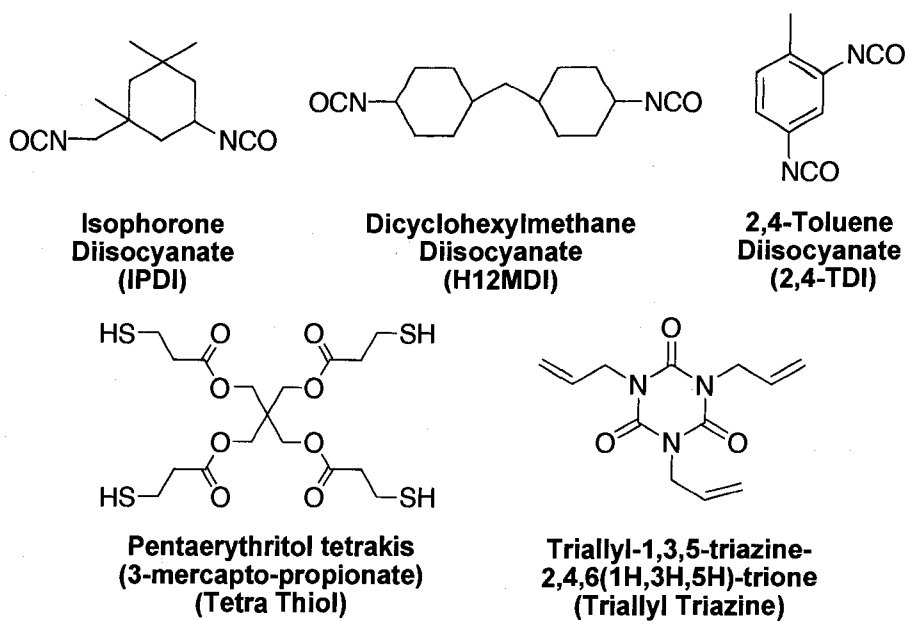


Chart 5.1. Structures of components.

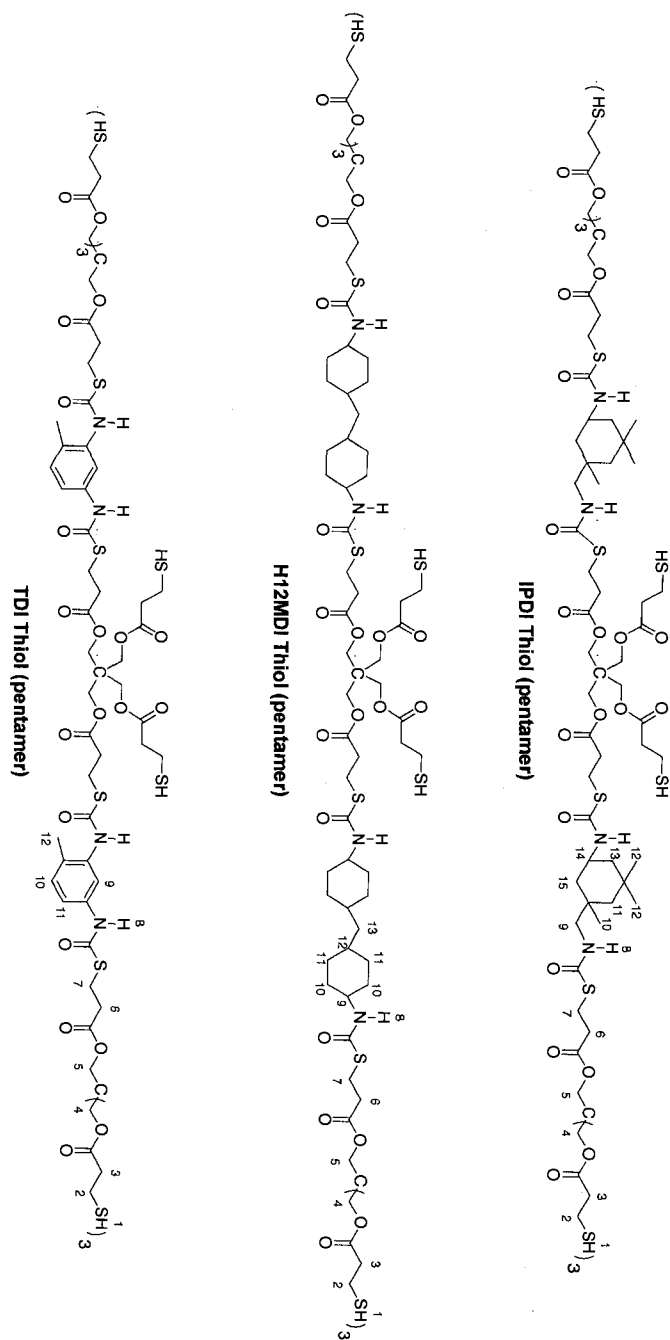
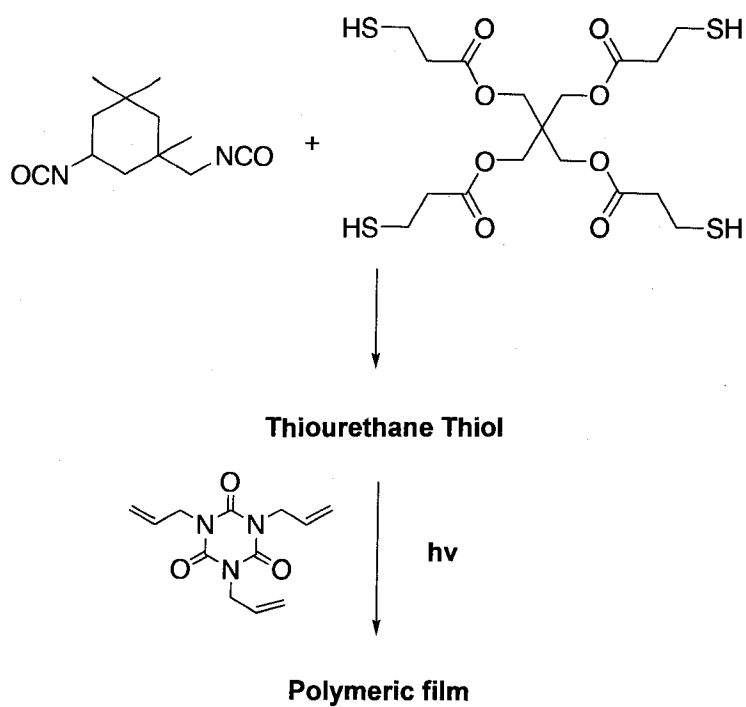


Chart 5.2. Representative average structures of the three thiol end-capped oligomers: IPDI Thiol pentamer, H12MDI Thiol pentamer and TDI Thiol pentamer (the hydrogens are numbered and their ^1H NMR chemical shifts are listed in Table 5.1 under the same number).



Scheme 5.1. Synthesis of IPDI Thiol and formation of the corresponding TUTE film.

Table 5.1. ^1H NMR chemical shifts of the SH end-capped oligomers.

H	δ (ppm)		
	IPDI Thiol	H12MDI Thiol	TDI Thiol
1	1.2	1.3	1.3
2	2.6-2.8	2.6-2.8	2.6-2.8
3	2.6-2.8	2.6-2.8	2.6-2.8
4	4.1	4.2	4.2
5	4.1	4.2	4.2
6	2.6-2.8	2.6-2.8	2.6-2.8
7	2.9-3.1	3.2	3.2
8	5.5-6.5	5.5-6.0	6.9-8.5
9	2.9-3.1	3.7	6.9-8.5
10	0.9-1.1	1.7	6.9-8.5
11	1.5-1.8	1.7	6.9-8.5
12	0.9-1.1	1.0-1.2	2.3
13	1.5-1.8	1.0-1.2	
14	3.5-3.6		
15	1.5-1.8		

Table 5.2. T_g s ($^{\circ}\text{C}$) of aged TUTE films and 1:1 molar Tetra Thiol-Triallyl Triazine films. All T_g s were measured by DMA operating at 1Hz and 3 $^{\circ}\text{C}/\text{min}$.

Sample Component	Heat Treatment	T_g ($^{\circ}\text{C}$)		
		1,008 (mJ/cm^2)	5,040 (mJ/cm^2)	10,080 (mJ/cm^2)
IPDI Thiol-Triallyl Triazine films	Unannealed	78	92	101
	Annealed	91	96	108
H12MDI Thiol-Triallyl Triazine films	Unannealed	87	92	95
	Annealed	94	94	93
TDI Thiol-Triallyl Triazine films	Unannealed	79	77	72
	Annealed	85	91	92
Tetra Thiol-Triallyl Triazine films	Unannealed	55	61	62
	Annealed	65	69	66

Table 5.3. FWHM values of $\tan \delta$ peaks of aged IPDI Thiol-Triallyl Triazine films.

Sample Component	Heat Treatment	FWHM (°C)		
		1,008 (mJ/cm ²)	5,040 (mJ/cm ²)	10,080 (mJ/cm ²)
IPDI Thiol-Triallyl Triazine films	Unannealed	18	24	28
	Annealed	18	20	22

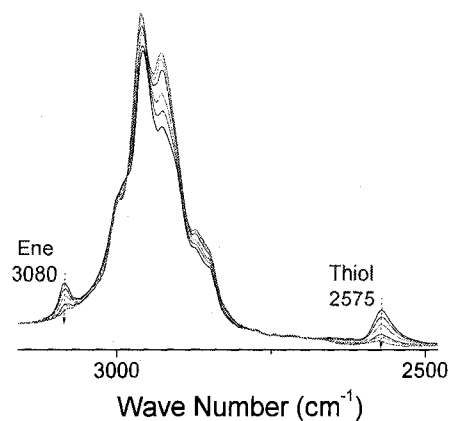
Table 5.4. Hardness of unaged TUTE films.

Sample Component	Persoz hardness (sec)		Pencil hardness	
	Unannealed	Annealed	Unannealed	Annealed
IPDI Thiol-Triallyl Triazine films	105	215	HB	7H
H12MDI Thiol-Triallyl Triazine films	45	186	5B	5H
TDI Thiol-Triallyl Triazine films	70	209	H	7H

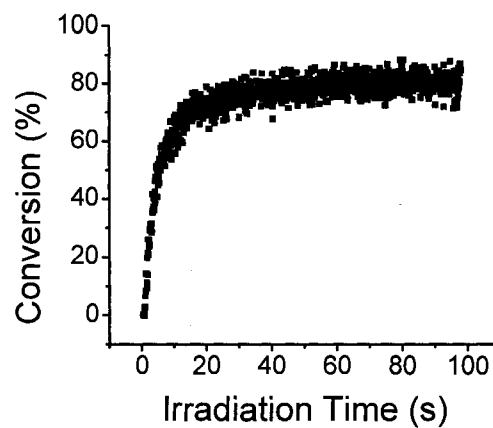
* Annealed samples were heated at 85 °C for 2 h

Table 5.5. Impact and elongation of unaged TUTE films.

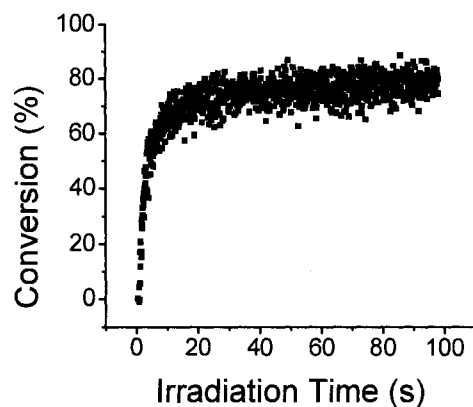
Sample Component	Impact		Bending	
	Direct (m-kg)	Reverse (m-kg)	Elongation (%)	Resistance to cracking (cm)
IPDI Thiol- Triallyl Triazine films	0.46	0.18	18.30	0.51
H12MDI Thiol- Triallyl Triazine films	0.86	0.46	19.10	0.33
TDI Thiol- Triallyl Triazine films	0.46	0.12	28.20	0.35



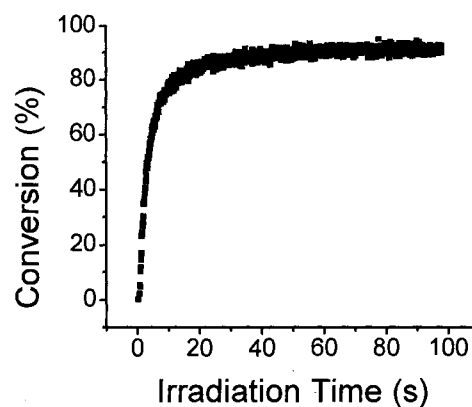
(a)



(b)



(c)



(d)

Figure 5.1. (a) RTIR spectra of thiol (2575 cm⁻¹) and ene (3083 cm⁻¹) in thiol-ene photopolymerization. Percent conversion of thiol group as a function of irradiation time of (b) IPDI Thiol-Triallyl Triazine, (c) H12MDI Thiol-Triallyl Triazine, and (d) TDI Thiol-Triallyl Triazine mixtures. Light intensity is 18.7 mW/cm² and 1 wt% of DMPA is used as photoinitiator.

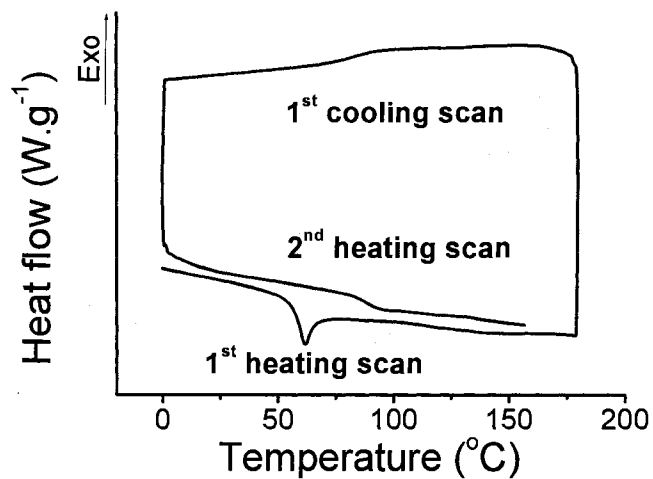
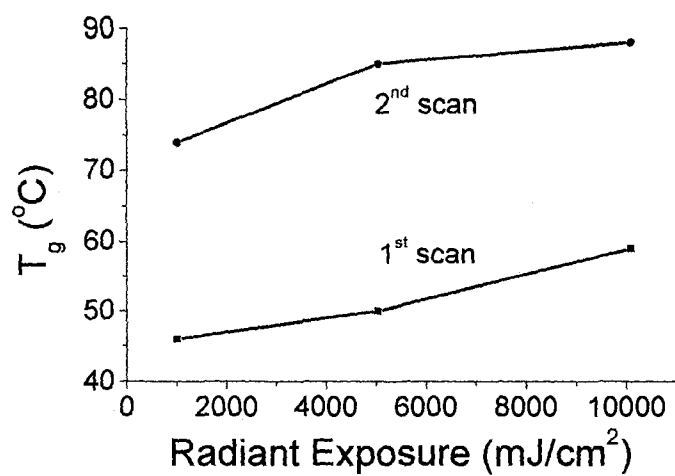
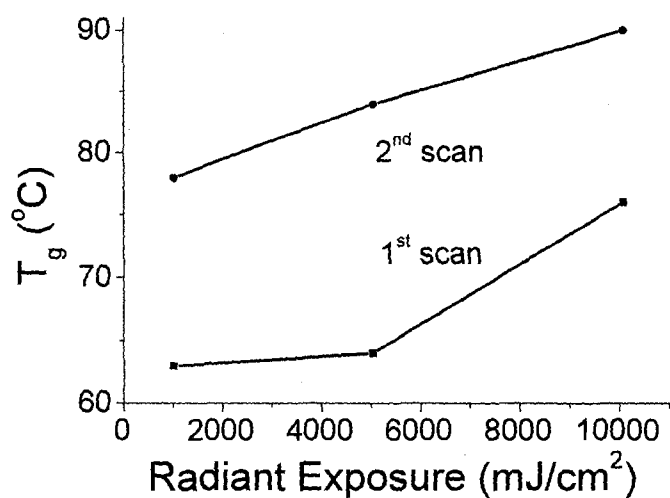


Figure 5.2. 1st and 2nd DSC heating scans and first DSC cooling scans for unaged IPDI Thiol-Triallyl Triazine films polymerized with UV radiant exposure of 10,080 mJ/cm^2 . All scans at 10 $^{\circ}\text{C}/\text{min}$.



(a)



(b)

Figure 5.3. T_g s of (a) unaged and (b) aged IPDI Thiol-Triallyl Triazine films determined from 1st and 2nd DSC heating scans at 10 °C/min.

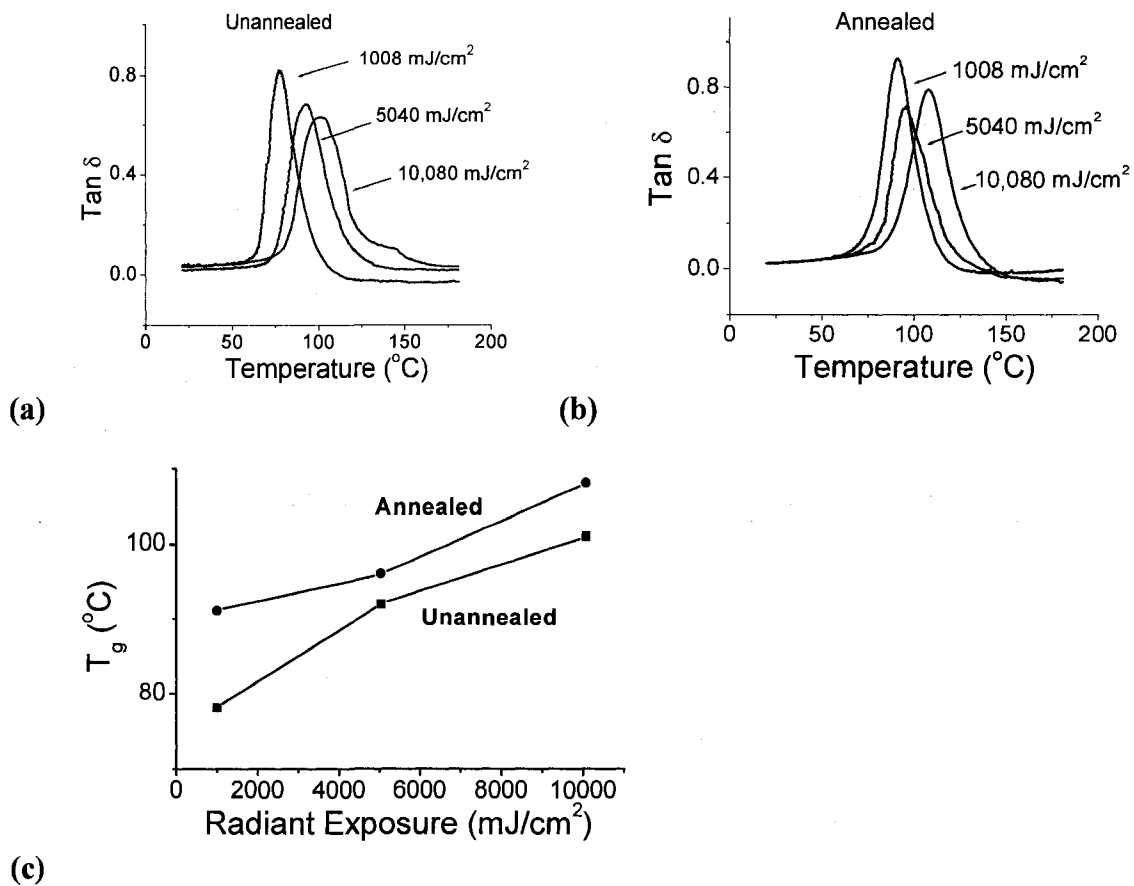
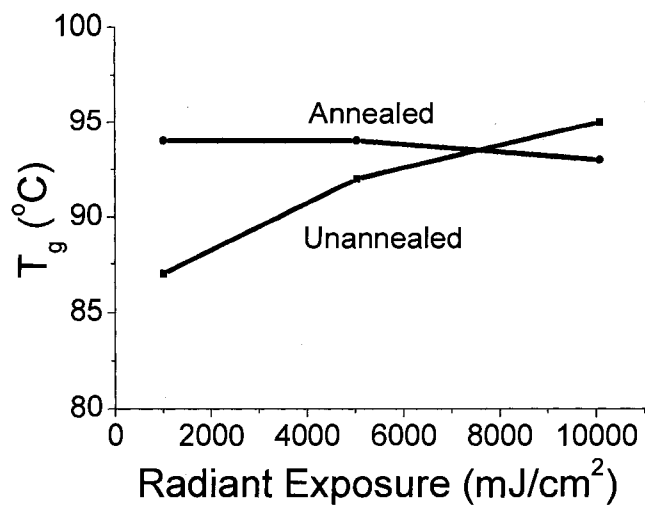
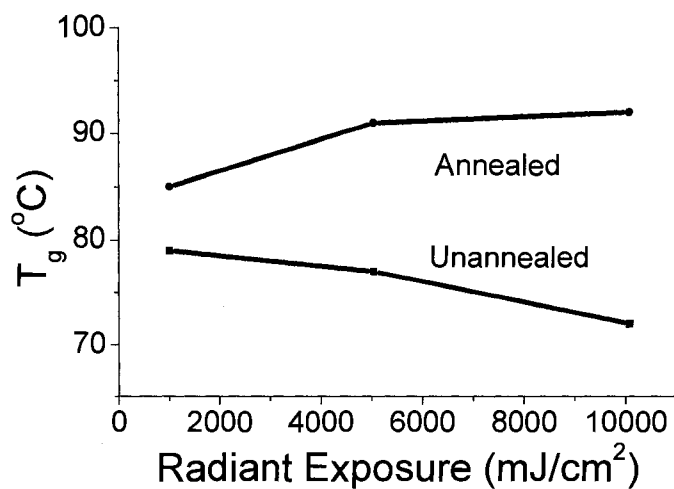


Figure 5.4. (a) $\tan \delta$ peaks for aged IPDI Thiol-Triallyl Triazine unannealed films. (b) $\tan \delta$ peaks for aged IPDI Thiol-Triallyl Triazine annealed (18 h, 85 $^{\circ}\text{C}$) films. (c) T_g obtained from $\tan \delta$ peak maxima in (a) and (b) vs. light radiant exposure. DMA scans obtained at 1Hz and 3 $^{\circ}\text{C}/\text{min}$.



(a)



(b)

Figure 5.5. (a) T_g of aged H12MDI Thiol-Triallyl Triazine films, and (b) T_g s of aged TDI Thiol-Triallyl Triazine films obtained by DMA at 1Hz and 3 °C/min. Annealed samples were heated at 85 °C for 18 h.

CHAPTER VI

PHYSICAL AGING OF THIOURETHANE THIOL-ENE NETWORKS

Abstract

The physical aging behavior of a class of photopolymerized thiourethane thiol-ene networks were characterized by thermal and spectroscopic analysis, the results of which are directly related to changes in macroscopic physical and mechanical properties. The hydrogen bonding associated with the thiourethane chemical structure exerts at most a slight retarding effect on the enthalpy relaxation, but there is a significant increase in the glass transition temperature of the thiourethane thiol-ene networks, an important implication for application of these materials and the stabilization of their physical, mechanical and thermal transition properties.

Introduction

When annealed at temperatures lower than its glass transition temperature, a polymer at a temperature below its glass transition temperature in the thermodynamic non-equilibrium state will approach the thermodynamic equilibrium state with coincident change in physical properties including a decrease in specific volume and enthalpy relaxation.^{1,2} The initial deviation from the equilibrium state at the physical aging temperature greatly depends on the thermal history of the glassy polymer which can be effectively removed by heating the polymer to the equilibrium state, approximately 50 °C higher than the glass transition temperature, and holding for more than 10 minutes.³ From

a practical point of view, physical aging is vital for any long-term application because the macroscopic properties of polymers change with time. This effect is accelerated when the polymer materials are maintained at a temperature close to their glass transition temperature.

Although hydrogen bonds, offering physical linkages within polymer matrices by restricting segmental and chain motions, may affect the relaxation process of macromolecules and help maintain the dimensional and physical properties of polymer materials, the physical aging of hydrogen bond containing polymer systems have not received much attention in the literature except for a limited number of reports.⁴⁻⁶

McGonigle et al.⁴ prepared a series of linear polystyrene copolymers that are capable of hydrogen bonding, the enthalpy relaxation and free volume changes of which were measured with differential scanning calorimetry (DSC) and positron annihilation lifetime spectroscopy (PALS). The physical aging process of these copolymers was shown to be sensitive to the formation of hydrogen bonds, resulting in slower relaxation rate during aging process compared to the polystyrene homopolymer. Through comparing the thermal properties of polystyrene, poly (4-hydroxystyrene) and poly (4-hydroxystyrene-co-styrene) measured by DSC, Yoshida et al. also found that the main chain motion and relaxation of polymers are restricted by hydrogen bonding. The relaxation time strongly depends on the content of hydroxyl groups in the copolymer.⁶ Upon characterizing the physical aging of the silica-poly(methyl methacrylate) (PMMA) nanocomposite by fluorescence spectroscopy, Priestley et al. found that the relaxation rate

of the 0.4 vol% silica-PMMA is 20 times slower than the PMMA polymer without nanoparticles.⁵ And via dielectric spectroscopy measurements, the strength of the β relaxation, being responsible for the physical aging and related to the motion of PMMA ester dipoles, was also reduced by about 50% for the silica-PMMA composite. These changes were attributed to the hydrogen bonds formed between the ester side groups of PMMA and the hydroxyl groups on the surface of the silica nanoparticles.

Understanding the effect of hydrogen bonding on sub- T_g aging in the glassy state is particularly important because of the wide applications of crosslinked polymers/polymer networks in industries including coatings and high performance materials. Hydrogen bonding containing thiourethane thiol-ene are ideal for probing such hydrogen bonding-aging effects due to their exceptional uniformity and high extent of hydrogen bonding.⁷ The uniform thiourethane thiol-ene networks were prepared from isocyanates, multifunctional thiol and multifunctional ene monomers as described in reference 7. It has been shown the glass transition temperatures of the thiourethane containing networks are significantly higher than the analogue hydrogen bonding free thiol-ene networks as a result of the formation of physical crosslinks due to hydrogen bonding. Herein, the thiourethane-thiol-ene networks were evaluated by DSC and the results were compared to base thiol-ene networks to illustrate the effect (very small) of hydrogen bonding on enthalpy relaxation (glass) of the networks. Changes in macroscopic properties such as the refractive index, Persoz pendulum hardness, and tensile stress/strain were also measured for samples subjected to sub- T_g aging.

Experimental

Materials

Dicyclohexyl methane diisocyanate (H12MDI), 2,4-toluene diisocyanate (TDI) and Isophorone diisocyanate (IPDI) were obtained from Bayer and used as received. Triallyl-1,3,5-triazine-2,4,6(1H,3H,5H)-trione (TTT) and pentaerythritol tetrakis(3-mercapto-propionate) (Tetra Thiol) were purchased from Aldrich Chemical Co. and used as received. The photoinitiator 2,2-dimethoxy-2-phenylacetophenone (DMPA) was obtained from Ciba Specialty Chemical Company. Other chemicals, such as anhydrous acetone, were also obtained from Aldrich Chemical Co. and used as received. The thiourethane thiol-ene (TUTE) films were prepared from diisocyanate, Tetra Thiol and TTT as described in detail elsewhere⁷ and shown in Scheme 6.1. TUTE films prepared from IPDI, TDI and H12MDI are designated IPDI Thiol-TTT, TDI Thiol-TTT and H12MDI Thiol-TTT, respectively. The base thiol-ene network, Tetra Thiol-TTT, was prepared from equal molar (based on functional groups) amounts of Tetra Thiol and TTT using 1 wt% of DMPA photoinitiator following a thiol-ene photopolymerization mechanism described elsewhere.^{7, 8} All films were postcured at temperatures higher than their glass transition temperature for 3-5 h to make sure complete conversion of functionalities was achieved; complete conversion was confirmed by FTIR showing no residual unreacted ene or thiol and DSC measurement which showed no shift in the glass transition temperature upon repeated heating scans for a specific sample.

Characterization

Tensile tests were conducted by clamping a piece of $\sim 125 \mu\text{m}$ film between the tensile clamps of a dynamic mechanical analysis (DMA), TA Q800 DMA (TA Instruments, Inc.), operating at a tension rate of 10 %/min with 0.05 N of preload force. The stress at break and strain at break was recorded as the tensile stress and tensile strain, respectively. The Persoz pendulum hardness of films ($\sim 125 \mu\text{m}$) on glass substrates was measured according to ASTM D-4366 using a BYK-Gardner pendulum hardness tester with a square frame pendulum. Refractive index of films ($\sim 125 \mu\text{m}$) was measured with a Bausch&Lomb ABBE-3L refractometer using 1-Bromonaphthalene as the contacting liquid between the sample film and the prism shield. A Bruker IFS 88 FTIR spectrometer operating at 5 scans/s was used to investigate films ($\sim 20 \mu\text{m}$) located in a sample chamber controlled by a Harrick temperature controller with an accuracy of $\pm 1 \text{ }^\circ\text{C}$. All differential scanning calorimetry (DSC) measurements were conducted with a TA Q100 (TA Instruments, Inc.). To investigate the effect of temperature on enthalpy relaxation of TUTE and base thiol-ene networks, $\sim 6 \text{ mg}$ of samples were annealed in situ in the DSC at various temperatures for 1 h (isochronal measurements), cooled down to $T_g - 50 \text{ }^\circ\text{C}$ and then reheated to $T_g + 50 \text{ }^\circ\text{C}$ to obtain the enthalpy relaxation peak (Figure 6.1a). To investigate the annealing time effect on enthalpy relaxation, films were annealed in situ in the DSC at $T_g - 10 \text{ }^\circ\text{C}$ for various period of time (isothermal experiments), cooled down to $T_g - 50 \text{ }^\circ\text{C}$ and then reheated to $T_g + 50 \text{ }^\circ\text{C}$ to obtain the enthalpy relaxation peak (Figure 6.1b). All cooling and heating rates were $10 \text{ }^\circ\text{C}/\text{min}$. In each DSC measurement, the sample was first annealed at $T_g + 50 \text{ }^\circ\text{C}$ for 30 min to remove any thermal history,

followed by cooling down to $T_g - 50$ °C and a subsequent heating scan to obtain the reference curve. Using TA Universal Analysis (V3.9A) software, the reference curve was subtracted from the following scan curves to produce recovery peaks around the glass transition region which are integrated to give the enthalpy loss values.

Results and Discussion

Physical and Mechanical Property Changes

The glass transition temperatures determined by DSC for all samples are listed in Table 6.1. Before measuring by DSC, all films were postcured for 20 h at temperatures higher than T_g to convert all unreacted functional groups and eliminate any postcuring effects on the DSC results. For all thiourethane thiol-ene films prepared from isocyanates, T_g s much higher than those of base thiol-ene films were observed. This is, at least partially, because of the hydrogen bonding associated with thiourethane linkages as reported in a previous publication.⁷ There may also be some effect on the T_g due to the higher functionality of the thiourethane thiol-ene films; however for thiols with functionality greater than four, the functionality is not expected to play a large role in determining the T_g since looping results from multiple reactions between interacting thiol and ene molecules.

It is well known that physical aging can cause changes in both microstructural and macrostructural properties include enthalpy, dielectric response and mechanical performance.¹ As shown in Figure 6.2, by annealing the IPDI Thiol-TTT film at 10 °C

lower than T_g for 20 h, increases in tensile stress, strain and Young's modulus are observed. This is due to the densification of network structure as well as the coincident conditions facilitating the formation of hydrogen bonding. The physical aging process, in principle, is reversible, resulting in reversible changes in physical properties. This is demonstrated in Figure 6.3 for the IPDI Thiol-TTT film, where the pendulum hardness of the IPDI Thiol-TTT film (measured at room temperature for each film) increases to over 250 s upon annealing at T_g-10 °C for 20 h. Upon further heating at 50 °C above the T_g for 30 min to remove the sub- T_g thermal aging history, the pendulum hardness of the film at room temperature returns to the original unannealed value, i.e., the sub- T_g aging process is recyclable.

Refractive index has also been used to monitor the physical aging process of polymers.⁹ In our case, both a thiourethane thiol-ene and a thiol-ene based film exhibit reversible changes in refractive indices upon annealing and heating. As shown in Figure 6.4, the refractive index of the IPDI Thiol-TTT film apparently increases upon annealing due to the increase in film density as suggested by the Lorentz-Lorenz equation,¹⁰

$$\frac{n^2 - 1}{n^2 + 2} = \frac{\rho N_{av} \alpha}{3M_0 \epsilon_0} \quad (1)$$

where n is the refractive index, ρ is the density of polymer, α is the average polarizability, ϵ_0 is the vacuum permittivity, N_{av} is the Avogadro constant and M_0 is the polymer molecular weight. Further heating of the film in the equilibrium rubbery state removes the thermal history and the refractive index of the film returns to the initial value. The

reversible change in refractive index is also observed for the TetraThiol-TTT based thiol-ene film.

Isochronal Measurements

In order to investigate the effect of annealing temperature (T_a) on sub- T_g aging of the thiourethane thiol-ene and thiol-ene films, enthalpy relaxation was measured by DSC as described in the Experimental section. As shown for an example system in Figure 6.5a, IPDI Thiol-TTT films were annealed in the DSC at various temperatures ranging from 10 °C above T_g to 25 °C below T_g . The relaxed enthalpy obtained by subtracting the reference peak area from the enthalpy recovery peak area is plotted as a function of T_a in Figure 6.5b. At annealing temperatures higher than T_g where molecular chains are mobile, no enthalpy recovery peaks are detected. With the decrease of annealing temperature to T_g , enthalpy recovery peaks appear implying that network relaxation occurs, which is reasonable considering that the glass transition region extends over a finite temperatures range. With a further decrease of the annealing temperature, significant enthalpy recovery peaks are observed at T_g-5 °C to T_g-15 °C. When the annealing temperature is too low to activate effective segmental motion, e.g. T_g-20 °C and T_g-25 °C, enthalpy relaxation is hindered and therefore, in the 1 h annealing process, only a very limited amount of enthalpy recovery will be obtained. The same trend can be observed in Figure 6.6 for the Tetra Thiol-TTT film. It is noted that the relaxed enthalpy of the IPDI Thiol-TTT film approaches zero for T_g-T_a values less than 20 °C, while that of Tetra Thiol-TTT remains measurable at temperatures up to T_g-40 °C. This small effect may reflect the role of

hydrogen bonding in limiting the extent of enthalpy relaxation during the 1 h annealing period; however, no conclusions can be made.

All of the other thiourethane thiol-ene films were measured by DSC following the same procedures used to obtain the data in Figure 6.5, and the recovered enthalpy is plotted as a function of annealing temperature in Figure 6.7. At essentially all annealing temperatures, the TetraThiol-TTT sample exhibited a little greater enthalpy relaxation than all of the thiourethane thiol-ene samples, and a significant amount of relaxation for the 1 h aging process can still be observed even at 40 °C below T_g . The slightly lower relaxation tendency of the thiourethane thiol-ene networks may be related to the hydrogen bonding. But the retarding effect of hydrogen bonding is not as great as those shown for linear polymers reported in the literature.^{4,5} This is presumably because that the physical aging of the networks prepared from multifunctional thiol and enes has already been greatly restricted by the very high network density. Therefore, the additional hydrogen bonding may not generate any significantly effect on the already restricted relaxation of molecular chains.

Isothermal Measurements

To compare the enthalpy relaxation rate of TetraThiol-TTT and the thiourethane thiol-ene networks, the films were annealed at a specific temperature for different periods of time and measured by DSC scans at 10 °C/min as described in the Experimental section. For all samples, T_g-10 °C was selected as the annealing temperature where the highest extent of relaxation was found for each system in the 1 h annealing process

(Figure 6.7).

As seen in Figure 6.8 for the TetraThiol-TTT and IPDI Thiol-TTT networks, an increase in enthalpy relaxation occurs with an increase in annealing time. As shown in Figure 6.9, the slope of the enthalpy relaxation versus log annealing time plot typically used to assess the rate of enthalpy relaxation¹¹⁻¹⁸ is greatest for the TetraThiol-TTT network. This may reflect a restrictive effect of hydrogen bonding on the relaxation of the network structure. However, due to the significant difference in the chemical structures of the thiols, it must be concluded that any effect of hydrogen bonding, if any, is very small. The enthalpy relaxation rate, β_H ,¹¹⁻¹⁹

$$\beta_H = -\frac{d\Delta H}{d \log t_a} \quad (1)$$

for each of the networks calculated from the linear least-square fit of the relaxation loss data shown in Figure 6.9 is given in Table 6.2. Again, slightly slower enthalpy relaxation rates were found for each of the thiourethane thiol-ene networks, but this may not be correlated with a retarding effect of hydrogen bonding on the relaxation process^{4-6, 20} since the difference in β_H are very small and again there are significant structural differences in the thiols. We note that the linear relationship between enthalpy loss and log annealing time in Figure 6.9 is clear over the measured time range with no signs of leveling off. It has been noted that the time required for achieving enthalpic equilibrium states in linear polymers is very long.²¹ For example, the reported polystyrene with the β_H of 0.85 at $T_g - 15$ °C requires over 100 h to achieve its enthalpic equilibrium states. The

thiol-ene based networks, clearly do not achieve enthalpic equilibrium within the 20 h annealing period.

FTIR Investigation

Thiourethane linkages (-N(H)-C(=O)-S-) have similar hydrogen bonding capabilities that are essentially identical to the analogous urethane groups (-N(H)-C(=O)-O-).²² Since hydrogen bonding is an vital factor affecting properties of urethane type polymers, it is important to understand the effect of physical aging on hydrogen bonding. The change of hydrogen bonding before, during and after physical aging process of thiourethane thiol-ene networks can be easily monitored by FTIR. Basically, when a functional group, e.g. the NH group in thiourethanes, is involved in hydrogen bonding, its IR characteristic band will shift to lower frequencies.^{23, 24} When hydrogen bonding is disrupted at elevated temperature its IR band will shift to higher frequencies.^{23, 24} As shown in Figure 6.10, the IR spectra of the IPDI Thiol-TTT film in the region of the hydrogen bonded N-H stretching band at $\sim 3350\text{ cm}^{-1}$, heated to $T_g+50\text{ }^\circ\text{C}$ to remove thermal history, followed by annealing at $T_g-10\text{ }^\circ\text{C}$, or $83\text{ }^\circ\text{C}$, for 20 h (curve b, measured at $83\text{ }^\circ\text{C}$ immediately after annealing and curve c, measured when the annealed sample is cooled to $25\text{ }^\circ\text{C}$) shows no noticeable shift in the NH band compared to the spectrum recorded before the 20 h annealing process (curve a). A semiquantitative analysis of N-H hydrogen bonding fraction, $F_{b,NH}$, can be obtained using equation 2,²⁴⁻²⁶

$$F_{b,NH} = \frac{1}{1 + 3.46 \frac{A_{f,NH}}{A_{b,NH}}} \quad (2)$$

where $A_{f,NH}$ and $A_{b,NH}$ are the absorbance of free ($\sim 3236 \text{ cm}^{-1}$) and hydrogen bonded NH groups ($\sim 3360 \text{ cm}^{-1}$), respectively. The area of the free and hydrogen bonded bands are obtained through a peak deconvolution method described elsewhere.²⁴ The results in Figure 6.11 show that $F_{b,NH}$ for the aged IPDI Thiol-TTT (84.0 % for curve b and 86.4% for curve c) is essentially identical to the value of $F_{b,NH}$ (85.4%) for the same sample prior to the 20 h annealing process.

Conclusions

The effect of annealing temperature and annealing time on the enthalpy relaxation of thiol-ene and thiourethane thiol-ene networks have been investigated qualitatively by DSC, and quantitatively by relaxation rate calculations. Compared with a model thiol-ene network, all of the hydrogen bonding containing thiourethane thiol-ene networks exhibit almost identical enthalpy relaxation rates at $T_g - 10 \text{ }^\circ\text{C}$. FTIR analysis of IPDI Thiol-TTT films indicated no change in the extent of hydrogen bonding upon sub- T_g aging. The hydrogen bonding associated with the thiourethane linkages thus influence the networks in one distinct way. By introducing hydrogen bonding, the glass transition temperatures of the networks are very high compared to traditional thiol-ene systems. However, there appears to be little effect of hydrogen bonding on enthalpy relaxation of these dense networks.

Acknowledgements

This work was supported by the MRSEC Program of the National Science Foundation under Award Number DMR 0213883. Materials were generously provided by Bayer Materials Science, Bruno Bock and Ciba Specialty Chemicals.

References

1. Hutchinson, J. M. *Progress in Polymer Science* **1995**, 20, 703-760.
2. Cowie, J. M. G.; Ferguson, R. *Macromolecules* **1989**, 22, 2307.
3. Cowie, J. M. G.; Ferguson, R. *Polymer Communication* **1986**, 27, 258.
4. McGonigle, E.-A.; Cowie, J. M. G.; Arrighi, V. *Journal of Materials Science* **2005**, 40, 1869.
5. Priestley, R. D.; Rittigstein, P.; Broadbelt, L. J.; Fukao, K.; Torkelson, J. M. *Journal of Physics: Condensed Matter* **2007**, 19, 205120.
6. Yoshida, H.; Nakamura, K.; Kobayashi, Y. *Polymer Journal* **1982**, 14, (11), 855.
7. Li, Q.; Zhou, H.; Wicks, D. A.; Hoyle, C. E. *Journal of Polymer Science: Part A: Polymer Chemistry* **2007**, 45, 5103.
8. Hoyle, C. E.; Lee, T. Y.; Roper, T. *Journal of Polymer Science: Part A: Polymer Chemistry* **2004**, 42, 5301.
9. Robertson, C. G.; Wilkes, G. L. *Polymer* **1998**, 39 (11), 2129.
10. Mills, N. J., In *Encyclopedia of Polymer Science and Engineering*, 2 ed.; Mark, H. F.; Bikales, N. M.; Overberger, C. G.; Menges, G.; Kroschwitz., J. I., Eds. John Wiley and Sons: New York, 1987; Vol. 10, p 493.
11. Bauwens-Crowet, C.; Bauwens, J. C. *Polymer* **1986**, 27, 709.
12. Wang, C.-H.; Filisko, F. E. *Polymeric Materials Science and Engineering* **1990**, 62, 782.
13. Bair, H. E.; Johnson, G. E.; Anderson, E. W.; Matsuoka, S. *Polymer Engineering and*

Science **1981**, 21, 930.

14. Cowie, J. M. G.; Elliott, S.; Ferguson, R.; Simha, R. *Polymer Communication* **1987**, 28, 298.

15. Roe, R.-J.; Millman, G. M. *Polymer Engineering and Science* **1983**, 23, 318.

16. Montserrat, S.; Colomer, P.; Belana, J. *Journal of Materials Chemistry* **1992**, 2, 217.

17. Pappin, A. J.; Hutchinson, J. M.; Ingram, M. D. *Macromolecules* **1992**, 25, 1084.

18. Montserrat, S. *Journal of Polymer Science: Part B: Polymer Physics* **1994**, 32, 509.

19. Pan, P.; Zhu, B.; Inoue, Y. *Macromolecules* **2007**, 40, 9664.

20. Yoshida, H.; Kanbara, H.; Takemura, N.; Kobayashi, Y. *Sen'i Gakkaishi* **1983**, 39, (12), T512.

21. Petrie, S. E. B. *Journal of Polymer Science: Part A2* **1972**, 10, 1255.

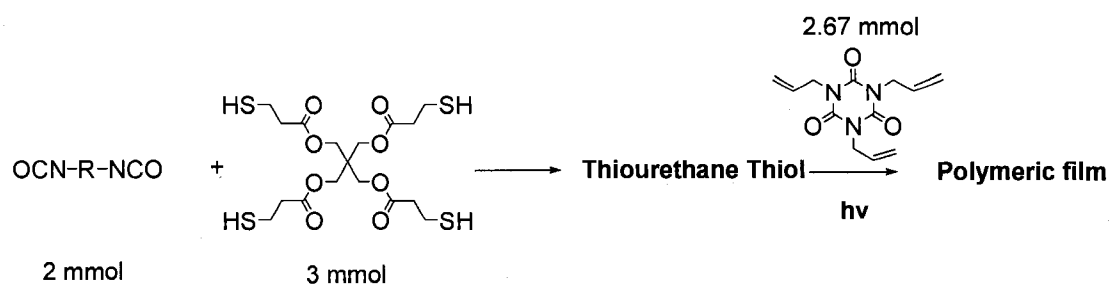
22. Li, Q.; Zhou, H.; Hoyle, C. E.; Magers, D.; Wicks, D. A. *Submitted to Macromolecules* **2008**.

23. Joesten, M. D.; Schaad, L. J., *Hydrogen Bonding*. Marcel Dekker, Inc: New York, 1974.

24. Zhou, H.; Li, Q.; Lee, T. Y.; Guymon, A. C.; Jonsson, S. E.; Hoyle, C. E. *Macromolecules* **2006**, 39, 8269-8273.

25. Seymour, R. W.; Estes, G. M.; Cooper, S. L. *Macromolecules* **1970**, 3, 579.

26. Xiu, Y.; Zhang, Z.; Wang, D.; Ying, S.; Li, J. *Polymer* **1992**, 33, 1335.



Scheme 6.1. Preparation of thiourethane-thiol-ene films. IPDI, TDI and H12MDI were used as the diisocyanates to prepare thiourethane thiols with different structures.

Table 6.1. Glass transition temperatures of thiourethane-thiol-ene and the base thiol-ene networks measured with DSC operating at 10 °C/min and full width of half maximum (FWHM) of Tan δ peaks measured with DMA operating at 3 °C/min.

	Tetra Thiol-TTT	IPDI Thiol-TTT	H12MDI Thiol-TTT	TDI Thiol-TTT
T_g (°C)	47	93	86	83

Table 6.2. Enthalpy relaxation rate of thiol-ene and thiourethane-thiol-ene networks.

	Tetra Thiol-TTT	IPDI Thiol-TTT	H12MDI Thiol-TTT	TDI Thiol-TTT
β_H (Jg ⁻¹ per decade)	0.88	0.83	0.77	0.76
R	0.997	0.998	0.998	0.997

* R is the correlation coefficients of the linear fit.

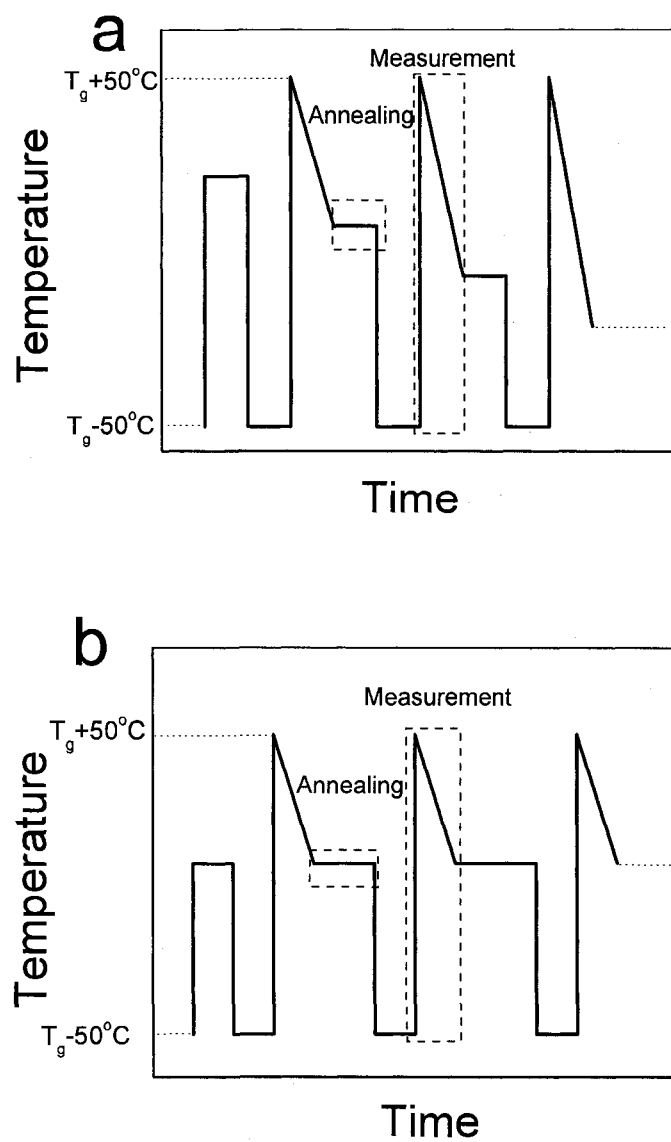


Figure 6.1. Schematic illustration of DSC measurements of enthalpy relaxation.

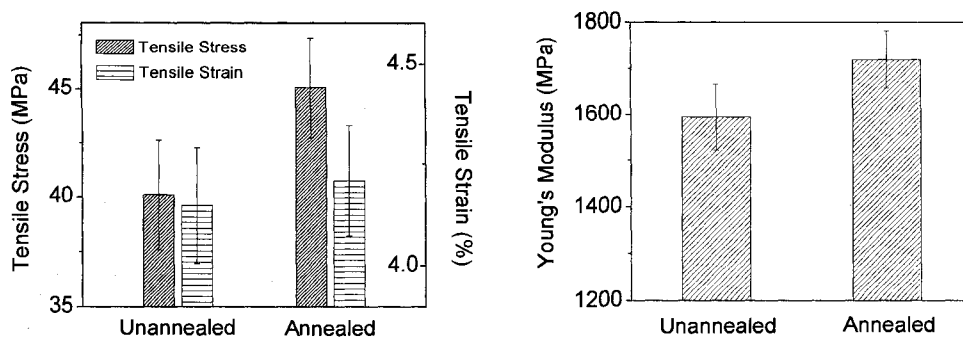


Figure 6.2. Tensile stress and strain of unannealed and annealed (T_g-10 °C for 20 h) IPDI Thiol-TTT film measured at room temperature.

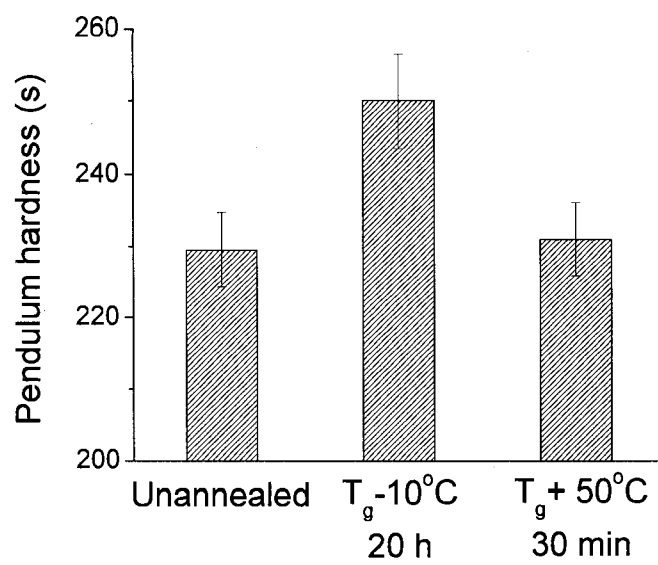


Figure 6.3. Pendulum hardness of IPDI Thiol-TTT film measured at room temperature.

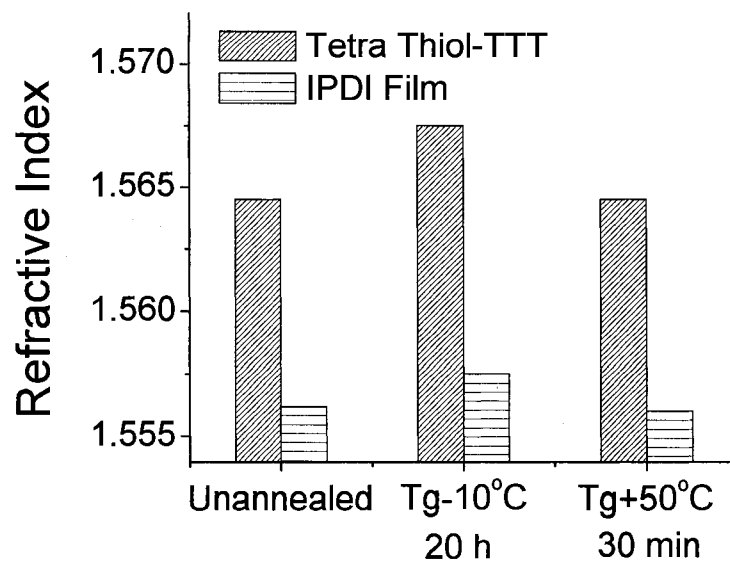
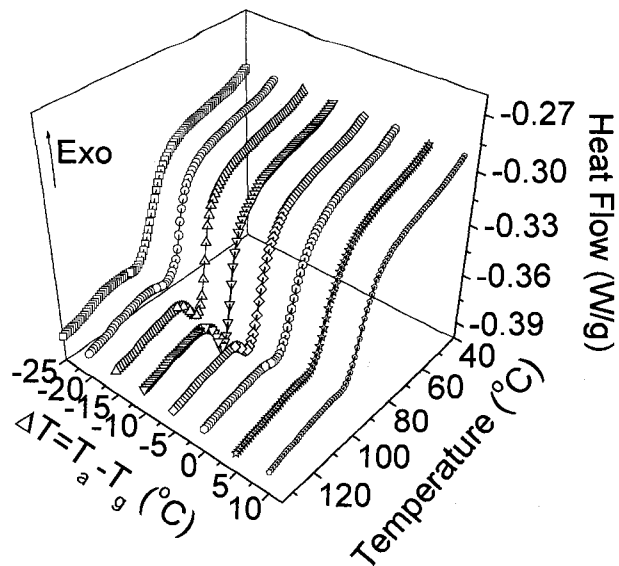
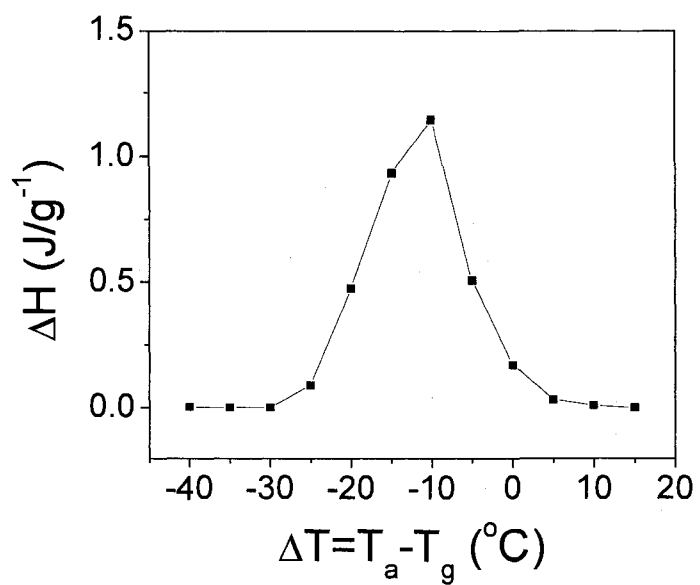


Figure 6.4. Refractive index of IPDI Thiol-TTT and Tetra Thiol-TTT films measured at room temperature.

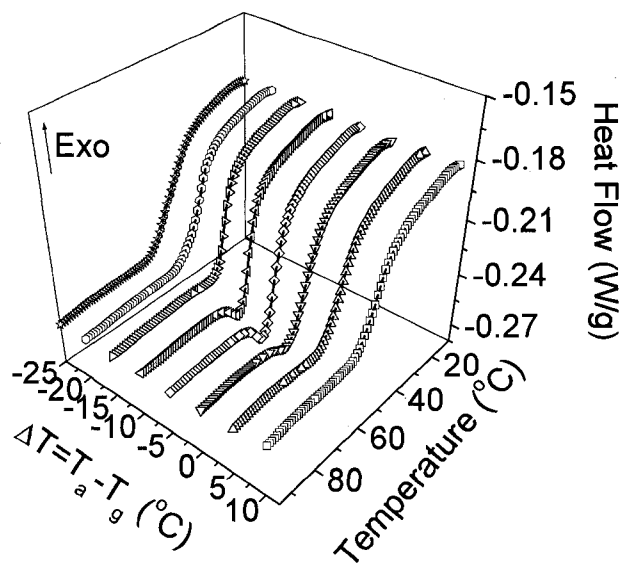


a

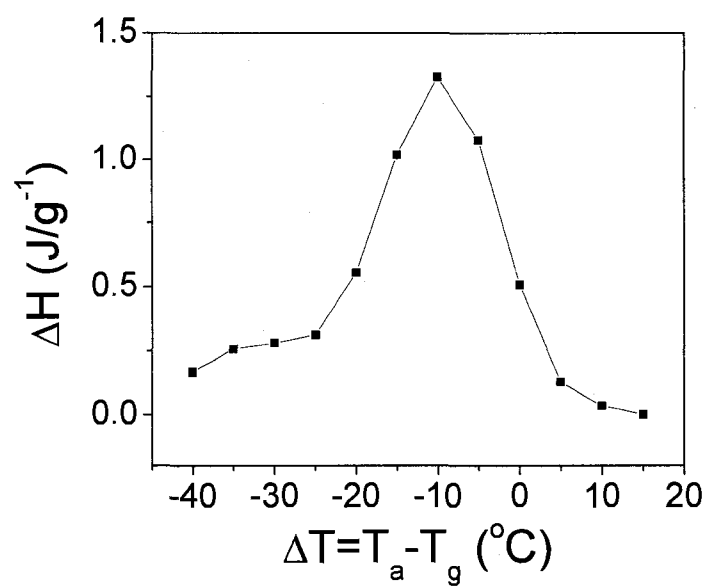


b

Figure 6.5. Enthalpy relaxation of IPDI Thiol-TTT film annealed for 1 h at various temperatures measured with DSC.



a



b

Figure 6.6. Enthalpy relaxation of TetraThiol-TTT film annealed at various temperatures measured with DSC.

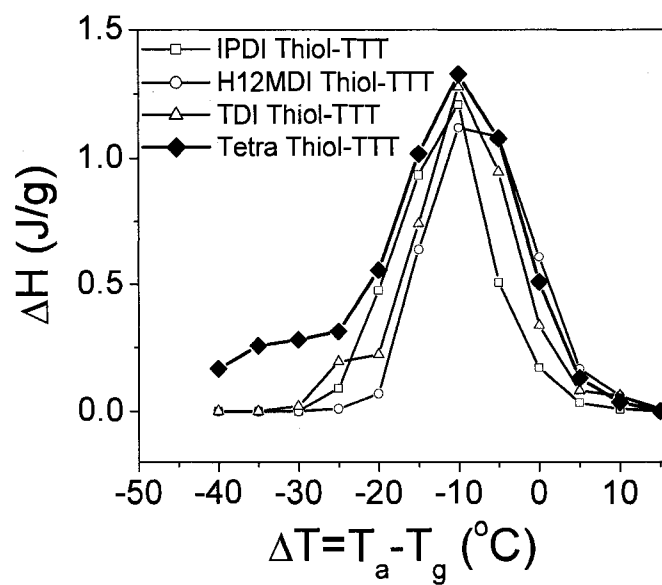


Figure 6.7. Relaxed enthalpy of all thiol-ene films as a function of annealing temperature.

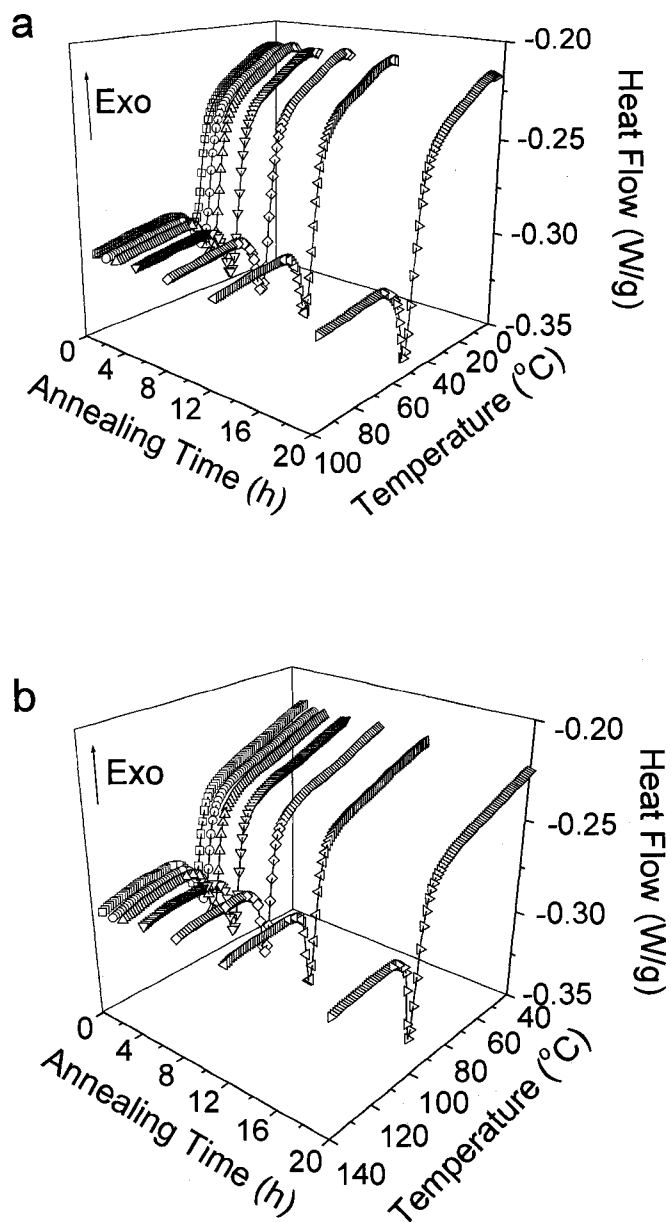


Figure 6.8. DSC curve of (a) Tetra Thiol-TTT network and (b) IPDI Thiol-TTT network annealed for different time periods.

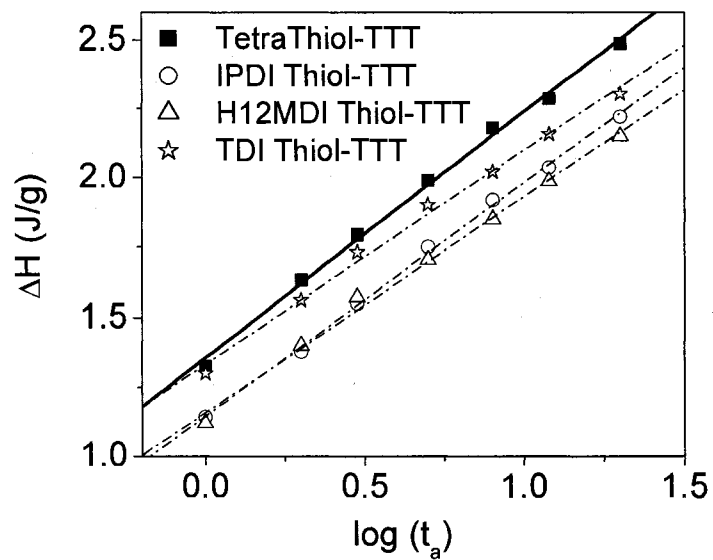


Figure 6.9. Enthalpy relaxation of thiol-ene and thiourethane thiol-ene networks as a function of annealing time (t_a) at T_g-10 °C.

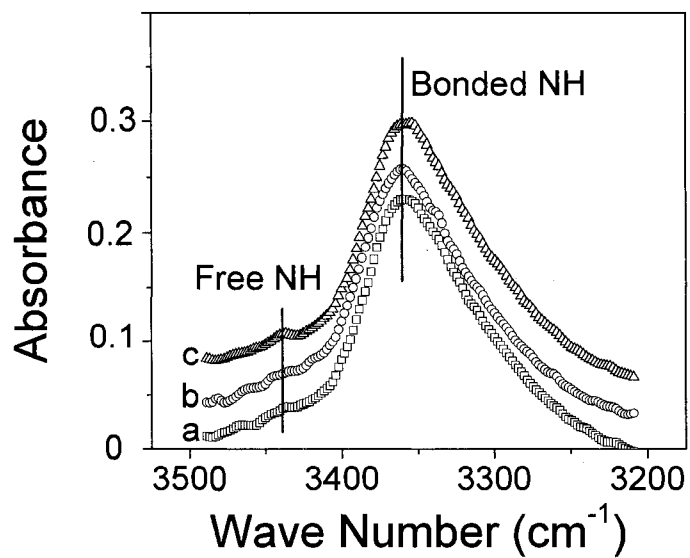


Figure 6.10. FTIR spectra of the NH group of the IPDI Thiol-TTT network measured at different conditions: (a) unannealed, (b) immediately after annealing at T_g-10 °C for 20h, and (c) when the annealed sample is cooled to 25 °C. The thermal history has been removed by heating at 150 °C for 30 min before FTIR measurements.

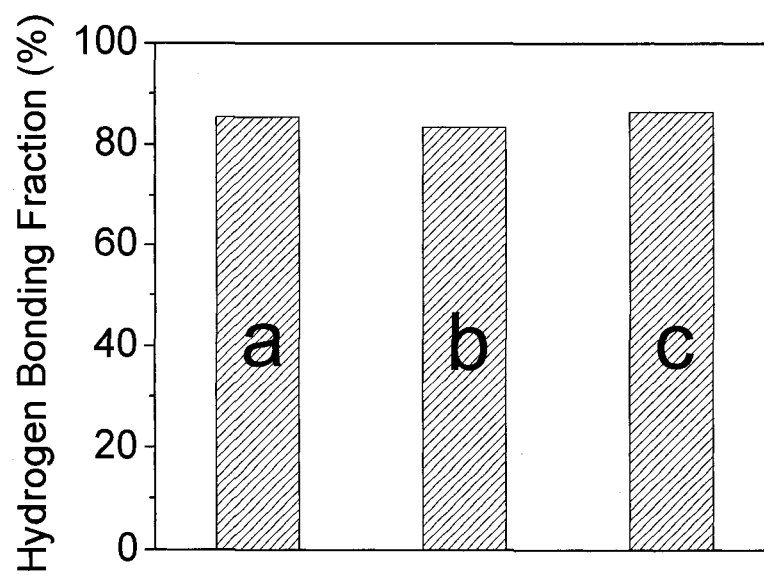


Figure 6.11. Hydrogen bonding fraction of samples a, b and c in Figure 6.10.

CHAPTER VII

COMPARISON OF SMALL MOLECULE AND POLYMERIC URETHANES,
THIOURETHANES AND DITHIOURETHANES: HYDROGEN BONDING AND
THERMAL, PHYSICAL AND MECHANICAL PROPERTIES. PART 1

Abstract

The hydrogen bonding behavior of a homologous series of small molecule and polymeric carbamate, thiocarbamates and dithiocarbamate, was investigated in solution, melt and solid states. The relative hydrogen bonding strengths in these systems were evaluated, and the results compared to theoretical calculations of hydrogen bonding strength. The polyurethane and polythiourethane were found to have approximately equivalent physical and mechanical properties as a result of a similar extent of hydrogen bonding, whereas the polydithiourethane model compound, due to a lower degree of hydrogen bonding, has reduced thermal and mechanical transition temperatures as well as lower hardness values. The polythiourethane and polydithiourethane networks exhibit narrower glass transitions compared to polyurethane networks, apparently the result of an efficient isocyanate/isothiocyanate-thiol reaction with little or no side products. Due to weakness of the C-S bond compared to the C-O bond, thiourethanes and dithiourethanes have lower thermal stability than corresponding urethanes. Finally the thiourethanes and dithiourethane have higher refractive index values than their urethane counterparts.

Introduction

Polyurethanes, since their discovery in 1947,¹ have been widely used in many coatings² and elastomer³ applications due to an extraordinary combination of physical and mechanical properties. Accordingly, the structure-property relationships of polyurethanes have been extensively studied.^{2, 4-11} Hydrogen bonding, providing physical linkages within the material matrix, is a vital factor that determines the microscopic and macroscopic properties of polyurethanes, including their phase behavior, glass transition temperature, strength and stiffness.^{8, 9} Considerable effort has been extended to understand the hydrogen bonding behavior of polyurethanes in both segmented systems and polymer blends.^{4, 6, 10, 11}

Although the reactions of thiols and isocyanates have also been known for a long time^{12, 13} and the resultant polythiourethanes (containing a structure unit as -N(H)-C(=O)-S-) are used in many modern applications including optical lenses due to high refractive index values^{14, 15} and advanced coatings,¹⁶⁻¹⁸ the basic physical and mechanical properties of thiourethanes/polythiourethanes have not been characterized to the same extent as their urethane counterparts, although limited literature can be found on synthesis/catalysis,^{12, 13} reaction kinetics,¹⁹ thermodynamic transitions²⁰ and hydrogen bonding.^{21, 22} Materials based on a similar structure, dithiourethane or dithiocarbamate, -N(H)-C(=S)-S-, have also been explored for use in optical applications due to their high refractive index values.^{14, 15}

One of the distinct advantages of thiourethane and dithiourethane chemical

structural units is the feasibility of incorporating them into photopolymerizable systems which has the potential of opening up whole new application areas. For example, in our previous study on photopolymerized thiol-ene films,²³ a notable enhancement in glass transition temperature was attained for thiourethane-thiol-ene (TUTE) systems presumably due to several factors including the hydrogen bonding associated with the thiourethane linkages. However, questions related to the strength of the hydrogen bonds of thiourethanes and dithiourethanes compared with those of ordinary urethanes and the corresponding effect on polymer properties remain to be delineated.

From both a basic and practical view point, a detailed investigation and comparative analysis of the hydrogen bonding behavior of a homologous family of structures including urethanes (-N(H)-C(=O)-O-), thiourethanes (-N(H)-C(=O)-S-) and dithiourethanes (-N(H)-C(=S)-S-), and the resulting correlation of polymer structure and physical, mechanical and optical properties is important in establishing guidelines for future development. Accordingly, to provide a comprehensive understanding of the hydrogen bonding behavior of each urethane type (polyurethane, polythiourethane and polydithiourethane) and to characterize critical structure-property relationships, a series of small molecule model compounds were synthesized. The relative strength of their hydrogen bonds was measured in solution and melt, and the results correlated with theoretical calculations. Based on the results of these simplified model systems, a contiguous set of polyurethane, polythiourethane and polydithiourethane networks were evaluated, and the effect of hydrogen bonding on physical and mechanical properties was

determined. The polyurethane and polythiourethanes were found to exhibit similar properties, quite different from those of polydithiourethanes, apparently due to differences in hydrogen bonding. The results reported herein are important in providing a clear theoretical and experimental basis for tailoring polymer properties through introducing different urethane type linkages, i.e., urethanes, thiourethanes and dithiourethanes.

Experimental

Materials

Chemicals for model compound synthesis, hexyl isocyanate (HI), hexyl isothiocyanate (HIT), 1-hexanol (HA), 1-hexanethiol (HT), butyl 3-mercaptopropionate (BMP), 1,6-hexanediol (HexDiol), 1,6-hexanedithiol(HexDithiol), dibutyltin dilaurate (DBTDL) and triethylamine (TEA) were purchased from Aldrich Chemical Co. and used as received. 1,6-Hexamethylene diisocyanate (HDI) and the HDI trimer or Desmodur® N3600 (3NCO) were obtained from Bayer Materials Science and used as received. 1,6-Hexane diisothiocyanate (HDIT) was purchased from Trans World Chemicals Inc. and used as received. Trimethylolpropane tris(3-mercaptopropionate) (TriThiol) was obtained from Bruno Bock Thiochemical and used as received. Other chemicals, such as anhydrous acetone, were also obtained from Aldrich Chemical Co. and used as received.

Preparation

Typical procedures for synthesizing the small molecule model compounds listed

in Scheme 7.1, N-hexyl hexylcarbamate (HIHA), N-hexyl S-hexylcarbamate (HIHT), and N-hexyl S-butyl 3-mercaptopropionate thiocarbamate (BMPHI), and N-hexyl S-butyl 3-mercaptopropionate dithiocarbamate (BMPHIT) are as follows (HIHA is taken as an example). 0.03 Mol of hexyl isocyanate and 0.03 mol of 1-hexanol were first charged into a 3 neck flask before 10 mL of hexane was added. The reactor was then purged with dry N₂ for 30 min followed by 0.02 wt% of dibutyltin dilaurate (DBTDL) being added and stirred. The mixture was allowed to react for 8 h at 65 °C under dry N₂ flow. All the model products were purified by recrystallization from hexane 2-3 times, and their structures verified by nuclear magnetic resonance spectroscopy (NMR). TEA was used in all thiol reactions with isocyanates or isothiocyanates due to its highly efficiency as a catalyst.²⁴ DBTDL was used in all alcohol reactions.

¹H NMR:

HIHA (CDCl₃): δ 0.89 (t, 6H, -CH₃), 1.30 (m, 12H, -CH₂-), 1.55 (m, 4H, -CH₂-), 3.17 (q, 2H, -CH₂-N), 4.04 (t, 2H, -CH₂-O-), 4.60 (s, 1H, -N(H)-).

HIHT (CDCl₃): δ 0.88 (t, 6H, -CH₃), 1.29 (m, 12H, -CH₂-), 1.55 (m, 4H, -CH₂-), 2.90 (q, 2H, -CH₂-N), 3.29 (t, 2H, -CH₂-S-), 5.25 (s, 1H, -N(H)-).

BMPHI (CDCl₃): δ 0.93 (t, 6H, -CH₃), 1.29 (m, 8H, -CH₂-), 1.56 (m, 4H, -CH₂-), 2.69 (t, 2H, -CH₂-C(=O)-), 3.15 (t, 2H, -CH₂-S-), 3.27 (q, 2H, -CH₂-N), 4.10 (t, 2H, -CH₂-O-), 5.27 (s, 1H, -N(H)-).

BMPHIT (CDCl₃): δ 0.93 (t, 6H, -CH₃), 1.32 (m, 8H, -CH₂-), 1.56 (m, 4H, -CH₂-), 2.77 (t, 2H, -CH₂-C(=S)-), 3.51 (t, 2H, -CH₂-S-), 3.72 (q, 2H, -CH₂-N), 4.11 (t, 2H,

-CH₂-O-), 7.02 (s, 1H, -N(H)-).

To prepare the polymeric networks, 3NCO-HexDiol and 3NCO-HexDithiol (Scheme 7.2), 0.03 mol of 3NCO and 0.02 mol of HexDiol (or HexDithiol) were first charged into a scintillation vial before 2 mL of anhydrous acetone was added to form a transparent solution. ~0.03 Wt% (based on the whole mixture) of DBTDL (or ~0.003 wt% of TEA) was then added to the monomer solution and mixed homogeneously. The solution was then evenly coated onto a piece of clean glass, followed by purging with dry N₂ in a sealable chamber for 1 h at room temperature, curing at 80 °C overnight and heating under vacuum (70 °C) for about 24 h. This yielded completely cured 200 μm thick film with no trace of solvent (verified by FTIR at 2272 cm⁻¹ and thermal gravimetric analysis). To prepare HDI-TriThiol and HDIT-TriThiol (Scheme 7.2), 0.006 mol of TriThiol and 0.009 mol of HDI (or HDIT) were charged into a scintillation vial and mixed homogeneously before 0.01 wt% (or 0.4 wt%) of TEA was added and mixed. The mixture was then coated onto a piece of clean glass using a 5 mil draw down bar, followed by purging with dry N₂ in a sealable chamber for 1 h, curing at 80 °C overnight and then heating under vacuum to yield transparent films with thicknesses of ~120 μm. The HDI-TriThiol films were completely cured (total loss of NCO groups at ~2272 cm⁻¹) and the conversion of isothiocyanate groups (~2082 cm⁻¹) in HDIT-TriThiol films was ~99%. The type and concentration of catalysts were adjusted for each system, as described above, to achieve efficient curing, while also allowing enough time for mixing and film coating.

Characterization

Proton nuclear magnetic resonance (^1H NMR) spectra were obtained on a Mercury 300 (Varian Inc.) spectrometer, the temperature of which was controlled by a Bruker Variable Temperature Unit equipped with a Eurotherm 818 Controller. Each spectrum was recorded as the co-addition of 64 scans after 25 min of equilibrium at the desired temperature. For regular NMR measurements, concentrations of 3.7 mM (in either CDCl_3 or d-DMSO) were used for small molecules in solution. Regular and temperature-resolved infrared spectra were collected on a Bruker IFS 88 FTIR spectrometer by holding samples (small molecules or polymer films prepared) sandwiched between two NaCl plates in a heating unit controlled by a Harrick temperature controller with an accuracy of ± 1 °C. Each spectrum was recorded after equilibrating for 25 min at the desired temperature. Peak deconvolution was conducted using a Gaussian function in Origin software to obtain free and hydrogen bonded NH peaks as described elsewhere.²⁵ Thermal stability of model polymers were measured with a TA Q60 (TA Instruments, Inc.) thermal gravimetric analysis (TGA) operating at a heating rate of 20 °C/min. Glass transition temperatures were measured with a TA Q1000 differential scanning calorimetry (DSC) operating at 10 °C/min and a TA Q800 dynamic mechanical analysis (DMA) operating at 1 Hz and 3 °C/min. Two heating scans were conducted for all samples and the second scan were selected to determine T_g values using TA Universal Analysis software (V 3.9A). Tensile properties measurements were also conducted on the TA Q800 DMA using the strain rate module operating at a strain rate of

10 %/min. Pencil hardness was measured according to ASTM D-3363. The Persoz pendulum hardness was measured according to ASTM D-4366 using a BYK-Gardner pendulum hardness tester with a square frame pendulum. At least six tests were performed for each film (different parts of the film) coated on a glass substrate and the average value of the six was taken as the final result. Adhesion tests were conducted according to ASTM D 3359-02. All of the computations of hydrogen bonding energy were performed using density function theory. The function employed was the three-parameter B3 hybrid function of Becke²⁶ and the LYP correlation function of Lee, Yang and Parr.²⁷ The basis sets used were the correlationally-consistent basis sets cc-pVDZ²⁸ and cc-pVTZ²⁹ created by Dunning and coworkers. The cc-pVDZ basis set uses a double-zeta description for valence electrons, while the cc-pVTZ basis employs a triple-zeta description for valence electrons. Both basis sets use a single-zeta description for core electrons, and both have a consistent set of polarization functions. Refractive index was measured by a Bausch&Lomb ABBE-3L refractometer at 24 °C at a wavelength of 589 nm. 1-Bromonaphthalene was applied between the sample film and the prism shield. The density of the polymers was measured using a density column constructed from toluene and carbon tetrachloride according to ASTM-D 1505.

Results and Discussion

Model Compounds in Solution

To ascertain the position of hydrogen bonded and free N-H peaks, model

compounds in solution were measured by infrared spectroscopy as described in the Experimental section. The FTIR spectra of the carbamate (HIHA), thiocarbamates (HIHT and BMPHI), and the dithiocarbamate (BMPHIT) are shown in Figure 7.1. At very low concentrations, e.g. 0.37 mM and 3.7 mM, where the model compounds are unable to associate through hydrogen bonding, only free N-H stretching peaks appear at about 3453 cm^{-1} (HIHA), 3428 cm^{-1} (HIHT), 3428 cm^{-1} (BMPHI), and 3376 cm^{-1} (BMPHIT). Generally, intermolecular hydrogen bonding is not likely to occur at a concentration lower than 10 mM in a nonpolar solvent.³⁰ Apparently, the difference in free N-H peaks position is due to a variation in hydrogen bonding strength caused by the electronegativity difference of sulfur and oxygen atoms in the urethane, thiourethane and dithiourethane groups. At higher concentrations, e.g. 74 mM and 185 mM, however, both the free N-H peak at higher frequencies and the hydrogen-bonded N-H peak at lower frequencies are present. The shift of the N-H peak reflects a decrease in bond strength resulting from the formation of hydrogen bonds. A big difference is observed between the spectra of BMPHI and BMPHIT. A significant contribution from the NH hydrogen bonded to the carbonyl oxygen is present in the BMPHI solution at a concentration of 185 mM, while for the dithiocarbamate BMPHIT, the hydrogen bonded NH peak is only found at a much higher concentration, i.e. 925 mM. This indicates a lower propensity for hydrogen bonding for the dithiourethane in solution compared to the urethane and thiourethane.

To confirm the above observations, the model compounds were dissolved in both

polar and nonpolar solvents and the ^1H NMR recorded to determine the effect of hydrogen bonding on the chemical shifts of the NH protons. Figure 7.2 shows the NMR spectra of HIHA in neat d-DMSO and CDCl_3 as an example. The concentration (3.7 mM) is so low that no inter- or intra- molecular hydrogen bonds are formed between HIHA molecules in the nonpolar solvent (CDCl_3) as observed by FTIR, and by inference in d-DMSO. The only possible hydrogen bonding is between HIHA and d-DMSO. In d-DMSO, hydrogen bonds are formed between the model compound NH groups and the sulphinyl group ($-\text{S}=\text{O}$) of d-DMSO, resulting in a downfield shift of the NH proton peak due to a decrease in electron density around the NH proton and a corresponding increase in the asymmetry of the electron density due to the polarization of the NH bond by the $-\text{S}=\text{O}$ group.³¹ The extent of this shift or the difference in chemical shifts for associated and unassociated NH is a direct indication of the ability of the NH group to form hydrogen bonds with an oxygen acceptor.³¹ The stronger the hydrogen bond formed, the greater the downfield shift. As already mentioned the unassociated NH chemical shift refers to that at infinite dilution. This was confirmed since the NMR results show no significant change in the NH peak upon diluting the HIHA/ CDCl_3 solution to as low as 0.37 mM (not shown). The chemical shift of the NH in CDCl_3 (3.7 mM) can thus be regarded as the unassociated value for comparison purposes. The chemical shift of NH in d-DMSO can then be taken as the associated NH value representing the hydrogen bonding between the NH of HIHA and the sulphinyl group of d-DMSO. NMR spectra were recorded for all the model compounds in a similar manner to that for HIHA in

Figure 7.2, and the results are plotted in Figure 7.3. As shown in Figure 7.3, there is only a small difference in the values ($\delta_{d\text{-DMSO}} - \delta_{\text{CDCl}_3}$) obtained for HIHA and HIHT, indicating similar strengths of the urethane and thiourethane hydrogen bonds. Also, BMPHIT does not show a lower shift value than BMPHI, indicating that the hydrogen bonding forming ability of the donor group, NH, is not adversely affected by the substitution of the carbonyl group with the thiocarbonyl. This suggests that the lower extent of hydrogen bonding found by FTIR in Figure 7.1 for BMPHIT results from the effect of sulfur on the hydrogen bonding capability of the carbonyl oxygen.

Another interesting characteristic of BMPHI and BMPHIT is the intramolecular hydrogen bonding that forms between the NH proton and the ester carbonyl hydrogen bonding acceptor, in addition to the NH proton hydrogen bonding with the carbonyl on the urethane/dithiourethane group. An effective way to quantify the extent of intramolecular hydrogen bonding can be expressed as

$$vr = \frac{\delta_{d\text{-DMSO}} - \delta_{\text{CDCl}_3}}{\delta_{\text{ref}}} \quad (1)$$

where δ_{ref} is the chemical shift of a reference compound with a similar structure to the compound being evaluated, but free of intramolecular hydrogen bonding.^{32, 33} A vr value smaller than 1.0 indicates the formation of intramolecular hydrogen bonding; the smaller the value, the greater the extent of intramolecular hydrogen bonding. Because of the similar structures of HIHT and BMPHI, HIHT can serve as a reference compound for BMPHI for comparison purposes. The calculated vr value of 1.03 indicates that no

intramolecular hydrogen bonds are formed. If any such bonds were formed, a significant bonded IR peak should have been observed at the concentrations around 3.7 mM.³⁴

However, as shown in Figure 7.1 and 7.2 this is clearly not the case for either BMPHI or BMPHIT.

Model Compounds: Melt

The melting point of the small model compounds measured by DSC are listed in Table 7.1. The two thiourethanes have similar melting points, higher than those of the urethane and the dithiourethane. The melting point is influenced by hydrogen bonding as well as other factors related to the unit crystal structure. Temperature-resolved infrared spectroscopy, an effective technique that has been extensively used to investigate hydrogen bonding,^{6, 7, 31, 35} was employed to measure the hydrogen bonding behavior of model compounds on a semiquantitative basis. Two distinctly separated NH peaks, representing free (higher frequency) and bonded (lower frequency) groups, are observed within the NH stretching region of HIHA and HIHT (Figure 7.4). A reduction in the bonded peak intensity and a corresponding increase in the intensity of the free peak with increasing temperature clearly illustrates disassociation of hydrogen bonds at elevated temperature. Similar changes are also observed in the IR spectra of BMPHI and BMPHIT. However, compared with the symmetrical and sharp bonded peaks of HIHA and HIHT, the bonded NH stretch bands of BMPHI and BMPHIT are unsymmetrical and much broader than those of HIHA and HIHT (Figure 7.4).

The absorbance of each peak, free and bonded, obtained through a peak

deconvolution method described previously,²⁵ can be used to approximate the hydrogen bonding fraction ($F_{b,NH}$), the percent of NH groups involved in hydrogen bonding, based on the equation given below^{5, 36}

$$F_{b,NH} = \frac{1}{1 + 3.46 \frac{A_{f,NH}}{A_{b,NH}}} \quad (2)$$

where $A_{f,NH}$ and $A_{b,NH}$ are the absorbance of free and hydrogen bonded NH groups, respectively, and the constant 3.46 is used as the extinction coefficient ratio of the bonded and free NH groups. Although, as stated in the literature,⁴ the extinction coefficient of the NH group changes with the strength of the hydrogen bond, for semi-quantitative comparison purposes, the error introduced by using 3.46 is minimal.

The NH stretching region of HIHA and HIHT can be deconvoluted into two distinct peaks, the free NH and the bonded NH peak. In the deconvolution process applied to BMPHI and BMPHIT, however, to obtain satisfactory curve fits, two peaks must be included in the bonded region (Figure 7.5). This is reasonable considering that two types of hydrogen bonding acceptors exist for BMPHI and BMPHIT, the ester carbonyl and the thiourethane carbonyl, or dithiourethane thiocarbonyl. The competition between different types of acceptors are well known in similar polyester and polyether urethanes.^{5, 37-39} The assignments of all the peaks are listed in Table 7.2 for comparison. The thiourethane bonded peaks in HIHT and BMPHI appear at exactly the same frequency with the same frequency shift value ($\Delta\nu$). The two ester bonded peaks in BMPHI and BMPHIT appear at different frequencies as a result of differences in electron

density, consistent with reported shifts of about 80 cm^{-1} for urethane systems.^{5, 37}

The hydrogen bonding fractions of each sample as a function of temperature, calculated using equation 2, are shown in Figure 7.6. The $A_{b,NH}$ values of BMPHI and BMPHIT are the result of adding the absorbances of the ester bonded peaks and the thiourethane/dithiourethane bonded peaks. In each case, with an increase in temperature, the hydrogen bonding fraction decreases as a result of disassociation. HIHA and HIHT show very similar hydrogen bonding fractions at a given temperature, indicative of similar hydrogen bonding ability. Due to the abundant hydrogen bonding acceptors present, BMPHI has the greatest extent of hydrogen bonding at a given temperature. Although the dithiocarbamate, BMPHIT, as a result of a high concentration of carbonyl acceptors, still has a hydrogen bonding fraction of over 70%, the weaker hydrogen bonding forming ability of thiocarbonyl results in measurably lower hydrogen bonding fraction at a given temperature than its thiourethane analogue, especially at elevated temperatures. These results are in agreement with the weaker hydrogen bonding ability of the thiocarbonyl (C=S) group compared to the carbonyl group (C=O) determined by FTIR and crystallographic measurements has been reported.^{22, 40}

The contributions of ester, thiourethane and dithiourethane groups can be quantitatively expressed by,

$$C_{\text{Ester}} = \frac{A_{b,\text{Ester}}}{A_{b,\text{Ester}} + A_{b,\text{Thiourethane}}} \quad (3)$$

$$C_{\text{Thiourethane}} = \frac{A_{\text{b,Thiourethane}}}{A_{\text{b,Ester}} + A_{\text{b,Thiourethane}}} \quad (4)$$

$$C_{\text{Dithiourethane}} = \frac{A_{\text{b,Dithiourethane}}}{A_{\text{b,Ester}} + A_{\text{b,Dithiourethane}}} \quad (5)$$

where C and A stand for the contribution and the NH group absorbance, respectively.

Although the extinction coefficient of NH groups bonded with different acceptors may be different, the results of these simple calculations are still reasonable for comparison purposes. As shown in Figure 7.7, for the thiocarbamate, BMPHI, the initial contribution (35°C) of the ester group, 33%, is much lower than that of the thiourethane group, 67%. These values change very little with an increase in temperature, indicating a stronger hydrogen bonding forming ability of the thiourethane carbonyl groups compared to the ester carbonyls. Interestingly, for BMPHIT, at room temperature, an equal amount of hydrogen bonds are formed between the NH hydrogen and the ester carbonyl and thiocarbonyl groups. With an increase in temperature, the contribution of the ester groups sharply increases to over 60% while that of the dithiourethane groups decreases to less than 40%, consistent with weaker and less stable hydrogen bonding between NH and the thiocarbonyl groups.

Model compounds were also investigated with temperature-resolved ^1H NMR spectroscopy. For all of the model compounds (the results for HIHA in Figure 7.8 are shown as an example), the NH peaks exhibit an upfield shift due to the disassociation of hydrogen bonds as temperature increases, while the position of all other peaks remain unchanged. Apparently, the extent of the shift ($\Delta\delta = \delta_{35^\circ\text{C}} - \delta_{105^\circ\text{C}}$) is related to hydrogen

bonding strength since more energy is required to reduce stronger hydrogen bonding. The temperature dependant chemical shift coefficient, $\Delta\delta/\Delta T$, that have been used to distinguish between free and bonded NH in peptides and amides,^{34, 41-43} can also be used to evaluate the extent of hydrogen bonding. As shown in Figure 7.9 and Table 7.3, as expected, the urethane, HIHA, and thiourethane, HIHT, have similar coefficient values that are larger than that of the ester containing BMPHI which has greater hydrogen bonding forming capability. Interestingly, BMPHIT, exhibiting lower extent of hydrogen bonding in all other measurements reported herein, has a lower value than BMPHI. This inconsistency were also observed in the literature³⁴ which claims that it is difficult to correlate the extent of hydrogen bonding with $\Delta\delta/\Delta T$ values because both free hydrogen bonds and very stable hydrogen bonds result in lower chemical shift coefficient values.

Theoretical Calculations

In order to substantiate the experimental results, *ab initial* calculations were conducted for urethane, thiourethane and dithiourethane models. To simplify the calculation process, the model compounds shown in Chart 7.1 were used to conduct the theoretical calculation. The conclusions regarding the relative strength of hydrogen bondings can be readily extended to the more complicated models in Scheme 7.1. As shown in Table 7.4, the urethane and the thiourethane models have almost identical hydrogen bonding energies between N-H and C=O, while weaker hydrogen bonds are calculated for the dithiourethane model. This supports the experimental FTIR and NMR results. We note that based upon the theoretical hydrogen bonding energies in Table 7.5

and the margin of error in the theoretical calculations, it is not possible to predict whether the carbamate or the thiocarbamate has a higher hydrogen bonding energy.

Polymer Networks

To achieve an understanding of the hydrogen bonding behavior of urethane, thiourethane and dithiourethane groups when incorporated into polymer structures, a polyurethane, two polythiourethanes and a polydithiourethane were prepared as described in the Experimental Section (see Scheme 7.2 for polymer acronyms). The mechanical, spectral, and thermal properties of the 3NCO-HexDiol and 3NCO-HexDithiol networks have been measured to provide an evaluation of any differences between the urethane (-N(H)-C(=O)-O-) and thiourethane (-N(H)-C(=O)-S-) linkages in the representative polymer networks. Differences in hydrogen bonding between thiourethane and dithiourethane (-N(H)-C(=S)-S-) groups in the networks will be evaluated by comparing corresponding experimental results for HDI-TriThiol and HDIT-TriThiol. Before continuing we point out that the protocol used to cure each film resulted in essentially quantitative conversion (confirmed by FTIR) of all isocyanates and isothiocyanates in each case. However, in the case of the 3NCO-HexDiol films, although the curing takes place in a dry N₂ atmosphere, there is the potential for side reactions which may consume some of the isocyanate groups.⁴⁴

Thermogravimetric analysis of each polymer was first conducted (Figure 7.10) at a heating rate of 20 °C/min. For 3NCO-HexDiol and 3NCO-HexDithiol, the onset of weight loss of the urethane and thiourethane linkages occurred at 291 °C and 258 °C,

respectively, followed presumably by decomposition of the isocyanurate at temperatures greater than 380 °C.⁴⁵ An enhanced thermal stability of the polyurethane is attributed to the higher bond energy of the C-O bond than the C-S bond.⁴⁶ HDI-TriThiol and HDIT-TriThiol also show a two-step decomposition process involving the thermal decomposition of the thiourethane and dithiourethane linkages followed by decomposition of the TriThiol segments at higher temperatures. The lower thermal stability of the polydithiourethane is consistent with a literature report that dithiourethanes undergo decomposition at temperatures between 150 °C and 200 °C with the aid of AgNO₃.⁴⁷ While the conditions for thermal decomposition in Figure 7.10 certainly do not include a catalytic process, the low onset temperature is consistent with that reported by Gomez et al.⁴⁷

Following the analysis used in the investigation of the small molecule models, temperature-resolved FTIR spectral measurements were also made for the four urethane-type polymers over a temperature range from 25 °C to 125 °C. Figure 7.11 shows a plot of the hydrogen bonding fraction of polymer networks as a function of temperature that is consistent with the results for the small molecule models. The fraction of hydrogen bonding for the polyurethane and two polythiourethane networks is greater than the hydrogen bonding fraction for the polydithiourethane. The thiourethane, HDI-TriThiol, benefits from the less sterically hindered ester groups of the flexible trithiol based species resulting in the highest extent of hydrogen bonding. As observed for the small molecule compounds, analysis of the contributions of the two different carbonyl

donors in HDI-TriThiol and HDIT-TriThiol indicates that the thiourethane carbonyl dominates the hydrogen bonding in the former polymer, while hydrogen bonding to the thiocarbonyl groups in the polydithiourethane at elevated temperature is significantly reduced (Figure 7.12).

In an attempt to determine any physical/thermal differences in the four urethane type polymers, a battery of thermal and mechanical property measurements were made. The DSC thermal scans in Figure 7.13, and corresponding T_g values in Table 7.5, are all above room temperature, although the T_g for HDIT-Trithiol is not much greater than room temperature. The T_g of 3NCO-HexDithiol is only 2 °C greater than 3NCO-HexDiol. Its glass transition region is very narrow and there is a distinct enthalpy relaxation peak. These results are strong indication of a very uniform structure in the case of the 3NCO-HexDithiol network. The polythiourethane (HDI-TriThiol) has a higher T_g than that of the polydithiourethane (HDIT-TriThiol). This can be attributed to the chain rigidity afforded by the higher hydrogen bonding fraction and hydrogen bond strength for HDI-Trithiol compared to HDIT-TriThiol (see Figures 7.11 and 7.12). However, it should be noted that the T_g difference between the polythiourethane and the polydithiourethane is only ~10 °C and both have narrow glass transitions and enthalpy relaxation peaks as evidenced by the DSC scans in Figure 7.13. This is indicative of very uniform networks. The narrow glass transition region found in the DSC scans in Figure 7.13 are confirmed by the DMA plots in Figure 7.14 for the 3NCO-HexDithiol and the HDI-TriThiol networks which have full-width at half maximum (FWHM) temperature ranges of 14 °C

and 12 °C, respectively, considerably smaller than the FWHM values for their 3NCO-HexDiol (30 °C) and HDIT-TriThiol (20 °C) counterparts. The very low FWHM values for HDI-TriThiol and 3NCO-HexDithiol are suggestive of and consistent with very efficient reactions between the aliphatic isocyanates and thiols with little or no side products compared to the isocyanate-alcohol reactions used to make the 3NCO-HexDiol network, which are well documented⁴⁸ to undergo side reactions presumably resulting in broadening of the thermal (Figure 7.13) mechanical (Figure 7.14) transitions. The near quantitative conversions for the reactions of isocyanates and thiols with no side products is indeed well documented.^{19, 24, 49} Interestingly, the HDIT-TriThiol network formed by reactions between the isothiocyanate and thiols also have very narrow glass transition regions, although the T_g of the HDIT-TriThiol network is lower than that of the HDI-TriThiol network due presumably to the higher extent of hydrogen bonding for the latter. Returning again to the results in Figure 7.13 and 7.14, we reiterate that it is remarkable that such narrow transitions occur in such high density networks. These results are reminiscent of the results obtained by photoinitiated thiol-ene free-radical step-growth polymerization where highly uniform networks are also formed.^{23, 50, 51} The thiol-isocyanate reaction is a clear candidate for a “click” process characterized by essentially quantitative conversions obtained under relatively benign conditions with little or no side reactions.⁵² This premise is under evaluation and will be reported on in future publications.

Although 3NCO-HexDiol and 3NCO-HexDithiol have many similar properties as

have been and will be shown, they still have some differences resulting from the network structure as discussed previously. To follow up on these differences, sub- T_g aging studies were conducted. DSC heating scans obtained after annealing, i.e. physical aging, at $T_g - 10$ °C for 3NCO-HexDiol and 3NCO-HexDithiol for a specific period of time are shown in Figure 7.15. As is well known for many linear polymers⁵³ and is demonstrated in Figure 7.15 for the urethane and thiourethane polymer networks, the enthalpy relaxation peak increases with the annealing time. The relaxed enthalpy, obtained from the integration of the enthalpy relaxation peak, and relaxation rate are different for the two networks as is obvious from the plots of the relaxed enthalpy versus time in Figure 7.16. The faster rate of enthalpy relaxation for 3NCO-HexDithiol compared to 3NCO-HexDiol is consistent with the narrowness of the glass transition region.

3NCO-HexDiol, 3NCO-HexDithiol and HDI-TriThiol all exhibit similar pendulum hardness indicating that energy damping even at 25 °C, well below the T_g of each polymer, is similar for all three systems (Table 7.6). The polydithiourethane (HDIT-TriThiol), however, exhibits significantly greater damping, i.e., the oscillation time is about 100 s lower than for the other three polymer films. This no doubt reflects the lower hydrogen bonding for HDIT-TriThiol and corresponding greater energy dissipation (i.e. energy damping) at room temperature. The polyurethane and polythiourethanes also exhibit better surface scratch resistance as indicated by higher pencil hardness (Table 7.6), while all four of the urethane type polymers exhibited excellent adhesion to glass (Table 7.6). A number of factors, including mechanical

interlocking, dipole-dipole interactions and covalent bonding⁵⁴ affect adhesion and hence it is not surprising that all four polymers adhere well to glass.

Results obtained from stress-strain curves (Figure 7.17) of each system are listed in Table 7.7 for comparison. The stress-strain curves for 3NCO-HexDiol and the two polythiourethane model compounds (3NCO-HexDithiol and HDI-TriThiol) are typical of non-crystalline polymers. In the first region, tensile stress increases linearly with strain that is recoverable (obeying Hook's law) when the external force is removed, due to relaxation of bond length and bond angle, until the polymer yields. The larger hydrogen bond fraction no doubt plays a key role in explaining the higher yield stress of HDI-TriThiol compared to HDIT-TriThiol (Table 7.7). The comparable yield stress for 3NCO-HexDiol and 3NCO-HexDithiol is consistent with the near equivalency of hydrogen bonding. In the second region, a plateau is achieved after passing the yield point as a result of chain segmental motion. Tensile strains greater than 50% are achieved by a combination of stretching/orientation and coincident breaking of intermolecular interactions (i.e. van der Waals force and hydrogen bonding). Interestingly, the stress plateau for HDI-TriThiol, which has a higher fraction of hydrogen bonding according to the FTIR results in Figure 7.11, appears at a higher level than its polydithiourethane analogue. The polymers prepared from 3NCO have very similar tensile properties in the second region due to only minor differences in their structures and hydrogen bonding behavior. The tensile stress increases sharply in the third region for each urethane type polymer due to further stretching of the orientated structures. The final break is a result of

covalent bonding cleavage and complete disassociation of secondary interactions such as van der Waals and hydrogen bonding. The difference between the stress at break (σ_b) of the two polymers prepared from 3NCO may well be due to the difference in bonding energy of C-O and C-S⁴⁶ since hydrogen bonding is almost equivalent for these two systems. The polydithiourethane exhibits the characteristics of rubbery materials, the tensile stress of which increases continuously after the linear elastic region until the polymer breaks at a relatively higher strain. This rubbery property and the lower tensile strength is partly the results of a lower fraction of hydrogen bonding resulting in a relatively lower glass transition region near 25 °C. Summarizing, comparing HDI-TriThiol with the other three polymer networks, it is reasonable to conclude that a combination of appropriate flexibility in the backbone and abundant sterically accessible hydrogen bonding acceptor sites leads to a tough and hard urethane type material as indicated by Young's modulus, the energy to break (area below the stress-strain curve) and hardness.

Although comprehensive analysis and discussions on hydrogen bonding behavior of urethane type polymers have been made based on several types of measurements, there is still one critical parameter that needs to be evaluated. Since mechanical and optical properties of network films can be related to density, the densities of each system were measured (Table 7.8). The results in Table 7.3 show that all of the cured networks have approximately equivalent densities, confirming that the property differences between the polydithiourethane and the polythiourethane are not directly related to differences in

density.

Finally, it is noted that a major interest in polythiourethane and polydithiourethanes is a result of their high refractive indices. The results in Table 7.8 clearly show that indeed the refractive index is directly related to the sulfur content in the films with 3NCO-HexDithiol having a higher refractive index than 3NCO-HexDiol and HDIT-TriThiol having the highest refractive index of all four systems.

Conclusions

A series of small molecule and polymeric urethane, thiourethane and dithiourethane compounds were prepared and measured by FTIR, NMR, DSC, and DMA establishing the order of the hydrogen bonding strength as: urethane \approx thiourethane > dithiourethane. Due to their similar hydrogen bonding behavior, polyurethane and polythiourethane networks have similar physical and mechanical properties, i.e., T_g , hardness and tensile properties. The polydithiourethane model compound with lower T_g is softer, more flexible and less tough because of weaker hydrogen bonding forming ability. The comprehensive characterization and comparison of urethane, thiourethane and dithiourethane compounds reported herein provides experimental and theoretical guidance for various applications of sulfur containing polyurethanes.

Acknowledgements

This work was supported by the MRSEC Program of the National Science Foundation under Award Number DMR 0213883. We also acknowledge Bayer Materials

Science for supplying isocyanates and Bruno Bock Thiochemical for providing thiols.

References

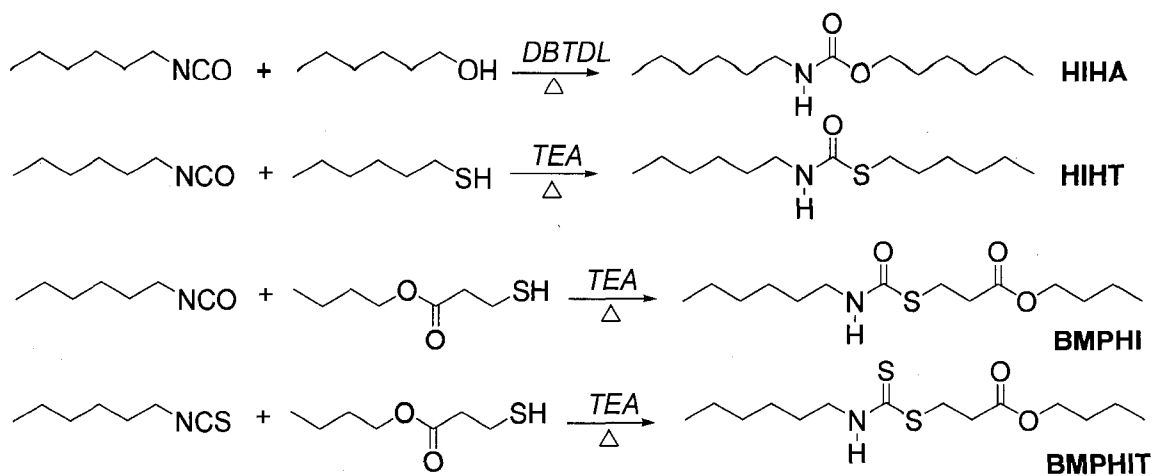
1. Bayer, O. *Angewandte Chemie* **1947**, A59, 257.
2. Chattopadhyay, D. K.; Raju, K. V. S. N. *Progress in Polymer Science* **2007**, 32, 352.
3. Pztrov, Z. S.; Ferguson, J. *Progress in Polymer Science* **1991**, 16, 695.
4. Coleman, M. M.; Lee, K. H.; Skrovanek, D. J.; Painter, P. C. *Macromolecules* **1986**, 19, 2149-2157.
5. Seymour, R. W.; Estes, G. M.; Cooper, S. L. *Macromolecules* **1970**, 3, 579.
6. Lee, H. S.; Wang, Y. K.; Hsu, S. L. *Macromolecules* **1987**, 20, 2089.
7. Pollack, S. K.; Smyth, G.; Papadimitrakopoulos, F.; Stenhouse, P. J.; Hsu, S. L.; MacKnight, W. J. *Macromolecules* **1992**, 25, 2381-2390.
8. Christenson, C. P.; Harthcock, M. A.; Meadows, M. D.; Spell, H. L.; Howard, W. L.; Creswick, M. W.; et al. *Journal of Polymer Science: Part B: Polymer Physics* **1986**, 24, 1404.
9. Mishra, A. K.; Chattopadhyay, D. K.; B., S.; Raju, K. V. S. N. *Progress in Organic Coatings* **2006**, 55, 231.
10. Wang, C. B.; Cooper, S. L. *Macromolecules* **1983**, 16, 775.
11. Yen, F.-S.; Hong, J.-L. *Macromolecules* **1997**, 30, 7927.
12. Dyer, E.; Osborne, D. W. *Journal of Polymer Science* **1960**, 47, 361.
13. Hastings, G. W.; Johnston, D. *British Polymer Journal* **1971**, 3, (2), 83.
14. Zhu, Z.; Risch, B. G.; Yang, Z.; Lin, Y.-N. European Patent Application. EP0780413A1, 1997.

15. Zhou, Y.; Lin, Y.-N.; Zhu, Z.; Risch, B. G. US Patent. US 6008296, 1999.
16. Tanaka, M.; et al. U.S. Patent Application 20050131203, 2005.
17. Shinohara, N.; et al. PCT International Application WO 2004078855, 2004.
18. Dietliker, K.; Misteli, K.; Jung, T.; Studer, K. In RadTech Europe 05: UV/EB--Join the Winning Technology (Conference Proceedings), Barcelona, Spain, Oct. 18-20, 2005; Barcelona, Spain, 2005; p 473.
19. Dyer, E.; Glenn, J. F.; Lendrat, E. G. *Journal of Organic Chemistry* **1961**, 26, 2919.
20. Freed, V. H.; et al. *Journal of Agriculture and Food Chemistry* **1967**, 15, (6), 1121.
21. Nagai, A.; Ochiiai, B.; Endo, T. *Journal of Polymer Science: Part A: Polymer Chemistry*, **2005**, 43, 1554.
22. Wheeler, K. A.; Harrington, B.; Zapp, M.; Casey, E. *CrystEngComm* **2003**, 5, (59), 337.
23. Li, Q.; Zhou, H.; Wicks, D. A.; Hoyle, C. E. *Journal of Polymer Science: Part A: Polymer Chemistry* **2007**, 45, (22), 5103-5111.
24. Dyer, E.; Glenn, J. F. *Journal of American Chemical Society* **1957**, 79, 366.
25. Zhou, H.; Li, Q.; Lee, T. Y.; Guymon, A. C.; Jonsson, S. E.; Hoyle, C. E. *Macromolecules* **2006**, 39, 8269-8273.
26. Becke, A. D. *Journal of Chemical Physics* **1993**, 98, 5648.
27. Lee, C.; Yang, W.; Parr, R. G. *Physics Review B* **1988**, 37, 785.
28. Woon, D. E.; Dunning, T. H. *Journal of Chemical Physics* **1993**, 98, 1358.
29. Kendall, R. A.; Dunning, T. H.; Harrison, R. J. *Journal of Chemical Physics* **1992**, 96,

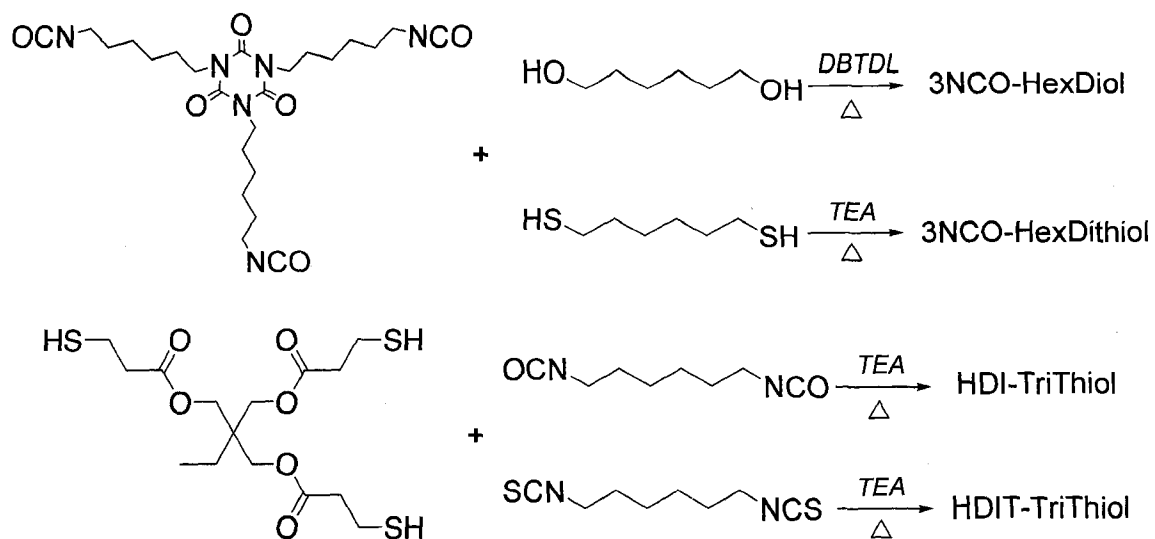
6796.

30. Silverstein, R. M.; Bassler, G. C.; Morrill, T. C., *Spectrometric Identification of Organic Compounds*. 4th ed.; John Wiley & Sons, Inc.: New York, 1981.
31. Joesten, M. D.; Schaad, L. J., *Hydrogen Bonding*. Marcel Dekker, Inc: New York, 1974.
32. Barisic, L.; Cakic, M.; Mahmoud, K. A.; Liu, Y.-N.; Kraatz, H.-B.; Pritzkow, H.; Kirin, S. I.; Metzler-Nolte, M.; Ropic, V. *Chemistry European Journal* **2006**, 12, 4965.
33. Ishimoto, B.; Tonan, K.; Ikawa, S.-i. *Spectrochimica Acta Part A* **1999**, 56, 201.
34. Winningham, M. J.; Sogah, D. Y. *Journal of American Chemical Society* **1994**, 116, 11173.
35. He, Y.; Zhu, B.; Inoue, Y. *Progress in Polymer Science* **2004**, 29, 1021.
36. Xiu, Y.; Zhang, Z.; Wang, D.; Ying, S.; Li, J. *Polymer* **1992**, 33, 1335.
37. Boyarchuk, Y. M.; Rappoport, L. Y.; Nikitin, V. N.; Apukhtine, N. P. *Polymer Science USSR* **1965**, 7, 859.
38. Tanaka, T.; Yokoyama, T.; Yamuguchi, Y. *Journal of Polymer Science: Part A-1* **1968**, 6, 2137.
39. Nakayama, K.; Ino, T.; Matsubara, I. *Journal of Macromolecular Science: Chemistry* **1969**, A3, (5), 1005.
40. Gramstad, T.; Sandstrom, H. J. *Spectrochimica Acta* **1969**, 25A, 31.
41. Tsang, K. Y.; Diaz, H.; Graciano, N.; Kelly, J. W. *Journal of American Chemical Society* **1994**, 116, 3988.

42. Diaz, H.; Espina, J. R.; Kelly, J. W. *Journal of American Chemical Society* **1992**, 114, 8316.
43. Dado, G. P.; Gellman, S. H. *Journal of American Chemical Society* **1994**, 116, 1054.
44. Oertel, G., *Polyurethane Handbook*. 2nd ed.; Hanser publishers: Munich-Vienna-New York, 1993.
45. Kordomenos, P. I.; Kresta, J. E.; Frisch, K. C. *Macromolecules* **1987**, 20, 2077.
46. Douglas, B.; McDaniel, D.; Alexander, J., *Concepts and Models of Inorganic Chemistry*. 3 ed.; Jonh Wiley & Sons, Inc.: New York, 1994.
47. Gomez, L.; Gellibert, F.; Wagner, A.; Mioskowski, C. *J. Comb. Chem.* **2000**, 2, 75.
48. Frisch, K. C.; Rumao, L. P. *Journal of Macromolecular Science: Review* **1970**, C5, 103.
49. Klemm, E.; Stockl, C. *Makromolekulare Chemie* **1991**, 192, 153.
50. Hoyle, C. E.; Lee, T. Y.; Roper, T. *Journal of Polymer Science: Part A: Polymer Chemistry* **2004**, 42, 5301.
51. Wei, H.; Li, Q.; Ojelade, M.; Madbouly, S.; Otaigbe, J. U.; Hoyle, C. E. *Macromolecules* **2007**, 40, 8788.
52. Kolb, H. C.; Finn, M. G.; Sharpless, K. B. *Angewandte Chemie: International Edition* **2001**, 40, 2004.
53. Hutchinson, J. M. *Progress in Polymer Science* **1995**, 20, 703-760.
54. Woods, J. G., In *Radiation Curing: Science and Technology*, Pappas, S. P., Ed. Springer: 1992; p 333.



Scheme 7.1. Synthesis of carbamate (HIHA), thiocarbamates (HIHT and BMPHI) and dithiocarbamate (BMPHIT).



Scheme 7.2. Preparation of polyurethane (3NCO-HexDiol), polythiourethanes (3NCO-HexDithiol and HDI-TriThiol) and polydithiourethane (HDIT-TriThiol).

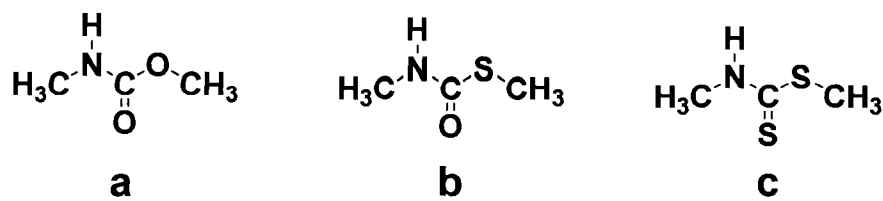


Chart 7.1. Molecular structures of (a) N-methyl methylcarbamate, (b) N-methyl S-methylthiocarbamate and (c) N-methyl S-methyldithiocarbamate used in hydrogen bonding strength calculation.

Table 7.1. Melting point (T_m) of small model compounds measured by DSC operating at 1 °C/min.

	HIHA	HIHT	BMPHI	BMPHIT
T_m (°C)	10	24	31	5

Table 7.2. Assignments of free and hydrogen bonded peaks in model compounds at 35 °C.

	Free	Bonded Peak (Acceptor 1)		Bonded Peak (Acceptor 2)	
	Wave Number (cm ⁻¹)	Wave Number (cm ⁻¹)	$\Delta\nu^*$ (cm ⁻¹)	Wave Number (cm ⁻¹)	$\Delta\nu$ (cm ⁻¹)
HIHA		Urethane			
	3459	3340	119		
HIHT		Thiourethane			
	3434	3311	123		
BMPHI		Thiourethane		Ester	
	3434	3311	123	3358	76
BMPHIT		Dithiourethane		Ester	
	3385	3247	138	3310	75

* $\Delta\nu$ is the wave number difference between bonded and free peaks.

Table 7.3. Slope and chemical shift difference for model compounds calculated from Figure 7.9.

	HIHA	HIHT	BMPHI	BMPHIT
$\Delta\delta$ (ppm)*	0.733	0.715	0.556	0.356
$\Delta\delta/\Delta T$ (* 10^{-3} ppm/K)	9.77	9.53	7.41	4.75

* $\Delta\delta = \delta_{35^\circ\text{C}} - \delta_{105^\circ\text{C}}$

Table 7.4. Hydrogen bonding energy of carbamate, thiocarbamate and dithiocarbamate.

	Carbamate	Thiocarbamate	Dithiocarbamate
Hydrogen bonding energy (kcal/mol)	5.36	5.18	4.44

Table 7.5. Glass transition temperatures of polymer networks measured by DSC and DMA.

	3NCO-HexDiol	3NCO-HexDithiol	HDI-TriThiol	HDIT-TriThiol
DSC (°C)	48	50	45	35
DMA (°C)	69	67	65	55

Table 7.6. Pendulum hardness and pencil hardness of polymer networks.

	3NCO-HexDiol	3NCO-HexDithiol	HDI-TriThiol	HDIT-TriThiol
Pendulum Hardness (s)	266 ± 3.0	270 ± 6.9	287 ± 5.3	178 ± 5.5
Pencil Hardness	5H	5H	5H	H
Cross Hatch Adhesion	5B	5B	5B	5B

Table 7.7. The yield stress (σ_y), yield strain (ϵ_y), stress at break (σ_b), strain at break (ϵ_b) and Young's modulus (E) of polymer networks.

	σ_y (MPa)	ϵ_y (%)	σ_b (MPa)	ϵ_b (%)	E (MPa)
3NCO-HexDiol	19.99 ± 2.68	3.48 ± 0.56	33.41 ± 3.26	91.73 ± 3.92	1057.83 ± 98.37
3NCO-HexDithiol	19.94 ± 0.63	3.73 ± 0.80	28.62 ± 0.60	90.52 ± 1.73	1074.68 ± 69.77
HDI-TriThiol	30.71 ± 3.44	3.97 ± 2.19	32.13 ± 3.05	107.80 ± 5.40	1676.60 ± 77.90
HDIT-TriThiol	4.67 ± 1.11	4.77 ± 1.50	27.83 ± 5.01	125.00 ± 6.88	310.50 ± 34.76

Table 7.8. Densities and refractive indices of polymer networks.

	3NCO-HexDiol	3NCO-HexDithiol	HDI-TriThiol	HDIT-TriThiol
Density (g/cm ³)	1.2518	1.2466	1.2698	1.2795
Refractive Index	1.5151	1.5505	1.5470	1.6092

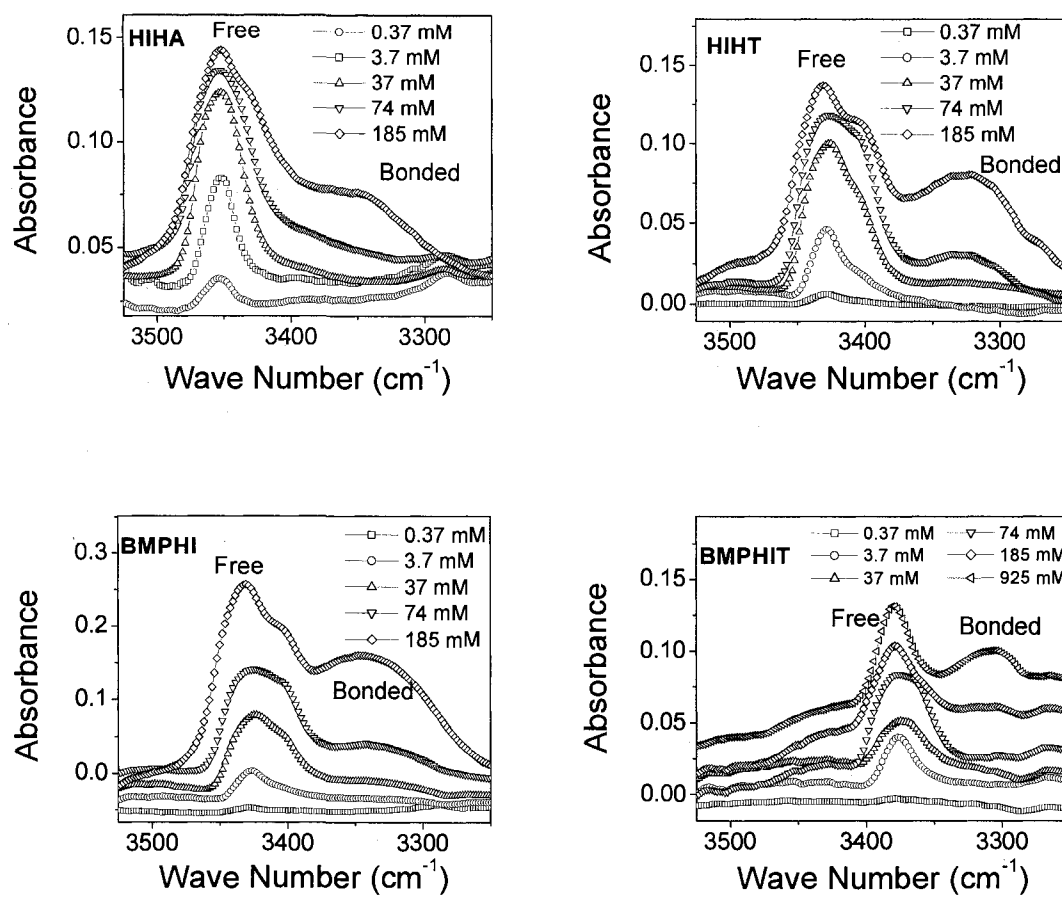


Figure 7.1. IR spectra of model compounds dissolved in chloroform. Note that the “bump” in the spectra for HIHA, HIHT and BMPHT between 3400 and 3500 cm⁻¹ is an instrumental artifact.

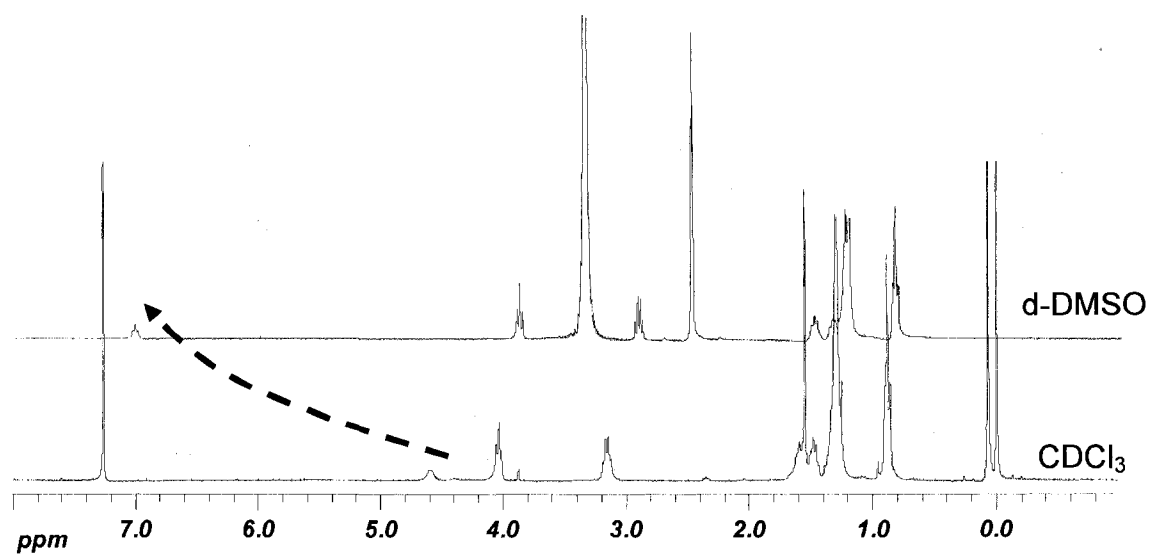


Figure 7.2. The ^1H NMR spectra of 3.7 mM HIHA in CDCl_3 and d-DMSO.

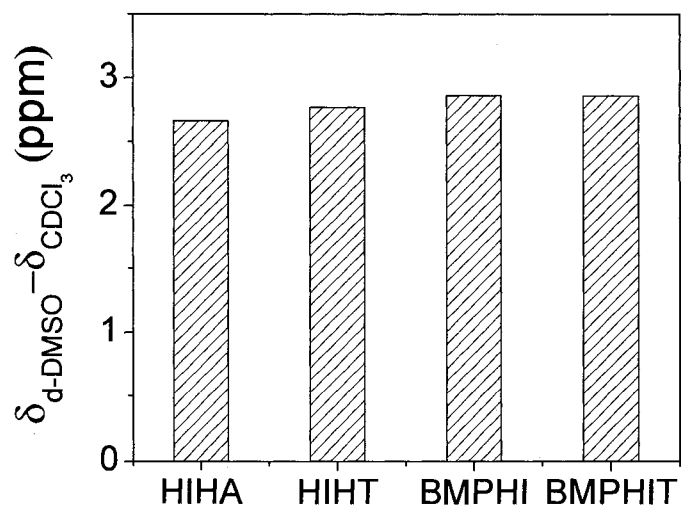


Figure 7.3. Chemical shift difference between NH protons in d-DMSO and CDCl₃.

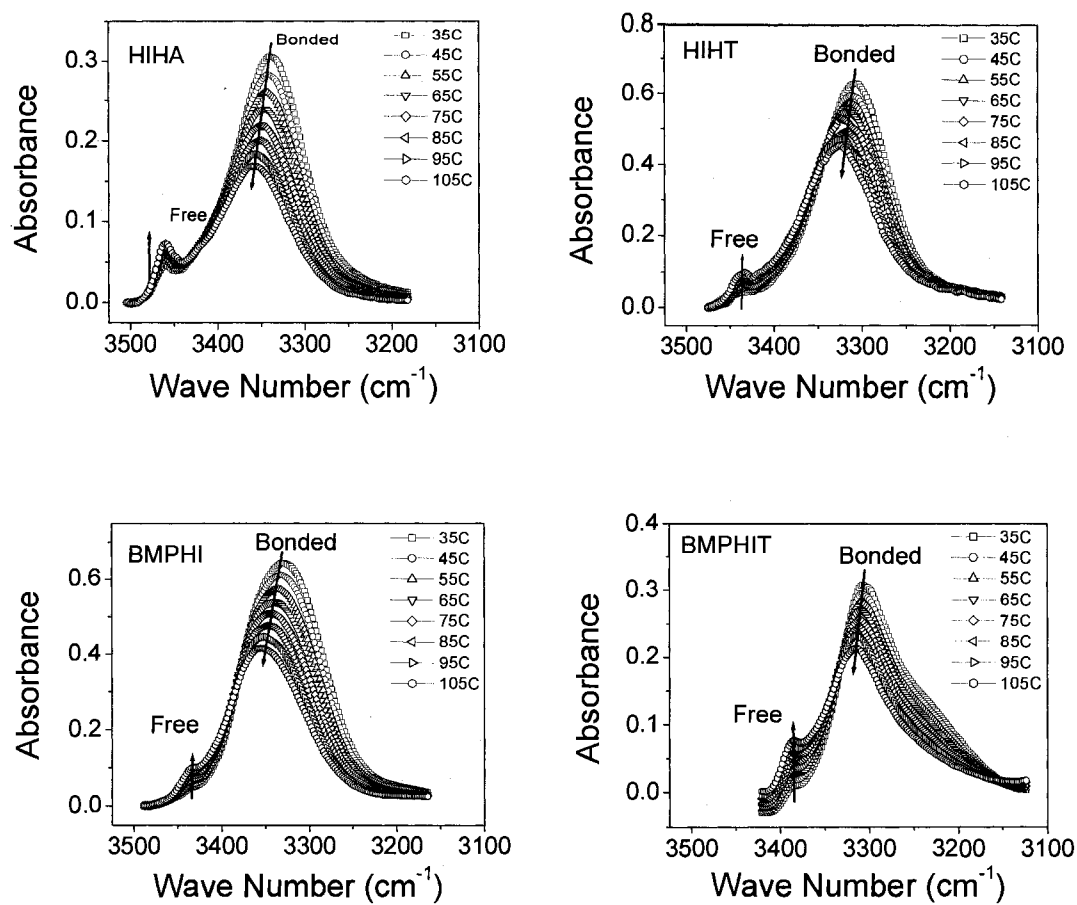


Figure 7.4. FTIR spectra of HIHA, HIHT, BMPHI and BMPHIT measured at different temperatures. The arrows indicate the direction of peak intensity as a function of temperature increase.

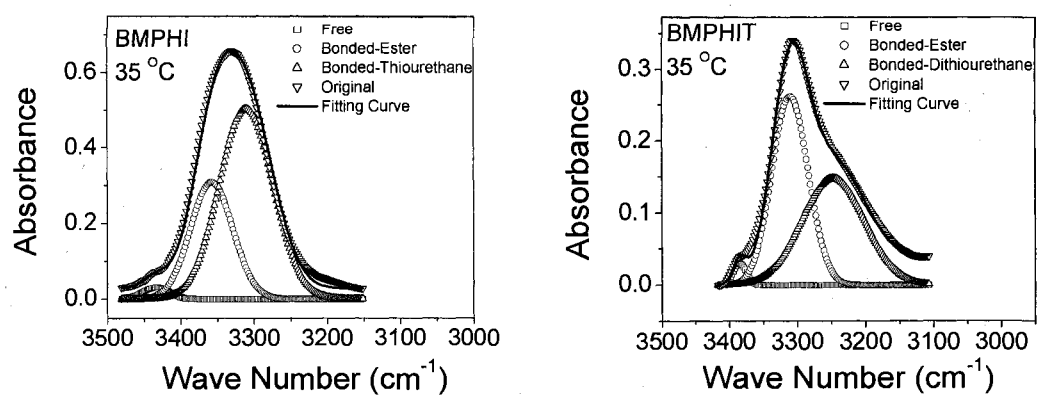


Figure 7.5. Peak deconvolution of the IR spectra of BMPHI and BMPHIT measured at 35 °C.

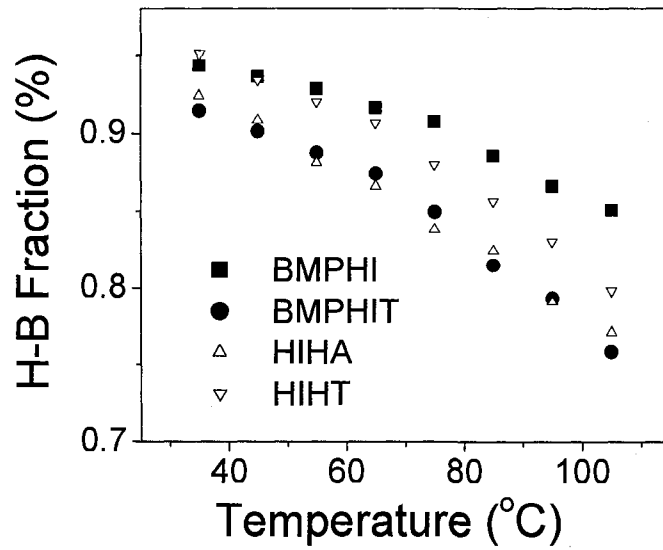


Figure 7.6. Hydrogen bonding fractions of model compounds.

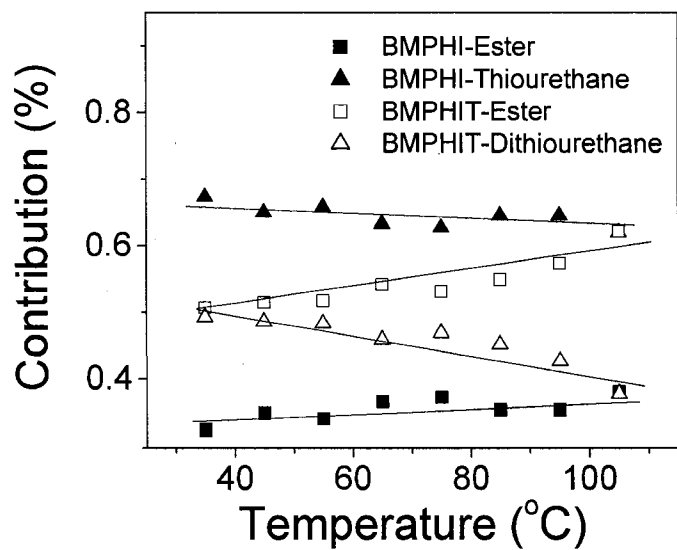


Figure 7.7. Contributions of different hydrogen bonding acceptors of BMPHI and BMPHIT model compounds.

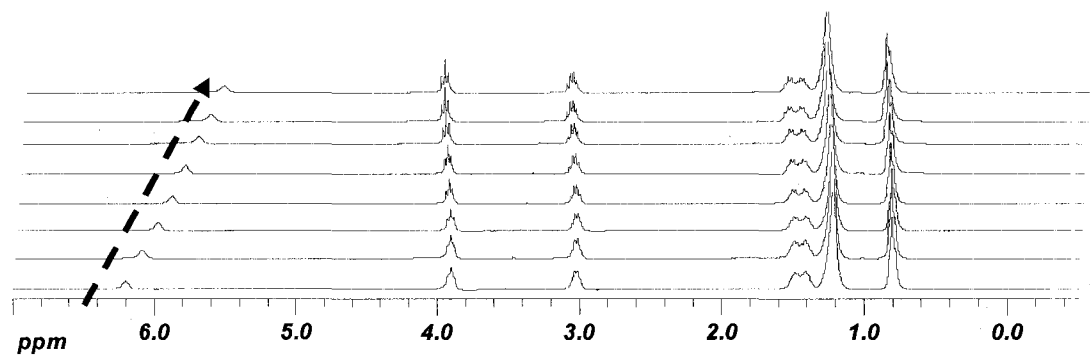


Figure 7.8. The ^1H NMR spectra of HIHA measured at temperatures from 35 °C to 105 °C with a 10 °C interval.

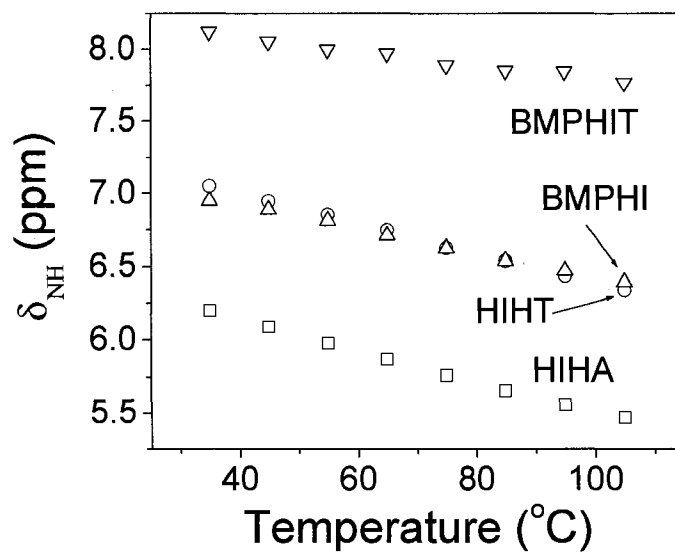


Figure 7.9. The chemical shift value of NH proton for model compounds as a function of temperature.

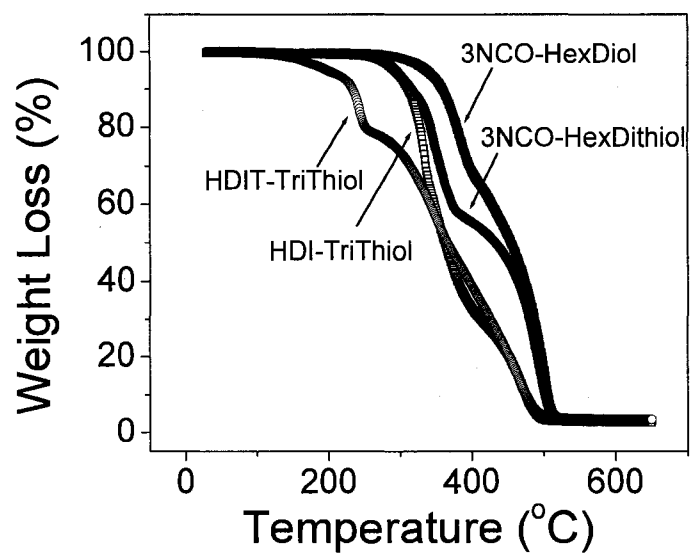


Figure 7.10. Thermogravimetric analysis of polymer networks.

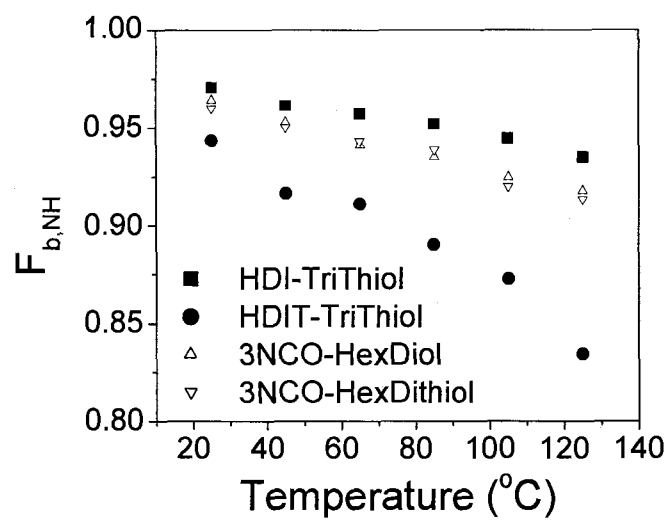


Figure 7.11. Hydrogen bonding fraction of polymer networks as a function of temperature.

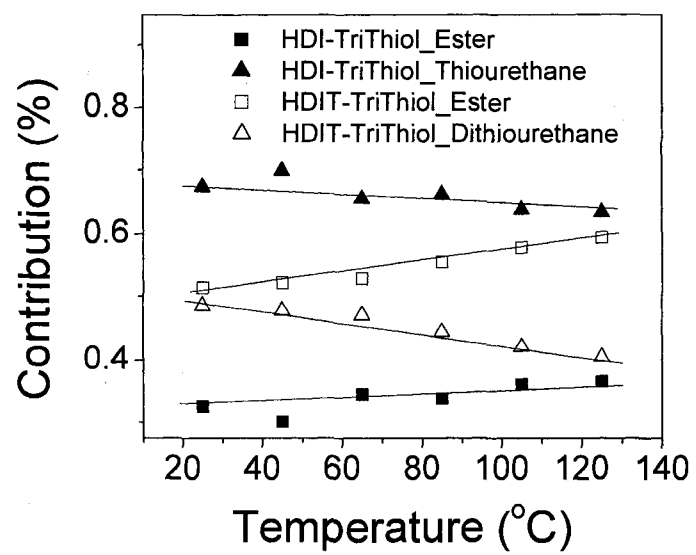


Figure 7.12. Contributions of different hydrogen bonding acceptors of HDI-TriThiol and HDIT-TriThiol.

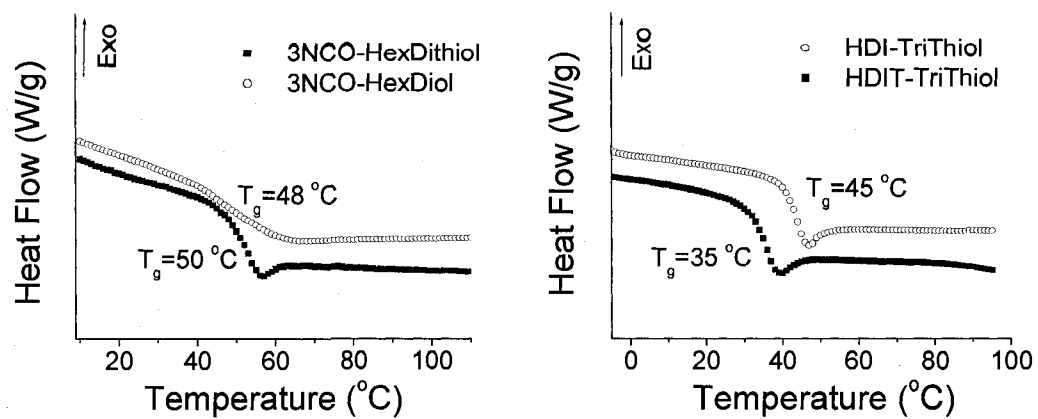


Figure 7.13. DSC scans of polymer networks.

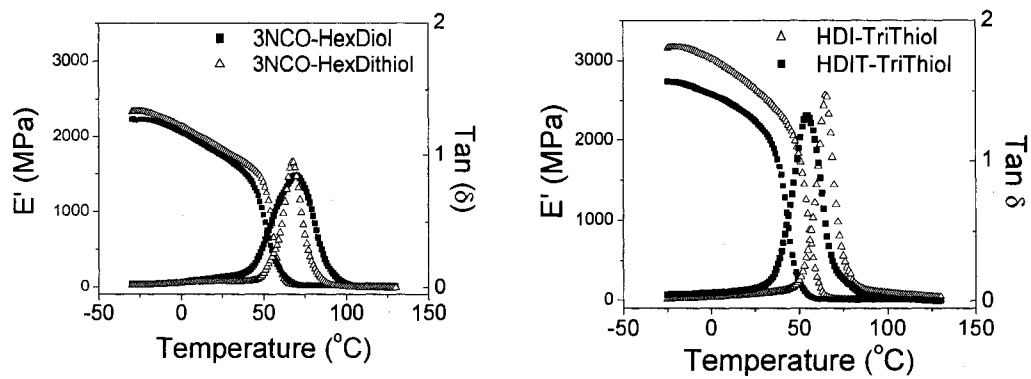


Figure 7.14. Storage modulus (E') and $\tan \delta$ of polymer networks measured by DMA operating at 3 °C/min.

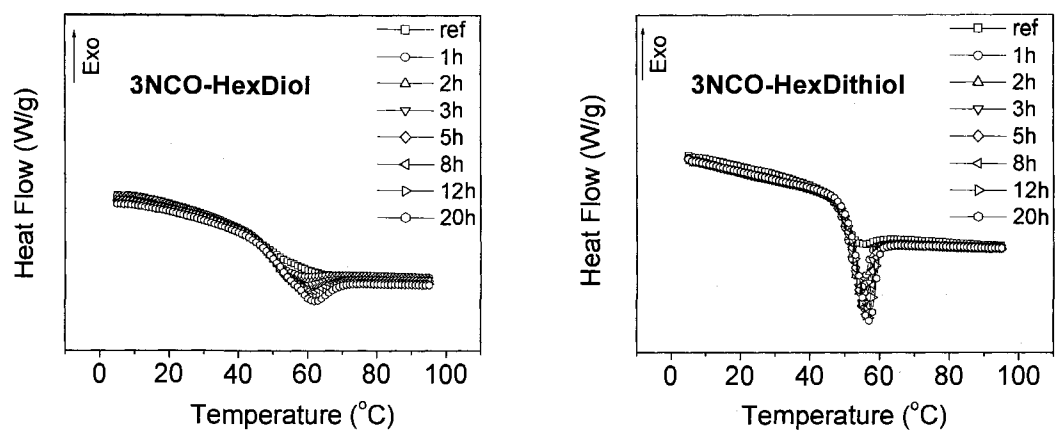


Figure 7.15. DSC curves of 3NCO-HexDiol and 3NCO-HexDithiol networks annealed for different times.

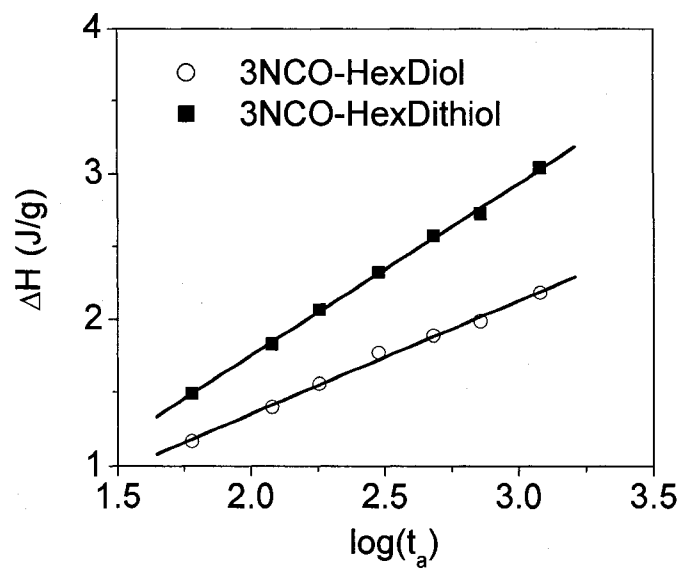


Figure 7.16. The enthalpy relaxation of 3NCO-HexDiol and 3NCO-HexDithiol as a function of sub- T_g aging time.

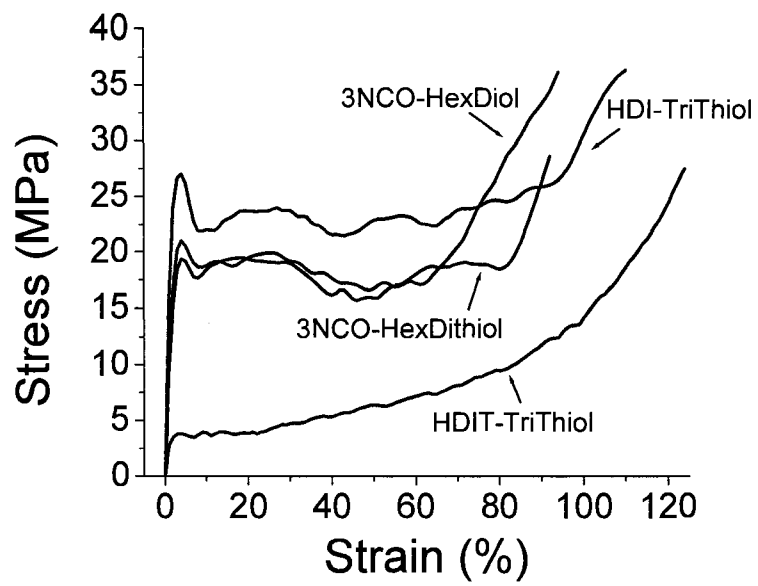


Figure 7.17. Stress-strain curve of model compounds measured at a strain rate of 10 %/min.

CHAPTER VIII

COMPARISON OF SMALL MOLECULE AND POLYMERIC URETHANES,
THIOURETHANES AND DITHIOURETHANES: HYDROGEN BONDING AND
THERMAL, PHYSICAL AND MECHANICAL PROPERTIES. PART 2

Abstract

A homologous family of small molecule and polymeric urethane, thiourethane and dithiourethane were prepared from both aliphatic and aromatic isocyanates and comprehensively characterized by a series of spectroscopic, thermal, physical and mechanical analysis measurements to define the relative hydrogen bond strength and its correlation with properties. The NMR, FTIR and XRD measurements of the small molecules in solution, melt and solid states indicate the relative hydrogen bonding strength as: urethane \approx thiourethane $>$ dithiourethane. The aromatic urethane is more stable under UV irradiation than the corresponding thiourethane analogues. Due to the weaker C-S bond compared to the polythiourethanes and polydithiourethane have reduced thermal stability compared to their urethane counterparts. Similar T_g values observed for the polyurethane and polythiourethanes are higher than those for the polydithiourethane, consistent with the lower hydrogen bonding in the latter.

Introduction

Hydrogen bonding is a type of strong noncovalent interaction which can be represented by A-H---B, where A and B are atoms that are more electronegative than

hydrogen (F, Cl, O, S, N, P).^{1,2} Since their recognition in the 1920s,³ hydrogen bonds have been extensively investigated because of the very important role they play in biological and polymer systems.^{1,2,4}

Polyurethanes, which exhibit extensive hydrogen bonding, have been widely used in many applications including coatings⁵ and elastomers⁶ due to an extraordinary combination of physical and mechanical properties. The structure-property relationships of polyurethanes have been thoroughly studied^{5,7-10} with an extensive effort in characterizing hydrogen bonding. Hydrogen bonding results in physical linkages within the material matrix and is a vital factor in defining the microscopic and macroscopic properties of polyurethanes, including their glass transition temperature, strength, stiffness and phase behavior.^{11,12}

The related polythiourethanes are prepared from thiol-isocyanate reactions.^{13,14} Although polythiourethanes (containing the structure unit -N(H)-C(=O)-S-) are extensively used in many modern applications including optical lenses and advanced coatings,¹⁵⁻¹⁷ the hydrogen bonding in polythiourethanes has not been thoroughly studied. Only limited literature can be found on subjects including synthesis/catalysis,^{13,14} kinetics of thiol-isocyanate reaction,¹⁸ thermodynamics of thiocarbamates¹⁹ and hydrogen bonding of polythiourethanes.²⁰ For polydithiourethanes or polydithiocarbamates, -N(H)-C(=S)-S-, which are also interesting because of their high refractive indices,²¹⁻²³ there are only limited reports on their hydrogen bonding behavior.²⁴ They have not been thoroughly characterized, especially with respect to structure-property relationships.

From both a basic and a practical point of view, a comprehensive investigation and comparison study of the hydrogen bonding behavior of a homologous family of both small molecule and polymer urethanes (-N(H)-C(=O)-O-), thiourethanes (-N(H)-C(=O)-S-), and dithiourethanes (-N(H)-C(=S)-S-) is necessary to provide a clear relationship between structure and properties in these important polymer materials. Herein, in order to achieve a thorough and complete comparison and evaluation of polyurethanes, polythiourethanes and polydithiourethanes, small molecule and polymeric urethanes, thiourethanes and dithiourethanes prepared from both aliphatic and aromatic secondary isocyanates, were characterized with respect to their hydrogen bonding behavior and structure-property relationships. The results show that urethanes and thiourethanes exhibit similar hydrogen bonding capabilities and mechanical/physical properties that are measurably different from those of the less hydrogen bonded dithiourethane. A theoretical and experimental starting point for further development of sulfur-containing aliphatic and aromatic urethane polymer materials is thus established.

Experimental

Materials

Chemicals for model compound synthesis, cyclohexyl isocyanate (CI), phenyl isocyanate (PI), phenyl isothiocyanate (PIT), 1-hexanol (HA), 1-hexanethiol (HT), 1,6-hexanediol (HexDiol), 1,6-hexanedithiol (HexDithiol), dibutyltin dilaurate (DBTDL) and triethylamine (TEA) were purchased from Aldrich Chemical Co. and used as

received. 1,6-Hexamethylene diisocyanate (HDI) and HDI trimer, or Desmodur® N3600 (3NCO), were obtained from Bayer Materials Science and used as received. 1,6-Hexane diisothiocyanate (HDIT) was purchased from Trans World Chemicals Inc. and used as received. Trimethylol propane tris(3-mercaptopropionate) (TriThiol) was obtained from Bruno Bock Thiochemical and used as received. Other chemicals, such as anhydrous acetone, were also obtained from Aldrich Chemical Co. and used as received.

Preparation

Typical procedures for synthesizing the small molecule model compounds listed in Scheme 8.1, N-cyclohexyl hexylcarbamate (CIHA), N-cyclohexyl S-hexylcarbamate (CIHT), N-phenyl hexylcarbamate (PIHA), N-phenyl S-hexylcarbamate (PIHT) and N-phenyl S-hexyldithiocarbamate (PITHT), are as follows (CIHA is taken as an example). 0.03 Mol of cyclohexyl isocyanate and 0.03 mol of 1-hexanol were first charged into a 3 neck flask before 10 mL of hexane was added. The reactor was then purged with dry N₂ for 30 min until 0.02 wt% of dibutyltin dilaurate (DBTDL) was added and stirred. The mixture was allowed to react for 8 h at 65 °C under dry N₂ flow. All the model products were purified by recrystallization from hexane 2-3 times, and their structures were verified with nuclear magnetic resonance spectroscopy (NMR). TEA was used in all thiol compounds reactions with isocyanates or isothiocyanates due to its highly efficiency as a catalyst.²⁵ DBTDL was used in all alcohol reactions for the same reason.

¹H NMR:

CIHA (CDCl₃): δ 0.89 (t, 3H, -CH₃), δ 1.30-1.94 (18H, -CH₂-), δ 3.49 (m, 1H,

-CH-N-), δ 4.03 (t, 2H, -CH₂-O-), δ 4.50 (s, 1H, -N(H)-).

CIHT (CDCl₃): δ 0.88 (t, 3H, -CH₃), δ 1.32-1.92 (18H, -CH₂-), δ 2.89 (t, 2H, -CH₂-S-), δ 3.75 (m, 1H, -CH-N-), δ 5.18 (s, 1H, -N(H)-).

PIHA (CDCl₃): δ 0.89 (t, 3H, -CH₃), δ 1.31 (6H, -CH₂-), δ 1.66 (m, 2H, -CH₂-C-O-), δ 4.15 (t, 2H, -CH₂-O-), δ 6.55 (s, 1H, -N(H)-), δ 7.05-7.54 (5H, benzene ring).

PIHT (CDCl₃): δ 0.90 (t, 3H, -CH₃), δ 1.32 (6H, -CH₂-), δ 1.66 (m, 2H, -CH₂-C-O-), δ 2.97 (t, 2H, -CH₂-O-), δ 7.00 (s, 1H, -N(H)-), δ 7.11-7.40 (5H, benzene ring).

PITHT (CDCl₃): δ 0.90 (t, 3H, -CH₃), δ 1.32 (6H, -CH₂-), δ 1.70 (m, 2H, -CH₂-C-O-), δ 3.29 (t, 2H, -CH₂-O-), δ 7.21-7.45 (5H, benzene ring), δ 8.73 (s, 1H, -N(H)-).

The polyurethanes, IPDI-HexDiol and TDI-HexDiol, polythiourethanes, IPDI-HexDithiol and TDI-HexDithiol, and polydithiourethane, TDIT-HexDithiol, were prepared as described below and are depicted in Scheme 8.2. 0.03 Mol of IPDI (IPDI-HexDiol is taken as an example) and 0.02 mol of HexDiol were first charged into a scintillation vial before 2 mL of anhydrous acetone was added to form a transparent solution. ~0.6 Wt% (based on the whole mixture) of DBTDL was then added into the monomer solution and mixed homogeneously. The solution was then evenly coated onto a piece of clean glass, followed by purging with dry N₂ in a sealable chamber for 1 h at room temperature. The sealed chamber was then moved to an oven set at 80 °C and kept

overnight, followed by heating under vacuum (70 °C) for about 24 h to yield a 200 μm thick film without any solvent (verified by thermal gravimetric analysis). The conversions of all films are greater than 95%. As described for the small models preparation, TEA is preferred as a catalyst for thiourethane and dithiourethane preparation. The type and concentration of catalysts were adjusted for each system to achieve efficient polymerization while also allowing enough time for mixing and film coating. The catalyst concentrations used for IPDI-HexDithiol, TDI-HexDiol, TDI-HexDithiol and TDIT-HexDithiol are 0.06 wt% (TEA), 0.18 wt% (DBTDL), 0.0002 wt% (TEA) and 0.4 wt% (TEA), respectively.

Characterization

Proton nuclear magnetic resonance (^1H NMR) spectra were obtained on a Mercury 300 (Varian Inc.) spectrometer, the temperature of which was controlled by a Bruker Variable Temperature Unit equipped with a Eurotherm 818 Controller. Each spectrum was recorded as the co-addition of 64 scans after 25 min of equilibrium at a given temperature. For regular NMR measurements, concentrations of 3.7 mM (in either CDCl_3 or $d\text{-DMSO}$) were used for small molecules in solution. Infrared spectra were collected on a Bruker IFS 88 FTIR spectrometer by holding samples sandwiched between two NaCl plates in a heating unit controlled by a Harrick temperature controller with an accuracy of ± 1 °C. Each spectrum was recorded after equilibrating for 25 min at the desired temperature. Peak fitting was conducted using a Gaussian function in Origin software to assign the free and hydrogen bonded NH peaks as described elsewhere.²⁶

Thermal stability of the polymers was measured with a TA Q60 (TA Instruments, Inc.) thermal gravimetric analysis (TGA) operating at a heating rate of 20 °C/min. Glass transition temperatures were measured with a TA Q1000 differential scanning calorimetry (DSC) operating at 10 °C/min. Two heating scans were conducted for all samples and the second scan were selected to determine T_g values using TA Universal Analysis software (V 3.9A). Pencil hardness was measured according to ASTM D-3363. Persoz pendulum hardness was measured according to ASTM D-4366 using a BYK-Gardner pendulum hardness tester with a square frame pendulum. At least six tests were performed for each film coated on a glass substrate at different parts of the film, and the average value of the six was taken as the final result. The crystallographic properties and data were collected using CuK α radiation and the charge-coupled area detector (CCD) on an Oxford Diffraction Systems Gemini S diffractometer at 296 K. The sample crystal was attached to the tip of a fine glass fibre and mounted on a goniometer head. The crystal structures were solved using by direct methods with SHELXS-86,²⁷ and refined with SHELXL.²⁸ The computations of hydrogen bonding energy were performed for N-methyl methylcarbamate, N-methyl S-methylthiocarbamate, and N-methyl S-methyldithiocarbamate using density function theory. The function employed was the three-parameter B3 hybrid function of Becke²⁹ and the LYP correlation function of Lee, Yang and Parr.³⁰ The basis sets used were the correlationally-consistent basis sets cc-pVDZ³¹ and cc-pVTZ³² created by Dunning and coworkers. The cc-pVDZ basis set uses a double-zeta description for valence electrons, while the cc-pVTZ basis employs a

triple-zeta description for valence electrons. Both basis sets use a single-zeta description for core electrons, and both have a consistent set of polarization functions.

Results and Discussion

Solution

NMR spectra of model compounds dissolved in both polar and nonpolar solvents were recorded to show the effect of hydrogen bonding on the NH proton chemical shifts. Figure 8.1 shows the NMR spectra of CIHA in pure and co-solvents of CDCl_3 and d-DMSO as an example. The concentration (3.7 mM) is low such that no intermolecular hydrogen bonds are formed, i.e., the only possible hydrogen bonding is between CIHA molecules and the d-DMSO solvent molecules. With an increase of the d-DMSO concentration, hydrogen bonding occurs between the model compound NH groups and the sulphonyl group ($-\text{S}=\text{O}$) of d-DMSO, resulting in a downfield shift of the NH peak. This can be explained by the decrease in electron density around the NH proton and an increase in the asymmetry of the electron density due to polarization of the NH bond by $-\text{S}=\text{O}$ group.² The extent of this shift, or the difference in chemical shifts for associated and unassociated NH, is a direct indication of the hydrogen bonding strength.² The stronger the hydrogen bonding, the greater the downfield shift that occurs. Although, theoretically, the unassociated NH proton chemical shift refers to that at infinite dilution, since NMR results show no significant shift in the NH peak upon diluting the CIHA/ CDCl_3 solution to as low as 0.37 mM (not shown), the chemical shift of NH in

CDCl_3 (3.7 mM) can be regarded as the unassociated value for comparison purposes. And the chemical shift of NH for CIHA in d-DMSO can represent the hydrogen bonding between NH of the model compounds and sulphonyl groups of d-DMSO. As shown in Figure 8.2, essentially equivalent values are obtained for thiocarbamates and carbamates in terms of the NMR downfield shift for both the aliphatic (CIHA and CIHT) and aromatic (PIHA and PIHT) compounds, indicating similar hydrogen bonding strength in the carbamates and thiocarbamates. The shift for the dithiocarbamate compound, however, is lower than its analogues, implying weaker hydrogen bonding between the NH proton in PITHT and the sulphonyl oxygen in d-DMSO. This is reasonable considering that, comparing with the urethane linkage, $-\text{N}(\text{H})-\text{C}(=\text{O})-\text{O}-$, and even the thiourethane linkage, $-\text{N}(\text{H})-\text{C}(=\text{O})-\text{S}-$, the lower electronegativity of the two sulphur atoms results in a less electrophilic N-H hydrogen in the dithiourethane linkage, $-\text{N}(\text{H})-\text{C}(=\text{S})-\text{S}-$, reducing the tendency to form hydrogen bonds. We point out that the results in Figure 8.2 only reflect the hydrogen bonding forming ability of the N-H group of these model compounds, which is to say, in these NMR experiments, the model compounds only behave as hydrogen bonding donors.

Melt

Since temperature is one of the most important factors affecting hydrogen bonding, model compounds were also investigated by temperature-resolved ^1H NMR spectroscopy. For all model compounds (results for CIHA in Figure 8.3 is shown as an example), the NH peaks exhibit an upfield shift due to the disassociation of hydrogen

bondings as temperature increases, while the position of other peaks remain unchanged. The temperature dependence chemical shift coefficients, $\Delta\delta/\Delta T$, that have been used to distinguish between free and bonded NH in peptides and amides,³³⁻³⁶ can be used to evaluate the extent/strength of hydrogen bonding in the carbamates and thiocarbamates. As shown in Figure 8.4 and Table 8.1, no significant differences are observed between the carbamates and thiocarbamates, both aliphatic and aromatic, confirming that equally strong hydrogen bonds are formed in both cases. In accordance with the NMR solution study discussed earlier, the results for the dithiocarbamate, PITHT, gives a larger slope than both the carbamate, PIHA, and thiocarbamate, PIHT. The chemical shift difference between 65 °C and 105 °C, $\Delta\delta$, is also related to the strength of hydrogen bonding. As shown in Table 8.1, both the aliphatic and aromatic carbamates and thiocarbamates exhibit the same chemical shift difference while the dithiocarbamate shows a larger value for $\Delta\delta$, indicating the order of the hydrogen bonding strength as: carbamate \approx thiocarbamate > dithiocarbamate.

Temperature-dependent infrared spectroscopy, an effective technique that has been extensively used to investigate hydrogen bonding,^{2, 9, 10, 37} was also used to measure the hydrogen bonding behavior of the model compounds, and provide a semiquantitative analysis of the hydrogen bonding. Distinctly separated NH peaks, representing free (higher frequency) and bonded (lower frequency) groups, are observed in the NH stretch region of all five model compounds (CIHA and CIHT are shown in Figure 8.5 as examples). A direct observation is the reduction in the bonded peak intensity and relative

enhancement in the intensity of the free peak with temperature increase due to disassociation of hydrogen bonding at elevated temperatures. The absorbance of each peak, obtained through a peak deconvolution method described previously,²⁶ can be used to calculate the approximate hydrogen bonding fraction ($F_{b,NH}$), the percent of NH groups involved in hydrogen bonding, based on the equation given below^{8, 38}

$$F_{b,NH} = \frac{1}{1 + 3.46 \frac{A_{f,NH}}{A_{b,NH}}}$$

where $A_{f,NH}$ and $A_{b,NH}$ are the absorbance of free and hydrogen bonded NH groups, respectively, and the constant 3.46 is used as the extinction coefficient ratio of the bonded and free NH groups. Although, as stated in reference 7, the extinction coefficient of the NH group changes with the strength of the hydrogen bond, for semi-quantitative comparison purposes in our case over the narrow temperature range from 45-95 °C, the error introduced by using 3.46 is minimal. As shown in Figure 8.6, with an increase in temperature, $F_{b,NH}$ decreases as a result of hydrogen bonding disassociation as expected. Carbamates and thiocarbamates shows very similar hydrogen bonding fractions, an indication of similar hydrogen bonding ability in these compounds, whereas the dithiocarbamate exhibits a lower hydrogen bonding fraction. The results are in agreement with the weaker hydrogen bonding ability of the thiocarbonyl (C=S) group compared to the carbonyl group (C=O) reported previously via FTIR and crystallographic measurements of related systems.^{24, 39}

Crystals

X-ray diffraction provides an effective basis for qualitatively assessing intermolecular interactions which bear on crystal properties such as density, melting point, and heat of fusion. In the present study, both carbamates and thiocarbamates show hydrogen-bonding between functional groups. The interactions link the molecules in chains in the fashion of β -sheets, with nearly linear N-H...O contacts. The metrics are summarized in Table 8.2 and 8.3, and show the relatively long N...O distances (3.0Å) typical of neutral donor and acceptor groups, and consistent with the generally lower melting points of the compounds. Crystal forms for the carbamates are nearly isomorphous with the analogous thiocarbamates, and the hydrogen-bonding metrics are similar. Both the distance values and angle values of the carbamates and thiocarbamates are very close (Table 8.2), indicating similar hydrogen bonding strength. The dithiocarbamate phase is nicely crystalline but forms very slender needles; the XRD data are at poor resolution and therefore not included in this study. However, ab initial calculations have shown the hydrogen bonding strength of the dithiocarbamate (4.44 kcal/mol) to be less than that of the carbamate (5.36 kcal/mol) or the thiocarbamate (5.18 kcal/mol).

A comparison of the melting temperatures of the phases studied shows some interesting phenomena. The aliphatic carbamate (CIHA) and thiocarbamate (CIHT) have similar melting points, consistent with their similar structures and hydrogen-bond forming abilities (Table 8.4). However, the aromatic thiocarbamate exhibits a

significantly higher melting point. This presumably results from the stronger π - π interactions between the phenyl rings in PIHT and may be connected to a somewhat better packing arrangement in crystals of PIHT as suggested by its higher density (1.192 g/cm³) compared to the corresponding carbamate PIHA (1.149 g/cm³). Interestingly, based on the comparison of linear polyurethanes and polythiourethanes, Dyer et al.¹³ claimed that the polythiourethanes generally have higher melting points than their oxygen analogs due to the greater molar cohesive energy of sulfide links than ether links.⁴⁰

Photolysis of Aromatic Model Compounds

In order to provide a comprehensive characterization, the photolytic decomposition of the aromatic species was investigated. As shown in Figure 8.7a, the primary bands of all samples decrease and small shoulders appear at higher wavelength after 20 min exposing to a medium pressure mercury lamp with output from 254 nm to over 400 nm. The absorbance of the primary band peak maxima of PIHA, PIHT and PITHT at 235 nm, 250 nm, and 286 nm are reduced by 30%, 68% and 76%, respectively, indicating the greater photostability of the urethane than the sulfur containing thiourethane or dithiourethane. It has been suggested that the photodegradation of urethanes occurs mainly through the cleavage of C-N and C-O/C-S bonds as shown in Chart 8.1.⁴¹ For PIHA (Figure 8.7b), after photodegradation, the new band appears at ~340 nm is due to the ortho photo-Fries product reported in the literature.^{42, 43} The corresponding band for the degraded PIHT sample shifts to 358 nm with higher absorbance. While for PITHT, only a tail appears in this region which implies a different

photodegradation mechanism. The solutions of the model compounds with equal absorbance at 254 nm were then irradiated with 254 nm UV lamps in the Rayonet photoreactor for 10 min (Figure 8.8). Interestingly, PIHA and PIHT exhibit significant increase in absorbance at long wavelengths above 300 nm. For PITHT, after the 10 min irradiation, the absorbance band at 285 nm almost completely disappears and a small tail appears at higher wavelengths. The formation of similar free radicals shown in Scheme 8.3^{41, 44} were suggested for aromatic carbamate and thiocarbamates as a result of cleavage reactions at the C=O groups. No literature references are available for the photostability of dithiourethanes. Although the retarding effect of hydrogen bonding on photolysis of aromatic polyurethanes has been reported,⁴⁵ the samples investigated herein are not affected by hydrogen bonding under the experimental conditions, 0.06 mM concentration in dichloromethane.

Polymer Properties

To understand the effect of hydrogen bonding on polymer properties, two polyurethanes, two polythiourethanes and one polydithiourethane were prepared as described in the Experimental section (Scheme 8.2).

The change in the N-H hydrogen bonding fraction, $F_{b,NH}$, of each polymer as a function of temperature (25 °C- 105 °C) was measured by FTIR using a similar method to that for evaluating the small molecules model compounds in Figure 8.5. As shown in Figure 8.9, the values for $F_{b,NH}$ as a function of temperature for the two polyurethanes, IPDI-HexDiol and TDI-HexDiol, exhibit values similar to the two polythiourethanes,

IPDI-HexDithiol and TDI-HexDithiol. The polydithiourethane, TDIT-HexDithiol, exhibits the lowest hydrogen bonding fraction with a significant decrease in hydrogen bonding at the higher temperatures.

In order to determine any physical difference between the polyurethanes, the polythiourethanes and the polydithiourethane, a series of physical measurements were conducted. As indicated by the absence of any melting peaks for any of the polymers upon heating in the DSC up to 300 °C, the model polymers are amorphous. The glass transition temperatures, measured by DSC scans, are shown in Figure 8.10 and Table 8.5. As expected, the glass transitions of the polyurethanes and polythiourethanes appears at about the same temperature range, both higher than that of the polydithiourethane.

Films of the polyurethanes and the polythiourethanes all exhibit similar Persoz hardness values as indicated in Table 8.5, consistent with the glass transition temperature and hydrogen bonding results. The polydithiourethane has only a slightly lower Persoz hardness value, presumably due to the hydrogen bonding fraction that is very close to those of polyurethanes and polythiourethanes at the testing temperature (23 °C). Finally all of the films exhibited very good surface scratch resistance as indicated by the pencil hardness test results in Table 8.5.

To investigate thermal stability, thermogravimetric analysis was conducted (Figure 8.11 and Table 8.5). Polyurethanes and polythiourethanes show very similar degradation behavior. Both the aliphatic and aromatic polyurethanes exhibit greater thermal stability than the polythiourethanes which have about 30 °C lower $T_{5\%}$ values

(temperature at 5% weight loss). The lower bond energy for C-O compared to that of C-S contributes to the thermal stability differences between polyurethanes and polythiourethanes.⁴⁶ The polydithiourethane, TDIT-HexDithiol, is much less stable than either the polyurethanes or the polythiourethanes. The much lower thermal stability of a polydithiourethane with the $-N(H)-C(=S)-S-$ linkage has been reported.⁴⁷

Conclusions

The hydrogen bonding and structure-property relationships of a series of small molecule and polymeric urethane, thiourethane and dithiourethane systems prepared from both aliphatic and aromatic secondary isocyanates were characterized. The extent of hydrogen bonding for the urethanes and thiourethanes was greater than that of the dithiourethane. Similar physical and mechanical properties for the polyurethanes and polythiourethanes (both aliphatic and aromatic) were consistent with the hydrogen bonding results. The dithiourethane based small molecule model and polymer exhibited a lower melting point (small molecule) and glass transition temperature (polymer) than the urethane and thiourethane counterparts.

Acknowledgements

This work was supported by the MRSEC Program of the National Science Foundation under Award Number DMR 0213883. We also acknowledge Bayer Materials Science for supplying isocyanates.

References

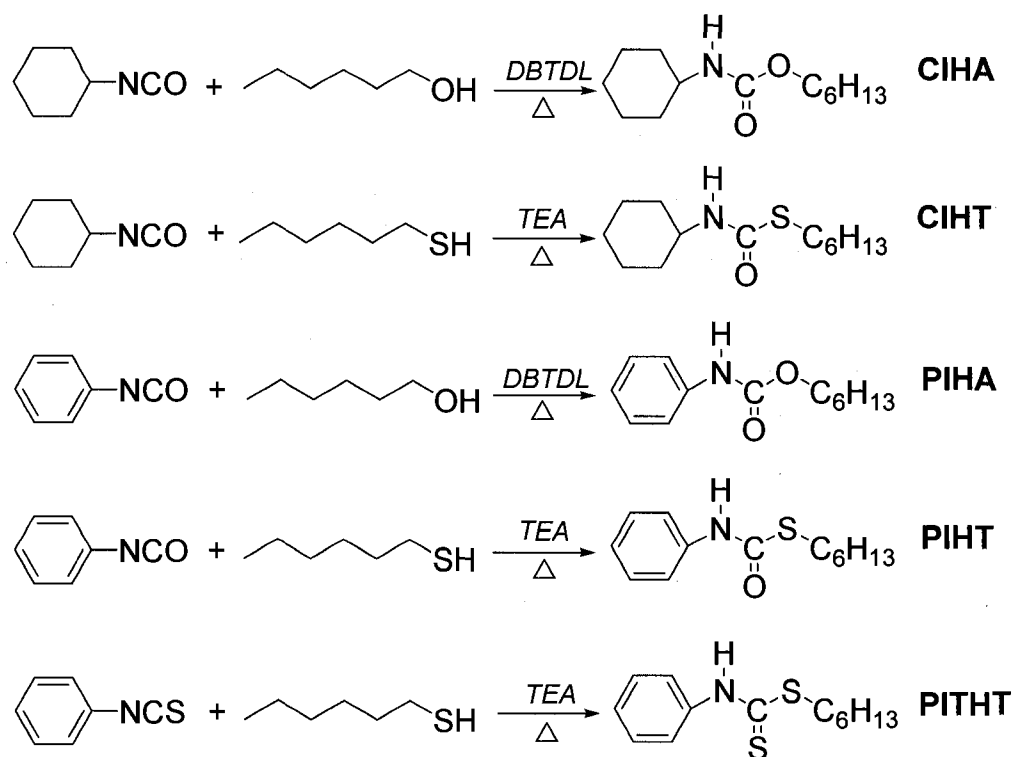
1. Jeffrey, G. A., *An Introduction to Hydrogen Bonding*. Oxford Univeristy Press: New York-Oxford 1997.
2. Joesten, M. D.; Schaad, L. J., *Hydrogen Bonding*. Marcel Dekker, Inc: New York, 1974.
3. Lewis, G. N., *Valence and the Structure of Atoms and Molecules*. Chemical Catalog Co.: New York, 1923.
4. Bandekar, J.; Klima, S. *Journal of Molecular Structure* **1991**, 263, 45.
5. Chattopadhyay, D. K.; Raju, K. V. S. N. *Progress in Polymer Science* **2007**, 32, 352.
6. Pztrov, Z. S.; Ferguson, J. *Progress in Polymer Science* **1991**, 16, 695.
7. Coleman, M. M.; Lee, K. H.; Skrovanek, D. J.; Painter, P. C. *Macromolecules* **1986**, 19, 2149-2157.
8. Seymour, R. W.; Estes, G. M.; Cooper, S. L. *Macromolecules* **1970**, 3, 579.
9. Lee, H. S.; Wang, Y. K.; Hsu, S. L. *Macromolecules* **1987**, 20, 2089.
10. Pollack, S. K.; Smyth, G.; Papadimitrakopoulos, F.; Stenhouse, P. J.; Hsu, S. L.; MacKnight, W. J. *Macromolecules* **1992**, 25, 2381-2390.
11. Christenson, C. P.; Harthcock, M. A.; Meadows, M. D.; Spell, H. L.; Howard, W. L.; Creswick, M. W.; et al. *Journal of Polymer Science:Part B:Polymer Physics* **1986**, 24, 1404.
12. Mishra, A. K.; Chattopadhyay, D. K.; B., S.; Raju, K. V. S. N. *Progress in Organic Coatings* **2006**, 55, 231.

13. Dyer, E.; Osborne, D. W. *Journal of Polymer Science* **1960**, 47, 361.
14. Hastings, G. W.; Johnston, D. *British Polymer Journal* **1971**, 3, (2), 83.
15. Tanaka, M.; et al. U.S. Patent Application 20050131203, 2005.
16. Shinohara, N.; et al. PCT Int. Appl. WO 2004078855, 2004.
17. Dietliker, K.; Misteli, K.; Jung, T.; Studer, K. In RadTech Europe 05: UV/EB--Join the Winning Technology (Conference Proceedings), Barcelona, Spain, Oct. 18-20, 2005; Barcelona, Spain, 2005; p 473.
18. Dyer, E.; et al. *Journal of Organic Chemistry* **1961**, 26, 2919.
19. Freed, V. H.; et al. *Journal of Agriculture and Food Chemistry* **1967**, 15, (6), 1121.
20. Nagai, A.; Ochiiai, B.; Endo, T. *Journal of Polymer Science: Part A: Polymer Chemistry*, **2005**, 43, 1554.
21. Risch, B. G.; Yang, Z.; Lin, Y.-N. 1996.
22. Nakayama, N.; Hayashi, T. *Progress in Organic Coatings* **2008**, 62, (3), 274.
23. Saito, T.; Kanai, T. PCT International Application. WO 2007126124, 2007.
24. Wheeler, K. A.; Harrington, B.; Zapp, M.; Casey, E. *CrystEngComm* **2003**, 5, (59), 337.
25. Dyer, E.; Glenn, J. F. *Journal of American Chemical Society* **1957**, 79, 366.
26. Zhou, H.; Li, Q.; Lee, T. Y.; Guymon, A. C.; Jonsson, S. E.; Hoyle, C. E. *Macromolecules* **2006**, 39, 8269-8273.
27. Sheldrick, G. *SHELXS-86 Program for Crystal Structure Solution*, Institut für Anorganische Chemie der Universität: Tammanstrasse 4, D-3400 Gottingen, Germany,

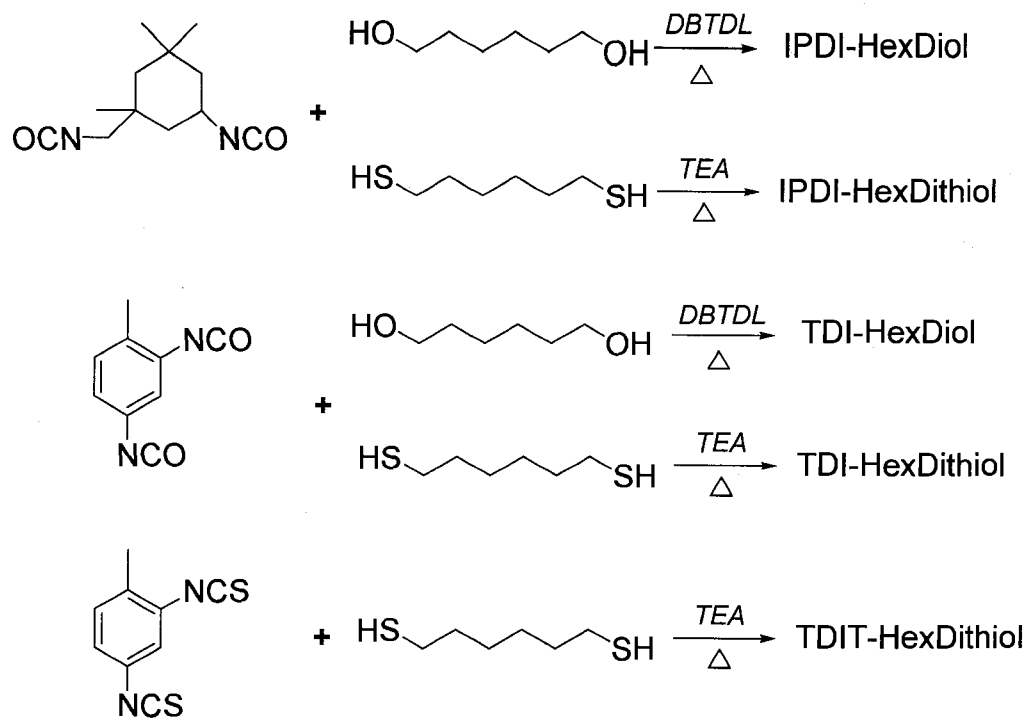
1986.

28. Sheldrick, G. M. *SHELX97 [Includes SHELXS97, SHELXL97, CIFTAB] - Programs for Crystal Structure Analysis (Release 97-2)*, Institut für Anorganische Chemie der Universität: Tammanstrasse 4, D-3400 Göttingen, Germany, 1998.
29. Becke, A. D. *Journal of Chemical Physics* **1993**, 98, 5648.
30. Lee, C.; Yang, W.; Parr, R. G. *Physics Review B* **1988**, 37, 785.
31. Woon, D. E.; Dunning, T. H. *Journal of Chemical Physics* **1993**, 98, 1358.
32. Kendall, R. A.; Dunning, T. H.; Harrison, R. J. *Journal of Chemical Physics* **1992**, 96, 6796.
33. Winningham, M. J.; Sogah, D. Y. *Journal of American Chemical Society* **1994**, 116, 11173.
34. Tsang, K. Y.; Diaz, H.; Graciano, N.; Kelly, J. W. *Journal of American Chemical Society* **1994**, 116, 3988.
35. Diaz, H.; Espina, J. R.; Kelly, J. W. *Journal of American Chemical Society* **1992**, 114, 8316.
36. Dado, G. P.; Gellman, S. H. *Journal of American Chemical Society* **1994**, 116, 1054.
37. He, Y.; Zhu, B.; Inoue, Y. *Progress in Polymer Science* **2004**, 29, 1021.
38. Xiu, Y.; Zhang, Z.; Wang, D.; Ying, S.; Li, J. *Polymer* **1992**, 33, 1335.
39. Gramstad, T.; Sandstrom, H. J. *Spectrochimica Acta* **1969**, 25A, 31.
40. Bunn, C. W. *Journal of Polymer Science* **1955**, 16, 323.
41. Osawa, Z., In *Developments in Polymer Photochemistry-3*

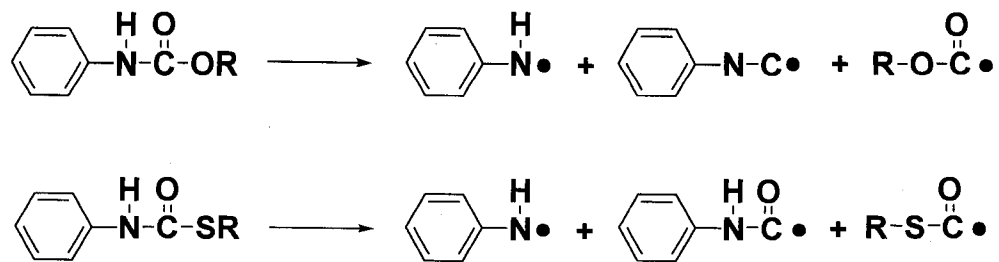
- Allen, N. S., Ed. Applied Science Publishers Ltd.: London, England, 1982.
42. Beachell, H. C.; Chang, I. L. *Polymer Science: Part A* **1972**, 10, 503.
43. Hoyle, C. E.; Herweh, J. E. *Journal of Organic Chemistry* **1980**, 11, 2195.
44. Gaber, A. M.; Aly, M. M.; Fahmy, A. M. *Phosphorus, Sulfur and Silicon* **2000**, 166, 243.
45. Hoyle, C. E.; Kim, K.-J.; No, Y. G.; Nelson, G. L. *Journal of Applied Polymer Science* **1987**, 34, 763.
46. Douglas, B.; McDaniel, D.; Alexander, J., *Concepts and Models of Inorganic Chemistry*. 3 ed.; John Wiley & Sons, Inc.: New York, 1994.
47. Gomez, L.; Gellibert, F.; Wagner, A.; Mioskowski, C. *J. Comb. Chem.* **2000**, 2, 75.



Scheme 8.1. Synthesis of carbamates (CIHA and PIHA), thiocarbamates (CIHT and PIHT) and dithiocarbamates (PITHT).



Scheme 8.2. Synthesis of polyurethanes, IPDI-HexDiol and TDI-HexDiol, polythiourethanes, IPDI-HexDithiol and TDI-HexDithiol, and polydithiourethane, TDIT-HexDithiol.



Scheme 8.3. Free radicals formed in the photolysis of aromatic urethane and thiourethane.

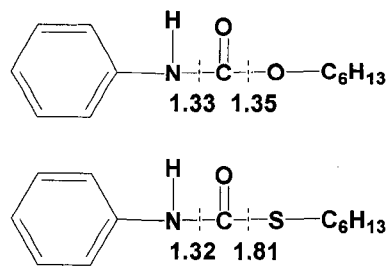


Chart 8.1. Structures and bond length (Å) of PIHA and PIHT. Bond length values are measured by X-Ray diffraction.

Table 8.1. Temperature dependent chemical shift coefficients, $\Delta\delta/\Delta T$, and variation in chemical shift, $\Delta\delta$, of model compounds.

	CIHA	CIHT	PIHA	PIHT	PITHT
$\Delta\delta/\Delta T$ (ppm/K * 10^{-3})	11.2	1.12	0.94	0.88	1.17
$\Delta\delta$ (ppm)*	0.45	0.45	0.38	0.35	0.47

* $\Delta\delta = \delta_{65^\circ\text{C}} - \delta_{105^\circ\text{C}}$

Table 8.2. Hydrogen-bonding metrics from crystal structures.

	CIHA	CIHT	PIHA	PIHT
N-H---O (Å)	2.930(3)	3.015(6)	2.992(7)	3.078(9)
Angle at H (°)	161.2(2)	162.2(4)	159.3(4)	160.7(5)

Table 8.3. Crystallographic data for crystal structures.

		CIHA	CIHT	PIHA	PIHT
Space Group		P2 ₁ 2 ₁ 2 ₁ (#19)	P-1 (#2) (Z=4)	P-1 (#2)	P-1 (#2)
Cell Constants	a (Å)	5.0663(2)	5.1365(5)	5.1270(6)	5.2198(3)
	b (Å)	13.4317(8)	15.567(3)	7.8674(13)	7.8737(6)
	c (Å)	21.1721(12)	19.266(3)	16.5435(17)	16.9331(16)
	α (°)	90	73.196(14)	88.855(11)	88.951(7)
	β (°)	90	88.684(10)	84.942(9)	95.277(7)
	γ (°)	90	89.231(10)	74.160(12)	107.335(6)
Volume (Å ³)		1440.74(13)	1474.3(4)	639.46(15)	661.48(9)

Table 8.4. Melting point of model compounds measured by DSC at a heating rate of 1 °C/min.

	CIHA	CIHT	PIHA	PIHT	PITHT
T _m (°C)	37	35	39	60	42

Table 8.5. Polymer properties.

	IPDI-HexDiol	IPDI-HexDithiol	TDI-HexDiol	TDI-HexDithiol	TDIT-HexDithiol
T _g (°C)	71	74	86	84	62
Pencil Hardness	5H	5H	5H	6H	5H
Persoz Hardness	284±5	288±4.9	267±5.2	293±6.1	250±5.2
T (5%)*	285	255	270	240	140

*T(5%) is temperature at 5% weight loss

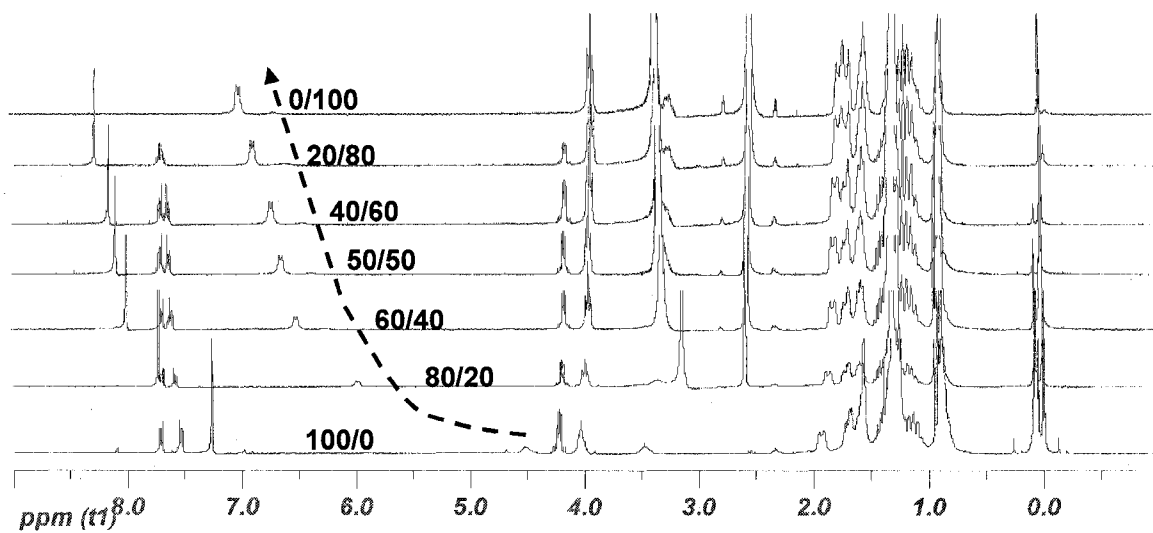
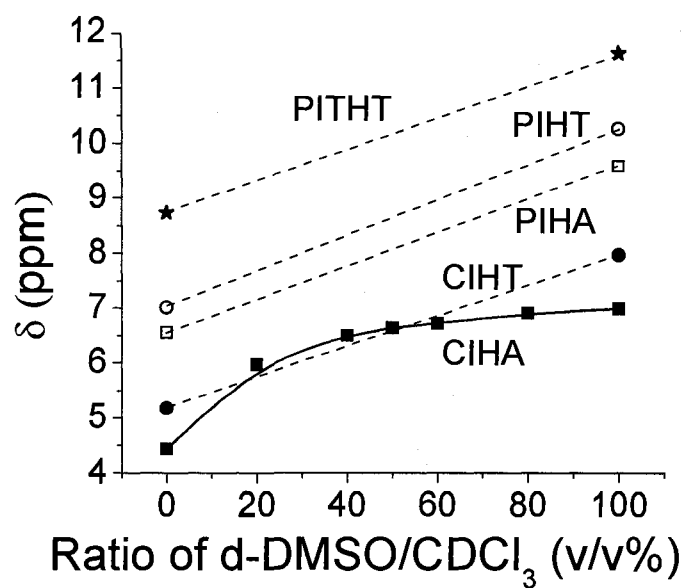
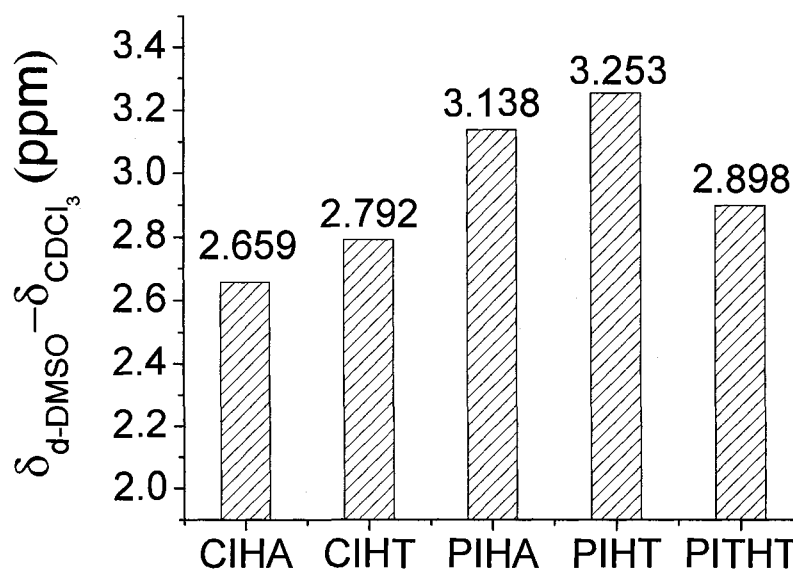


Figure 8.1. The ^1H NMR spectra of 3.7 mM CIHA in $\text{CDCl}_3/d\text{-DMSO}$ solvent mixtures. The numbers in the figure indicate the volume ratios of the two solvents.



a



b

Figure 8.2. (a) Chemical shift values of NH protons of model compounds as a function of volume ratio of d-DMSO/CDCl₃. (b) Chemical shift difference between NH protons in d-DMSO and CDCl₃.

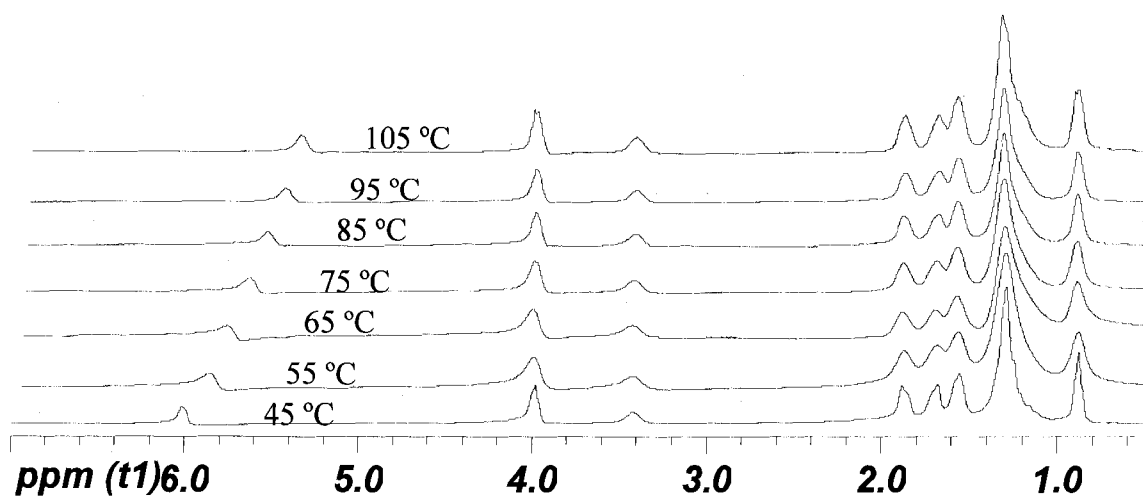


Figure 8.3. The ^1H NMR spectra of CIHA measured at different temperature.

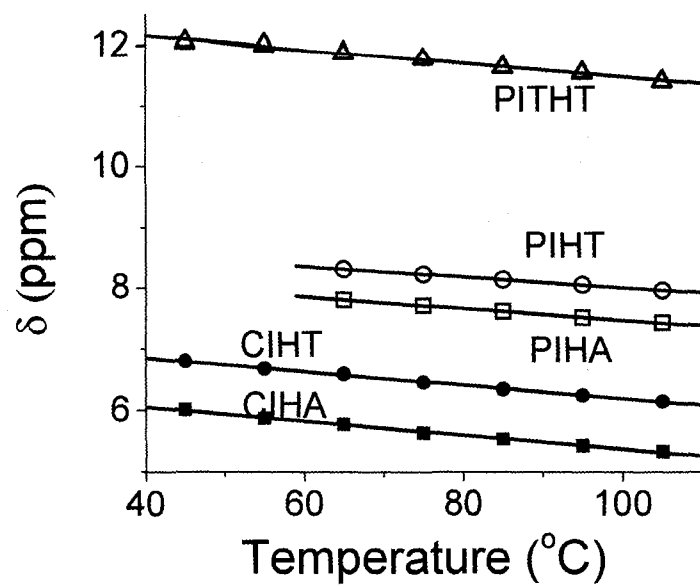


Figure 8.4. Chemical shift of model compounds as a function of temperature.

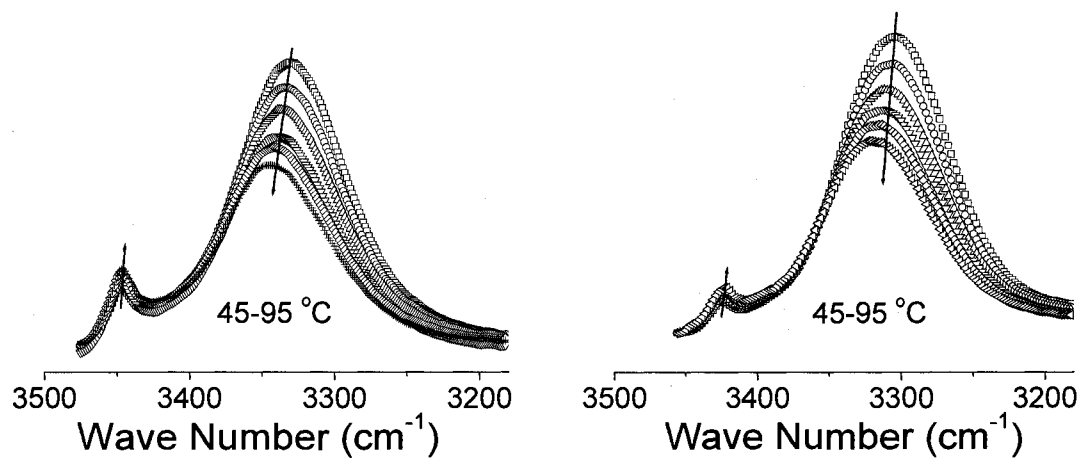


Figure 8.5. FTIR spectra of CIHA and CIHT measured at temperatures from 45 to 95°C with a 10 degrees interval. The arrows indicate the direction of temperature increase.

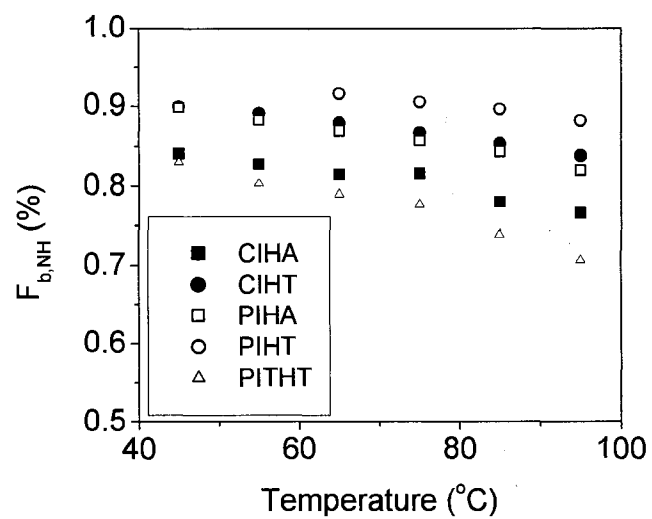


Figure 8.6. $F_{b,NH}$ of carbamates, thiocarbamates and dithiocarbamate as a function of temperature.

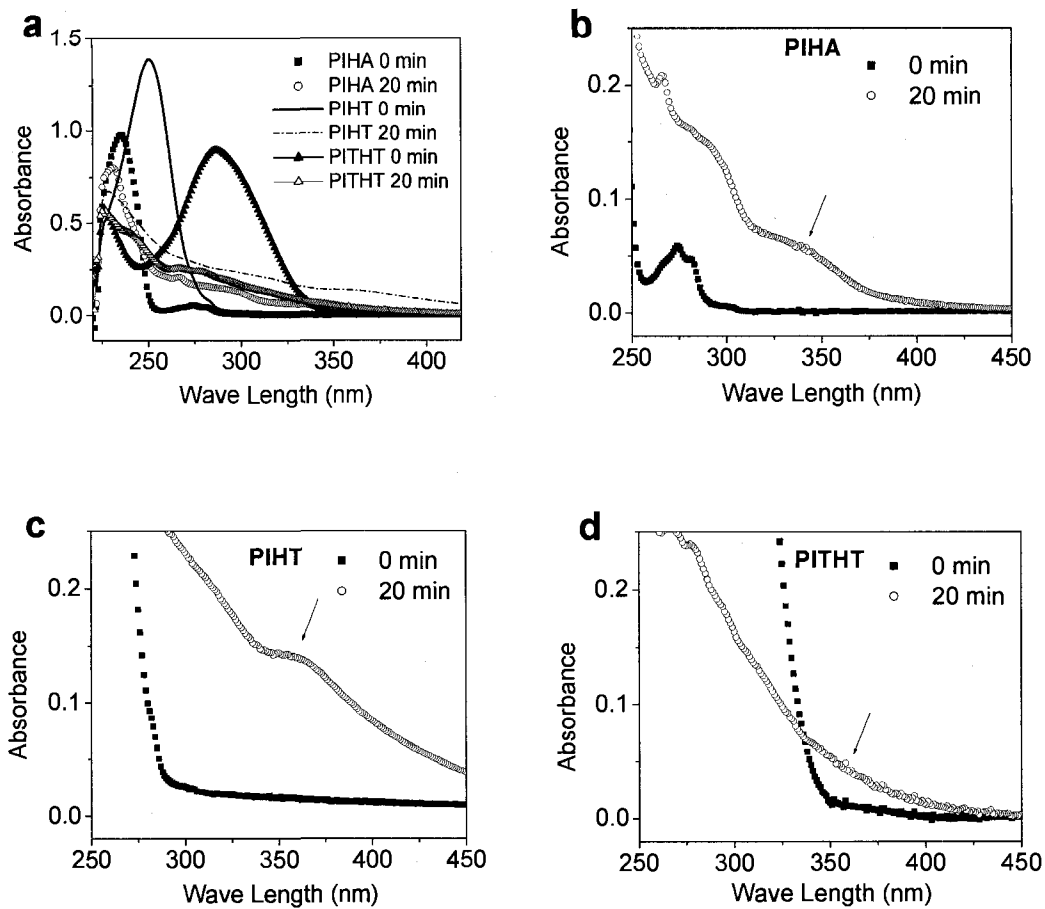


Figure 8.7. UV spectra of PIHA, PIHT and PITHT before and after photolysis conducted by exposing all samples dissolved in CH_2Cl_2 (0.06 mM) to the output of a medium pressure mercury lamp for 20 min.

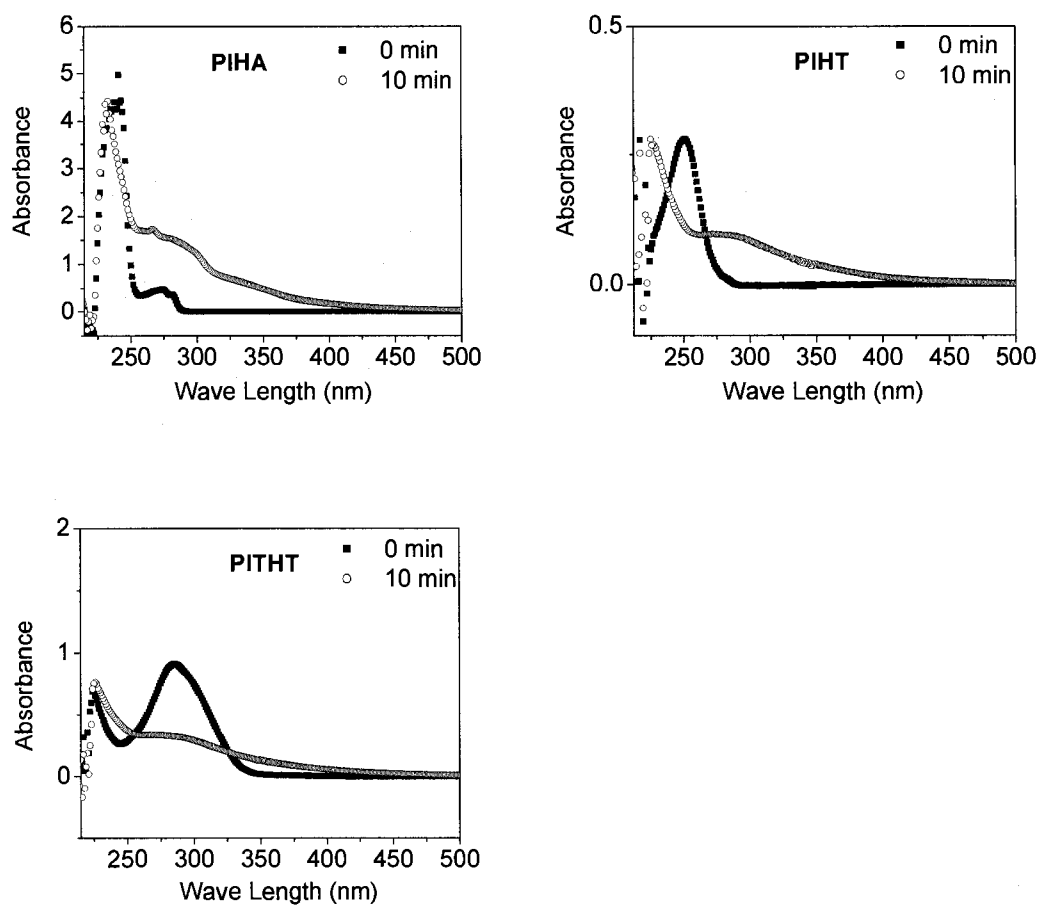


Figure 8.8. UV spectra of model compound solutions (in CH_2Cl_2) with equal absorbance at 254 nm before and after photolysis conducted by exposing all samples to the output of a Rayonet photoreactor equipped with 254 nm lamp.

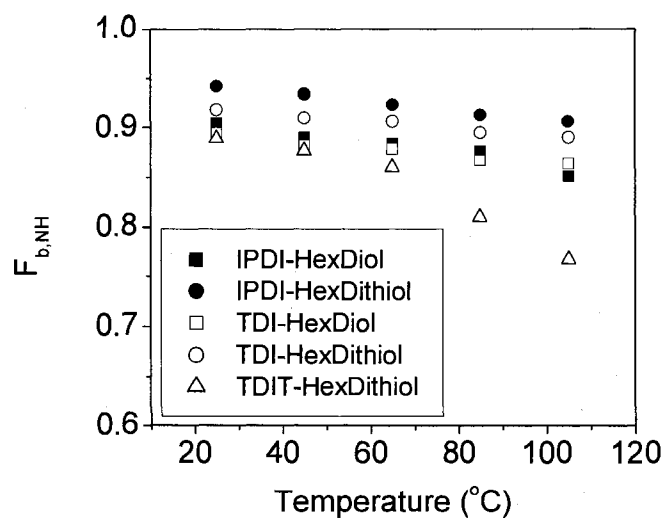


Figure 8.9. Hydrogen bonding fraction of polymers as a function of temperature.

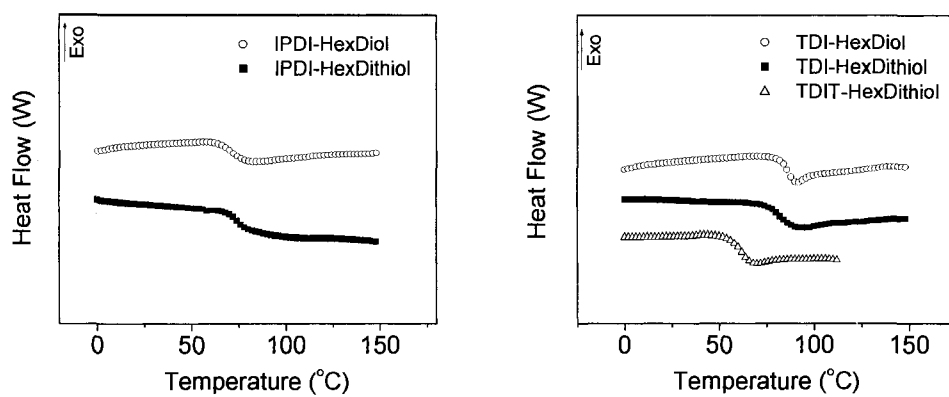


Figure 8.10. DSC curves of polymers.

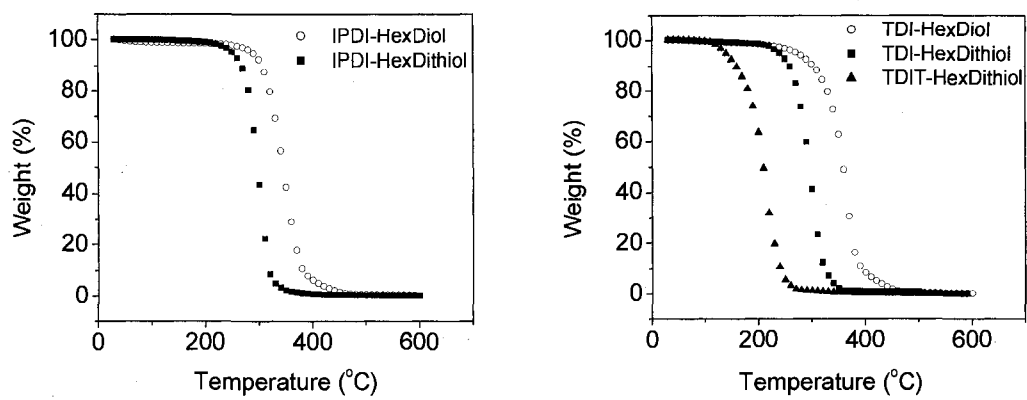


Figure 8.11. Thermogravimetric analysis of polymers.

CHAPTER IX

CONCLUSIONS AND RECOMMENDATIONS

The research reported in this dissertation has dealt with the photopolymerization and physical and mechanical property measurements of thiol-ene based systems and a comparison study of urethane, thiourethane and dithiourethane based materials. The main conclusions of each study are outlined in the following paragraphs.

The photopolymerization of four different types of enes with primary and secondary thiol was investigated and physical and mechanical properties of the thiol-ene networks measured. All ene monomers showed high reactivity with both thiols, with PEGDA homopolymerizing as well as copolymerizing with the thiol. Higher ΔC_p values were observed for the more flexible networks based on TEGDVE and PEGDA. The flexibility, surface scratch resistance and thermal stability of films based on the primary and secondary thiols were essentially identical. The trifunctional APE and TTT based networks with higher network densities, and in the case of TTT a rigid ring structure, had higher glass transition temperature, pencil hardness and refractive indices, and better mandrel bending performance. The difunctional and flexible TEGDVE and PEGDA based networks show lower T_g s, higher ΔC_p s and better impact resistance. Finally, all of the resin mixtures prepared from the commercial secondary thiol exhibited much better shelf-life than those prepared from the primary thiols, and the secondary thiol sample evaluated had little or no objectionable odor making it particularly suitable for many applications.

Real-time FTIR analysis shows that the photopolymerization of a trithiol and trivinyl ether mixture with excess vinyl ether proceeds by a rapid thiol-ene radical polymerization and a subsequent cationic vinyl ether polymerization. Dynamic rheology measurements confirm that the TriThiol-TriVinyl (25 to 75 mol%) sample gels at the end of the thiol-ene free-radical reaction followed by a cationic polymerization of residual vinyl ether groups. Mechanical property and impact measurements indicate an energy absorbing, tough material. The results suggest an important strategy for building networks via hybrid free-radical thiol-ene/cationic-ene polymerization processes.

Thiourethane-thiol-ene (TUTE) films with high glass transition temperatures were prepared from the thiol-ene polymerization of a triene with multifunctional thiol oligomers based upon three diisocyanates: IPDI, H12MDI and TDI. Further increases in T_g were achieved after the initial photocuring process by aging and/or annealing at 85 °C due to additional reaction of the thiol and ene functional groups, as well as the reaction of isocyanates formed during the photocuring process. All the aged and annealed TUTE thiol-ene films had T_g s greater than 90 °C. The hardness of the initially (unaged) cured TUTE films increased markedly after annealing. Also, the unaged TUTE films exhibit fairly good impact and bending properties.

The effect of annealing temperature and annealing time on the enthalpy relaxation of thiol-ene and thiourethane thiol-ene networks have been investigated qualitatively by DSC, and quantitatively by relaxation rate calculations. Compared with a model thiol-ene network, all of the hydrogen bonding containing thiourethane thiol-ene networks exhibit

almost identical enthalpy relaxation rates at $T_g - 10$ °C. FTIR analysis of IPDI Thiol-TTT films indicated no change in the extent of hydrogen bonding upon sub- T_g aging. The hydrogen bonding associated with the thiourethane linkages thus influences the networks in one distinct way. By introducing hydrogen bonding, the glass transition temperatures of the networks are very high compared to traditional thiol-ene systems. However, there appears to be little effect of hydrogen bonding on enthalpy relaxation of these dense networks.

A series of small molecule and polymeric urethane, thiourethane and dithiourethane model compounds were prepared and measured by FTIR, NMR, DSC, and DMA establishing the order of the hydrogen bonding strength as: urethane \approx thiourethane > dithiourethane. Due to their similar hydrogen bonding behavior, model polyurethane and polythiourethane networks have similar physical and mechanical properties, including close T_g , hardness and tensile properties. The polydithiourethane model compound with lower T_g is softer, more flexible and less tough because of weaker hydrogen bonding forming ability. The comprehensive characterization and comparison of urethane, thiourethane and dithiourethane compounds provides experimental and theoretical guidance for various applications of sulfur containing urethane materials based upon their unique features including high refractive index, the quantitative conversion of the isocyanate-thiol reaction, and the feasibility of incorporating them into photopolymerizable systems.

The hydrogen bonding and structure-property relationships of a series of small

molecular and polymeric urethane, thiourethane and dithiourethane systems prepared from both aliphatic and aromatic secondary isocyanates were characterized. The extent of hydrogen bonding for the urethanes and thiourethanes was greater than that of the dithiourethane. Similar physical and mechanical properties for the polyurethanes and polythiourethanes (both aliphatic and aromatic) were consistent with the hydrogen bonding results. The dithiourethane based model and polymers exhibited a lower melting point (small molecule) and glass transition temperature compared to the urethane and thiourethane counterparts.

Summarizing, the research reported in this dissertation has probed the effect of monomer structures on thiol-ene network properties and important strategies to prepare hybrid free-radical thiol-ene/cationic ene networks and high T_g thiol-ene networks with uniform structures. A comprehensive comparison and characterization was also conducted on a series of aliphatic, aromatic, primary and secondary isocyanate/isothiocyanate based urethane type materials to define any differences between urethanes, thiourethanes and dithiourethanes. Several suggestions can be made for future work as outlined in the following paragraphs.

To build up a complete set of structure-property relationships for thiol-ene networks, formulations containing an expanded set of thiol and ene structures should be investigated. Although, for primary and secondary Tetra Thiol based thiol-ene systems, almost no difference were observed in photopolymerization and film properties, it would still be interesting to investigate systems based on more hindered secondary thiols, such

as those with two methyl groups or a benzene ring attached to the α -carbon. This might significantly reduce the photopolymerization rate under the experimental conditions used in Chapter III and generate greater differences in network properties compared to those made from primary thiols.

Due to their excellent adhesion properties and complementary low shrinkage during curing, epoxides are worth to be incorporated into a free-radical/cationic hybrid thiol-ene system. Preliminary studies on TriThiol/4-vinyl-1-cyclohexene 1,2-epoxide (1:1 mol) shows that the propagating cationic chain ends are readily terminated by the nucleophilic sulfide linkages of the thiol-ene product. This was also reported in the literature. Thiol-ene polymers prepared from highly hindered secondary thiols, such as those mentioned in the above paragraph, may help reduce the chain end termination because of the steric hindrance around the sulfide bond.

The process for preparing thiourethane thiol-ene networks could be modified by mixing isocyanates, thiol and ene together and coating the mixture onto substrates. After the initial room-temperature isocyanate-thiol reaction was catalyzed by tertiary amine catalyst, such as triethyl amine or DABCO, the thiol-ene networks could be formed via the same conditions used in Chapter V. A combination of a rigid structure arising from thiourethane linkages and flexibility from more flexible enes may provide thiourethane thiol-ene films with better impact and mandrel bend performance.

Although a comprehensive investigation of the hydrogen bonding of thiourethanes and dithiourethanes in simplified small models, linear polymer and

polymer networks has been conducted, the hydrogen bonding behavior of thiourethanes and dithiourethanes in more complicated systems, such as phase separated polymers resembling polyester-polyurethane or polyether-polyurethane systems, would establish an even greater understanding of structure-property relationships in sulfur containing polyurethanes.

Thiol-ene photopolymerization offers an efficient process to form high density networks with uniform structures which have important potential applications. The conclusions drawn from this research and future work recommendations made in this section should result in the improvement of thiol-ene polymer properties. The conclusions regarding the thiourethanes and dithiourethanes should provide a theoretical and experimental basis for designing of new materials with enhanced performance.